

DEVELOPMENT OF ALUMINUM NITRIDE: A New Low-Cost Armor

**Final Report
August, 1988 - March, 1992**

DR. WILLIAM RAFANIELLO

December 1, 1992

U.S. ARMY RESEARCH OFFICE

DAAL03-88-C-0012

THE DOW CHEMICAL COMPANY

**Approved for Public Release:
Distribution Unlimited**



REPORT DOCUMENTATION PAGE			Form Approved OMB No. 0704-0188	
Public reporting burden for this collection of information is estimated to average 1 hour per response, including the time for reviewing instructions, searching existing data sources, gathering and maintaining the data needed, and completing and reviewing the collection of information. Send comments regarding this burden estimate or any other aspect of this collection of information, including suggestions for reducing this burden, to Washington Headquarters Services, Directorate for Information Operations and Reports, 1215 Jefferson Davis Highway, Suite 1204, Arlington, VA 22202-4302, and to the Office of Management and Budget, Paperwork Reduction Project (0704-0188), Washington, DC 20503.				
1. AGENCY USE ONLY (Leave blank)		2. REPORT DATE	3. REPORT TYPE AND DATES COVERED Final Report Aug. 1988 - March 1992	
4. TITLE AND SUBTITLE DEVELOPMENT OF ALUMINUM NITRIDE: A New Low-Cost Armor			5. FUNDING NUMBERS	
6. AUTHOR(S) W. Rafaniello				
7. PERFORMING ORGANIZATION NAME(S) AND ADDRESS(ES) The Dow Chemical Company 1776 Building Midland, MI 48674			8. PERFORMING ORGANIZATION REPORT NUMBER	
9. SPONSORING/MONITORING AGENCY NAME(S) AND ADDRESS(ES) U. S. Army Research Office P. O. Box 12211 Research Triangle Park, NC 27709-2211			10. SPONSORING/MONITORING AGENCY REPORT NUMBER	
11. SUPPLEMENTARY NOTES The view, opinions and/or findings contained in this report are those of the author(s) and should not be construed as an official Department of the Army position, policy, or decision, unless so designated by other documentation.				
12a. DISTRIBUTION/AVAILABILITY STATEMENT Approved for public release; distribution unlimited.			12b. DISTRIBUTION CODE	
13. ABSTRACT (Maximum 200 words) High performance and low cost are the two essential requirements necessary for advanced ceramics to be considered for incorporation into future armor systems. This work involved a comprehensive program, focused on aluminum nitride based ceramics, which examined the critical ceramic processing parameters and studied the impact these modifications had on ballistic performance. The accomplished objective was to demonstrate that low-cost fabrication methods could be utilized to produce high performance AlN based ceramics. Using a spray-dry, dry-press, pressureless sintering process, thick tiles were produced with ballistic performance equivalent to hot-pressed AlN materials. While penetration resistance against the long rod penetrator (LRP) was the ultimate measure of performance, several other ballistic tests were also performed. Ballistic limits were obtained for ceramic targets with a .30 caliber AP simulant and penetration tests were performed against .50 caliber APDS and SLAP rounds. These tests were used as screening tools to guide AlN powder and sintering aid optimization. Dynamic compressive strength, determined by a SHPB (split Hopkinson pressure bar), was also found to be useful in guiding material and process selection. Finally, AlN/SiC composites were found to have enhanced ballistic penetration resistance and offered the potential for even greater cost/performance benefits compared to the baseline materials.				
14. SUBJECT TERMS Aluminum nitride, sintering, powders, processing, armor, ballistic performance, dynamic properties, AlN/SiC composites, silicon carbide			15. NUMBER OF PAGES 141	
			16. PRICE CODE	
17. SECURITY CLASSIFICATION OF REPORT UNCLASSIFIED	18. SECURITY CLASSIFICATION OF THIS PAGE UNCLASSIFIED	19. SECURITY CLASSIFICATION OF ABSTRACT UNCLASSIFIED	20. LIMITATION OF ABSTRACT UL	

DEVELOPMENT OF ALUMINUM NITRIDE: A New Low-Cost Armor

**Final Report
August, 1988 - March, 1992**

DR. WILLIAM RAFANIELLO

December 1, 1992

U.S. ARMY RESEARCH OFFICE

DAAL03-88-C-0012

THE DOW CHEMICAL COMPANY

**Approved for Public Release:
Distribution Unlimited**

THE VIEW, OPINIONS, AND/OR FINDINGS CONTAINED IN THIS REPORT ARE THOSE OF THE AUTHOR(S) AND SHOULD NOT BE CONSTRUED AS AN OFFICIAL DEPARTMENT OF THE ARMY POSITION, POLICY, OR DECISION, UNLESS SO DESIGNATED BY OTHER DOCUMENTATION.

ACKNOWLEDGMENT

The author would first like to thank Dr. Andrew Crowson, ARO project monitor, and Lt. Col. P. Sullivan, DARPA armor program director at the time of this contract, for their support. This successful program was made possible only through the cooperative efforts of many individuals both within the Dow Chemical Company and outside in the armor community. For their efforts in dynamic and ballistic testing, I would like to recognize J. Lankford, C. Anderson and B. Morris at SwRI, and T. Williams, S. Hanchak, G. Abfalter, and S. Bless at UDRI. At the Dow Chemical Company, the work of F. Skeeel, I. Khoury and P. Bourns was invaluable in the critical development of a cost effective process for the manufacture of ceramic armor. Ron Hoffman and coworkers provided guidance in the selection of the most appropriate ballistic screening tests, and prepared many of the hundreds of ceramic targets which were tested. The exciting electron microscopy work was provided by D. Susnitzky and F. Shieu. I would also like to acknowledge the fine assistance of our Contracts R&D group, which provided the needed support for this contract from start to finish. Finally, I like to express my profound appreciation to my assistants, B. L. Stiehl and the late J. Lefevre, whose tremendous efforts and dedication made this endeavor a reality.

ABSTRACT

High performance and low cost are the two essential requirements necessary for advanced ceramics to be considered for incorporation into future armor systems. This work involved a comprehensive program, focused on aluminum nitride based ceramics, which examined the critical ceramic processing parameters and studied the impact these modifications had on ballistic performance. The accomplished objective was to demonstrate that low-cost fabrication methods could be utilized to produce high performance aluminum nitride based ceramics. Using a spray-dry, dry-press, pressureless sintering process, thick aluminum nitride tiles were produced with ballistic performance equivalent to hot-pressed AlN materials. Several grades of AlN powders with a broad range of chemistry and particle size characteristics were examined. Because of their potential impact on tile manufacturing costs, different sintering additives were also studied. Prior to ballistic testing, sinterability was first established for each formulation tested. While penetration resistance against a quarter scale tungsten long rod penetrator (LRP) was the ultimate measure of performance during this program, several other ballistic tests were also performed. Ballistic limits were obtained for ceramic targets with a .30 caliber AP simulant and depth of penetration tests were performed against .50 caliber APDS and SLAP rounds. The light caliber tests were used as screening tools to guide AlN powder and sintering aid optimization. Dynamic compressive strength, determined by a SHPB (split Hopkinson pressure bar), was also found to be useful in guiding material and process selection. Finally, AlN/SiC composites were found to have enhanced ballistic penetration resistance characteristics and offered the potential for even greater cost/performance benefits compared to the baseline materials.

TABLE OF CONTENTS

ACKNOWLEDGMENT.....	ii
ABSTRACT	iii
LIST OF TABLES	vi
LIST OF FIGURES	viii
1.0 INTRODUCTION	1
2.0 TECHNICAL WORK.....	4
2.1 HOT-PRESSED ALUMINUM NITRIDE	4
2.1.1 POWDER SELECTION & CHARACTERIZATION	4
2.1.2 HOT-PRESS OPTIMIZATION.....	8
2.1.3 PHYSICAL & MECHANICAL PROPERTIES.....	13
2.1.4 BALLISTIC STUDIES.....	21
2.1.5 DISCUSSION.....	29
2.2 SINTERED ALUMINUM NITRIDE.....	33
2.2.1 SINTERING SCREENING STUDY	33
2.2.2 PROCESS OPTIMIZATION.....	40
2.2.3 PREPARATION OF SINTERED TARGETS.....	50
2.2.4 PHYSICAL & MECHANICAL PROPERTIES.....	60
2.2.5 BALLISTIC STUDIES.....	67
2.2.5.1 LIGHT CALIBER TESTS.....	67
2.2.5.2 LRP and SLAP D.O.P. RESULTS	76
2.2.6 DISCUSSION.....	82
2.3 HOT-PRESSED AlN/SiC COMPOSITES.....	92
2.3.1 HOT-PRESS OPTIMIZATION.....	93
2.3.2 COMPOSITE TILE PREPARATION.....	100

2.3.3 BALLISTIC RESULTS.....	102
2.3.4 DISCUSSION.....	109
2.4 SINTERING OF AlN/SiC COMPOSITES.....	115
2.4.1 PROCESS OPTIMIZATION.....	115
2.4.2 SCREENING STUDY.....	121
3.0 SUMMARY.....	126
4.0 PUBLICATIONS AND TECHNICAL REPORTS	128
5.0 REFERENCES.....	129

LIST OF TABLES

I. AIN POWDERS EVALUATED DURING CONTRACT.....	5
II. HOT-PRESSING CONDITIONS FOR BALLISTIC TARGETS	12
III. PROPERTIES OF AIN POWDER USED FOR ARMOR TILES	13
IV. PHYSICAL PARAMETERS FOR HOT PRESSED BILLETS	17
V. MECHANICAL PROPERTIES OF HOT-PRESSED AIN.....	18
VI. CERAMIC TARGETS FOR LRP D.O.P. TESTING.....	22
VII. D.O.P. BALLISTIC RESULTS FOR LRP, L/D = 10.....	26
VIII. D.O.P. BALLISTIC RESULTS FOR LRP, L/D = 15.....	26
IX. SINTERING AIDS USED IN SCREENING EXPERIMENT	34
X. STATISTICAL RESULTS OF POWDER STUDY.....	36
XI. PROCESS SCREENING RESULTS FOR GREEN DENSITY	42
XII. PROCESS SCREENING RESULTS FOR FIRED DENSITY	44
XIII. TILE THICKNESS EFFECT ON GREEN DENSITY	46
XIV. SINTERED AIN SAMPLES FOR BALLISTIC EVALUATION	51
XV. SPRAY DRIED AIN PRODUCT FOR BALLISTIC SCREEN	51
XVI. AVERAGE VALUES FOR SINTERED AIN TILE SETS.....	54
XVII. AIN POWDER USED IN PREPARING SINTERED TILES.	55
XVIII. SELECTED SINTERED AIN FOR LRP TESTING.....	56
XIX. PROPERTIES OF SELECTED SINTERED AIN SAMPLES	61
XX. MECHANICAL CHARACTERIZATION OF SINTERED AIN COMPOSITIONS	64
XXI. SONIC PROPERTIES OF SINTERED AIN	66
XXII. .30 CALIBER BALLISTIC LIMITS FOR SINTERED AIN..	69
XXIII. MICROSCOPIC ANALYSIS OF BALLISTIC FRAGMENTS	73

XXIV.	PENETRATION RESULTS FOR L/D=10 LRP INTO AlN ...	77
XXV.	CORRELATION COEFFICIENTS FOR ALL PARAMETERS	87
XXVI.	RANKINGS OF SINTERED AlN COMPOSITIONS	90
XXVII.	RANK CORRELATION COEFFICIENTS.....	91
XXVIII.	POWDERS USED DURING TASKS ASSOCIATED WITH AlN/SiC COMPOSITES.....	93
XXIX.	DENSITY AND PHASE ANALYSIS OF AlN/SiC AT DIFFERENT HOT-PRESS TEMPERATURES.....	99
XXX.	HOT-PRESSING CONDITIONS FOR AlN/SiC BALLISTIC SAMPLES	101
XXXI.	L/D = 10 LRP PENETRATION RESULTS INTO AlN/SiC COMPOSITES.....	107
XXXII.	PROCESS OPTIMIZATION STUDY FOR SINTERED AlN/SiC COMPOSITES.....	117
XXXIII.	LEAST SQUARE COEFFICIENTS FOR AlN/SiC PROCESS OPTIMIZATION STUDY.....	120

LIST OF FIGURES

1. SEM PHOTOMICROGRAPHS OF AIN POWDERS	6
2. TYPICAL HOT-PRESS TEMPERATURE/PRESSURE CYCLE ...	9
3. HOT-PRESSED DENSITIES FOR AIN POWDERS.....	10
4. AVERAGE GRAIN SIZE OF HOT-PRESSED AIN POWDERS	11
5. PHOTOMICROGRAPHS OF HOT- PRESSED AIN BILLETS.....	15
6. SPLIT HOPKINSON PRESSURE BAR APPARATUS.....	19
7. COMPRESSIVE STRENGTH OF AIN POWDERS	20
8. SCHEMATIC OF BALLISTIC TEST PERFORMED AT SWRI	23
9. PENETRATION DATA FOR TUNGSTEN ALLOY PROJECTILES	24
10. REFINED PENETRATION DATA L/D =10 LRP.....	24
11. AVERAGE SCALED PENETRATION REDUCTION VALUES...	28
12. LRP D.O.P. AS A FUNCTION OF CERAMIC AREAL DENSITY	29
13. PERCENT THEORETICAL DENSITY OF SINTERED SAMPLES	35
14. PERCENT THEORETICAL DENSITY MEANS OF MAIN..... EFFECTS FOR AIN	37
15. PERCENT THEORETICAL DENSITY MEANS OF TWO FACTOR INTERACTION TERMS.....	38
16. PARAMETERS FOR THE SINTERED AIN SAMPLES.....	39
17. SCHEMATIC OF PROCESS TO FABRICATE AIN PARTS	40
18. PREDICTIVE MODELS FOR GREEN DENSITY	42
19. PREDICTIVE MODELS FOR FIRED DENSITY	43
20. EFFECT OF PEG MOLECULAR WEIGHT AND BINDER CERAMIC COMPOSITION ON THE BIAXIAL STRENGTH.....	45
21. EFFECT OF PEG MOLECULAR WEIGHT AND BINDER CERAMIC COMPOSITION ON THE DENSIFICATION OF AIN	45
22. WEIGHT LOSS OF AIN GREENWARE	47

23. CARBON DISTRIBUTION OF A GREEN AlN TILE	47
24. DIFFERENT PHASES OF SINTERED AlN.....	49
25. TYPICAL FAILURES IN FABRICATING LARGE AlN TILES	59
26. PHOTOMICROGRAPHS OF ETCHED POLISHED SECTIONS.	62
27. RANKED COMPRESSIVE STRENGTH OF AlN COMPOSITIONS	65
28. SCHEMATIC OF .30 CALIBER AP TARGET	68
29. PENETRATION RESULTS FOR .50 CALIBER APDS BULLETS	71
30. X-RAY PHOTOGRAPHS OF .50 CALIBER TARGETS.....	72
31. PHOTOMICROGRAPHS OF FRACTURE SURFACES	74
32. FRACTURE SURFACES OF BALLISTIC FRAGMENTS	75
33. RECOVERED PENETRATOR MASSES FOR AlN TARGETS	78
34. SCHEMATIC OF SLAP TARGET ASSEMBLY.....	80
35. PENETRATION VALUES FOR .50 CALIBER SLAP ROUNDS.	81
36. TEM PHOTOMICROGRAPHS OF FINE RUBBLE PARTICLES	84
37. TEM PHOTOMICROGRAPHS OF AlN WITH 0.5% CERIA.....	85
38. TEM PHOTOMICROGRAPHS OF AlN WITH 5.0% CERIA	86
39. SCATTER PLOTS FOR KEY MECHANICAL PROPERTIES	88
40. OPTICAL PHOTOMICROGRAPHS OF 90/10 AlN/SiC SAMPLES	98
41. OPTICAL PHOTOMICROGRAPHS OF 25/75 AlN/SiC SAMPLES	99
42. DENSITY OF AlN/SiC TILES SHOWING EFFECT OF POSITION IN DIE DURING HOT-PRESSING.....	101
43. RESIDUAL PENETRATION OF .50 CALIBER SLAP ROUNDS IN AlN/SiC COMPOSITE TARGETS.....	103
44. RESIDUAL PENETRATION OF .50 CALIBER SLAP ROUNDS	106
45. COMPARISON OF RESIDUAL PENETRATION OF TUNGSTEN LONG ROD PENETRATORS	108

46. TEM PHOTOMICROGRAPHS OF FINE RUBBLE PARTICLES FOR HOT-PRESSED AlN AND AlN/SiC COMPOSITES.....	113
47. TEM PHOTOMICROGRAPHS OF THIN SECTIONS TAKEN FROM LARGER (>3 mm) BALLISTIC FRAGMENTS.....	114
48. GRAPHICAL REPRESENTATION OF AlN/SiC RESULTS.....	118
49. AlN/SiC PROCESSING STUDY MAIN EFFECTS PLOT	119
50. BOX PLOT OF AlN/SiC SINTERING STUDY	123
51. CONTOUR PLOTS FOR SINTERED AlN/SiC COMPOSITES	125

1.0 INTRODUCTION

Ceramic armor has been identified as a potentially significant structural ceramic opportunity.¹ Based on the fit with its non-oxide technology base and the near term markets, The Dow Chemical Company has championed the recent development of ceramic based armor. However, despite impressive performance advantages, price has been a major stumbling block to the incorporation of ceramics into U.S. armored vehicles. The primary ceramics being considered for use as armor include alumina, boron carbide, titanium diboride and silicon carbide.² These materials are extremely hard, have high strength, are relatively lightweight and are typically expensive. Of these ceramics, only alumina is sintered and has the desired pricing for ceramic armor. Unfortunately, alumina does not offer the dramatic ballistic improvement to justify its use. Based on an economic analysis of ceramics production, cost was shown to be extremely volume sensitive.³ Currently, there are few applications for non-oxide, structural ceramics which offer the appropriate economies of scale (>1 million pounds).

Scientists at Lawrence Livermore National Laboratory (LLNL) reported that AlN plastically deformed under high pressure testing.⁴ The pressures studied are similar to those which occur during a ballistic event and postulated that, despite its atypical ceramic armor properties, it might be a useful armor material. Meanwhile, interest in aluminum nitride has grown rapidly over the past ten years because of the need for a high thermal conductivity electroceramic.⁵ The development of fine, high purity powders has enabled the densification of AlN and resulted in tremendous excitement for a high thermal conductivity substrate and BeO replacement. Dow has identified AlN as a potentially large ceramic powder opportunity and has developed the capability for producing large quantities of high quality AlN powder. Based on the potential economies of scale from the electroceramics applications and the surprising results by Heard and Cline at LLNL, AlN, as a dual use material, could meet both the performance and the cost requirements for ceramic armor.

A proposal, " Development of Aluminum Nitride: A New Low-Cost Ceramic Armor", was written to DARPA (Defense Advanced Research Project Agency)

in response to RFP (Request For Proposal) BAA-88-02, under a special Congressional Balanced Technology Initiative (BTI) program. Several technology areas were included in the BTI and armor was just one aspect of the broad based program. A contract was awarded to determine if aluminum nitride ceramics could provide the necessary combination of high penetration resistance and low manufacturing costs. Contract No. DAAL03-88-C-0012 was funded at \$390,000 over a 18 month period which started August 1, 1988. While the proposal included a provision for 2 optional years at ~\$250,000/year, only one of those was subsequently funded.

The overall objective of the aluminum nitride contract was to develop low cost processing technology to fabricate large, high performance, aluminum nitride tiles. Building on Dow's successes in the electroceramics area, a spray-dry, dry-press, sintering process was chosen for this program.⁶ By determining the interrelationships between ballistic performance and the critical processing variables, a relative cost/performance formula could be established. The initial phase of the contract was divided into two tasks. The first task involved establishing baseline data and determining the critical processing variables through a series of screening studies. The second task determined the ballistic performance of selected compositions with light threats and then based on this data, a few formulations were scaled up to a 10 cm dia. by 5 cm thick tile for quarter scale long rod penetrator (LRP) testing.

The first task of the contract involved the selection of aluminum nitride powders and establishing baseline properties on hot-pressed samples of the chosen powders. Hot-pressed ceramics are typically purer, have higher densities and usually result in superior mechanical properties than sintered products. By comparing the sintered results with those of the hot-pressed materials, one can ascertain the effect of the sintering parameters on the mechanical and ballistic performance of aluminum nitride ceramics. The baseline data generated during this phase of the contract, including ballistic and dynamic compressive test results from Southwest Research Institute (SwRI), will be described in this report. The selection and characteristics of the aluminum nitride powders will also be discussed. The hot-press conditions employed to prepare these samples and the resulting chemical and physical characteristics will be detailed as well.

Parallel to the hot-press study, two statistically designed screening studies were undertaken to establish sintering formulations and processing conditions suitable for achieving high densities. Based on the results of these two sets of designed experiments, twenty compositions were selected for an extensive evaluation of their ballistic and mechanical properties. Light caliber ballistic screening tests included ballistic limit determinations with a .30 caliber AP simulant and depth of penetration measurements with .50 caliber APDS and SLAP rounds. These tests were conducted at the University of Dayton Research Institute (UDRI). The intent of this evaluation was to guide the selection of a few promising AlN formulations which were expected to meet the performance and cost goals of the contract. Sintered tiles (10 cm dia. x 4.5 cm high) were then manufactured from the chosen compositions and tested against the LRP.

The final phase of the contract examined the ballistic characteristics of AlN/SiC composites. This composite system was chosen because both components have the potential of being low-cost, since they are sinterable materials with dual use capabilities. Silicon carbide and aluminum nitride have also been shown to have excellent ballistic properties against a variety of threats. While preliminary ballistic data⁷ and sintering studies of AlN/SiC⁸ materials have been encouraging, up until now a detailed analysis of this system for ballistic applications had not been done. Similar to the initial phase of this contract, a combination of processing and ballistic screening studies was utilized. The ballistic screening test was however, limited to .50 caliber SLAP D.O.P. measurements. Two composites were evaluated against the program standard LRP. Both of these sets of tests were performed at UDRI.

2.0 TECHNICAL WORK

2.1 Hot-Pressed Aluminum Nitride

2.1.1 POWDER SELECTION AND CHARACTERIZATION

Since the focus of this program was to establish cost/performance information, powders with different qualities, and potentially different values, were desired to establish differences. Therefore, powders were selected, from commercially available sources, primarily to achieve a range of chemical and particle size characteristics. It was not the intent of this study to critically evaluate the various powder grades or their manufacturers. In addition, since this program started in 1988, the powders used may not reflect the quality or grades that are currently available. Based on economic and resource limitations, only five grades of powder were studied during this contract.

Since the premise of this proposal involved the utilization of a potentially low cost supply of powder produced by The Dow Chemical Company, a Dow powder[∂] was the first material chosen. At the same time that Dow's AlN powder capabilities were being developed, AlN sintering and processing technology was being developed using Tokuyama Soda powder.⁹ This powder is prepared, similar to Dow, via the carbothermal route and was the premier AlN product being marketed at that time. A second carbothermal powder was needed for this contract as a comparison to the Dow powder. However, since so much was already known from earlier work about the sintering and ballistic characteristics of the Tokuyama Soda powder, there would be little value in repeating much of that work. Therefore, instead, the higher purity and finer Sumitomo Chemical powder, grade ANH-10 was chosen.[#] The remaining 3 powders selected were various grades of powders produced by the direct nitridation of aluminum metal. Denka AP-10^{\$} was selected because of its high surface area and moderate purity. Toyo Aluminum's TOYALNITE, F grade[§] was coarser but had lower impurity levels. The lowest quality powder

[∂] Armor Grade, the Dow Chemical Company, Midland, MI.

[#] ANH-10, Sumitomo Chemical Co. LTD, Niihama, Japan

^{\$} AP-10, DENKI KAGAKU KOGYO K. K., Tokyo, Japan

[§] TOYALNITE F Grade, TOYO ALUMINUM K. K., Osaka, Japan

chosen was ART grade 200.[‡] This product had a broad particle size distribution and high levels of metallic impurities.

The initial hot-press experiments used 1 kg powder samples which were evaluated under a previous research program.¹⁰ When the contract started and after the selection process was completed, the AlN powders were ordered in quantities of at least 25 kg. Larger amounts of Denka and Dow were purchased, since they were chosen as model powders which were used in other Phase I, screening studies. The lot numbers and physical characteristics of the original AlN powders used during the experimental stage of the hot-press study are detailed in Table I. From the representative SEM photomicrographs of the powders, shown in Figure 1, and the other measured parameters, it can be seen that each powder is clearly different and that a broad range of powder characteristics have been represented.

Table I
Aluminum Nitride Powders Evaluated During Contract

POWDER	ART	Sumitomo	TOYO AL	DOW	DENKA
GRADE	A200	ANH-10	F	ARMOR	AP-10
LOT #	870511	H17Z21	8F.007	36-24/25	10PF8612
TYPE	Nitrided Al	Carbothermal	Nitrided Al	Carbothermal	Nitrided Al
SIZE [#] (μm)	3.21	0.9	1.32	1.46	1.8
SEM values					
High (μm)	12	0.6	6	1.2	3
Low (μm)	0.2	0.1	0.2	0.2	0.1
Mean (μm)	4.0	0.3	1.5	0.3	1.0
BET [§] (m ² /g)	1.8	4.9	3.4	2.5	4.1
O* (wt. %)	1.68	1.78	1.53	1.20	1.80
C* (wt. %)	0.06	0.19	0.13	0.12	0.20
Fe (ppm)	500	< 5	49	49	141
Si (ppm)	150	76	176	114	125
Ca (ppm)	15	60	13	570	6
Cr (ppm)	11	13	11	ND < 10	5

Metallic Impurities measured by X-ray Fluorescence (XRF).[£]

[‡] ALNEL 200, Advanced Refractory Technologies, Buffalo, NY

[#] CAPA-700, Horiba, Ltd, Kyoto, Japan

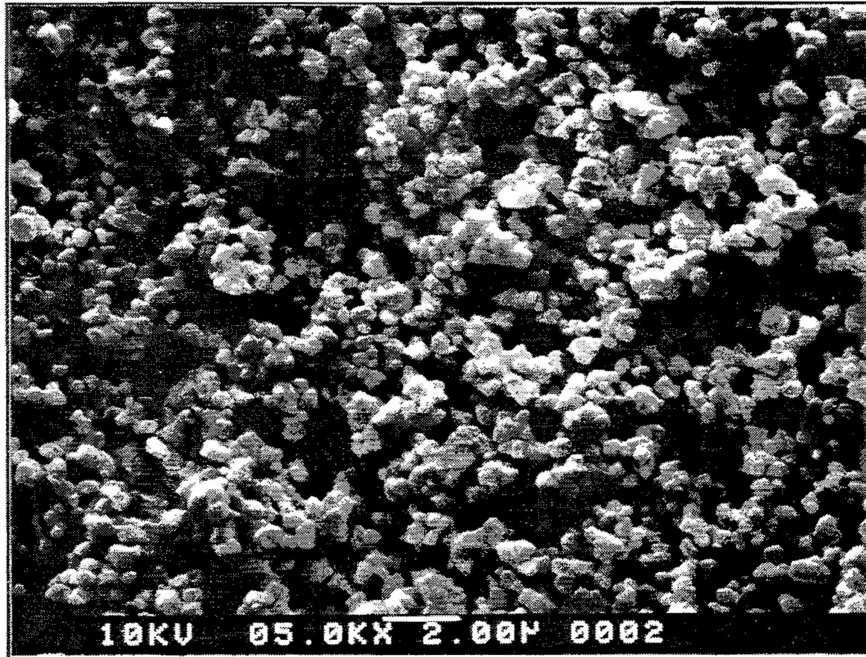
[§] Monosorb, Model MS-6, Quantachrome, Syosset, NY

^{*} TC-136 and IR 212, LECO Corp., St. Joseph, MI

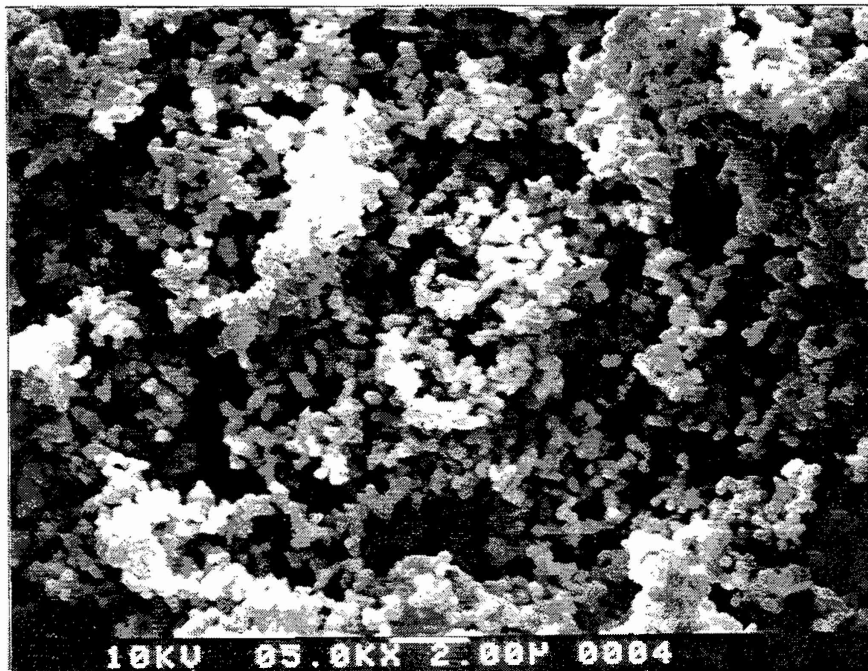
[£] Philips 1404, Mahwah, NJ

Fig. 1. SEM photomicrographs of the aluminum nitride powders used for this hot-press study and evaluation.

A. Carbothermal Aluminum Nitride Powders

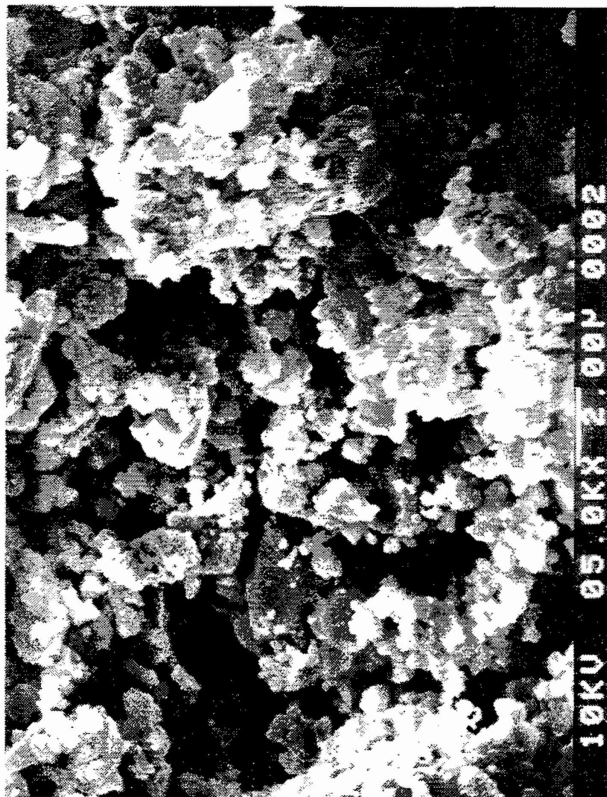


DOW (5000x)

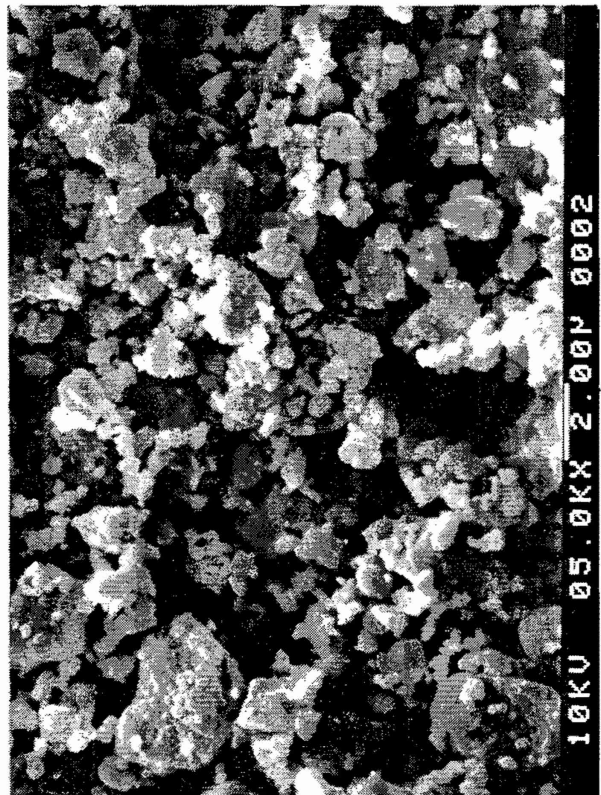


Sumitomo (5000x)

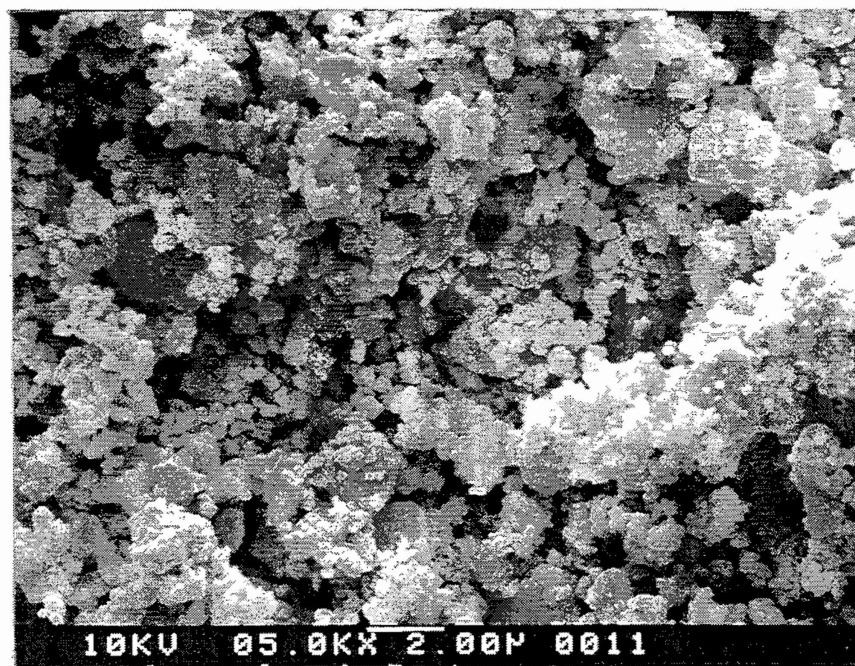
Fig. 1. B. Nitrided Aluminum AlN Powders



ART (5000x)



Toyo Al (5000x)



DENKA (5000x)

2.1.2 HOT-PRESS OPTIMIZATION

The first task of this hot-press program was to establish the optimum hot-press temperature for each powder being examined. From previous studies, it was determined that AlN could be densified in the temperature range of 1800 - 1900°C and 24 MPa (3500 psi) of pressure. Since densification is a function of average particle size and surface area, one would expect variations in the densification behavior of these five AlN powders. Also, in order to evaluate the impact of powder chemistry and particle size distribution on the mechanical and ballistic performance, average grain size of each sample should be roughly equivalent. Therefore, each powder was studied at 100°C intervals between 1700°C and 2000°C. The maximum pressure was kept constant at 34.5 MPa (5000 psi).

2.2 cm (7/8") diameter split cylinder graphite dies were used for most of the preliminary hot-press runs. The Dow samples were fabricated last and because of wear to the smaller dies, a 3.8 cm (1.5") diameter die was used. The split dies had a 7.6 cm (3") outer diameter and were supported by a 7.6 cm (3") x 15.2 cm (6") x 9.5 cm (3.75") solid graphite hoop. 12.5 g of AlN powder was loaded into the die which was lined with GRAFOIL®§. Two different powders were pressed at the same time and were separated from each other using two 0.025 cm (10 mil) GRAFOIL® sheets. The expected thickness for the hot-pressed parts was 1 cm. In order to obtain a sample of approximately equal thickness, 47 g of the Dow powder was used with the larger die.

The typical heating cycle employed was 33°C/min up to 1200°C, then 25°C/min to 1700°C, followed by 10°C/min to 1850°C and ending with the modest heating rate of 5°C/min up to the desired maximum temperature of 1900°C or 2000°C. When the desired temperature was 1700°C, then the heating rate reduction occurred at 1600°C. This heating schedule minimizes overshoot of the desired temperature, as well as maintaining a more uniform sample temperature. A 30 minute hold at the maximum temperature was consistent for all of the samples. An initial load equivalent to ~3.7 MPa (500 psi) was applied to the die stack during heat-up. The uniaxial load was increased over a five minute

§ GRAFOIL®, Union Carbide, Cleveland, OH

period to the maximum pressure at 1500°C. A representative heating and pressure schedule for a 1900°C hot-press run is shown in figure 2.

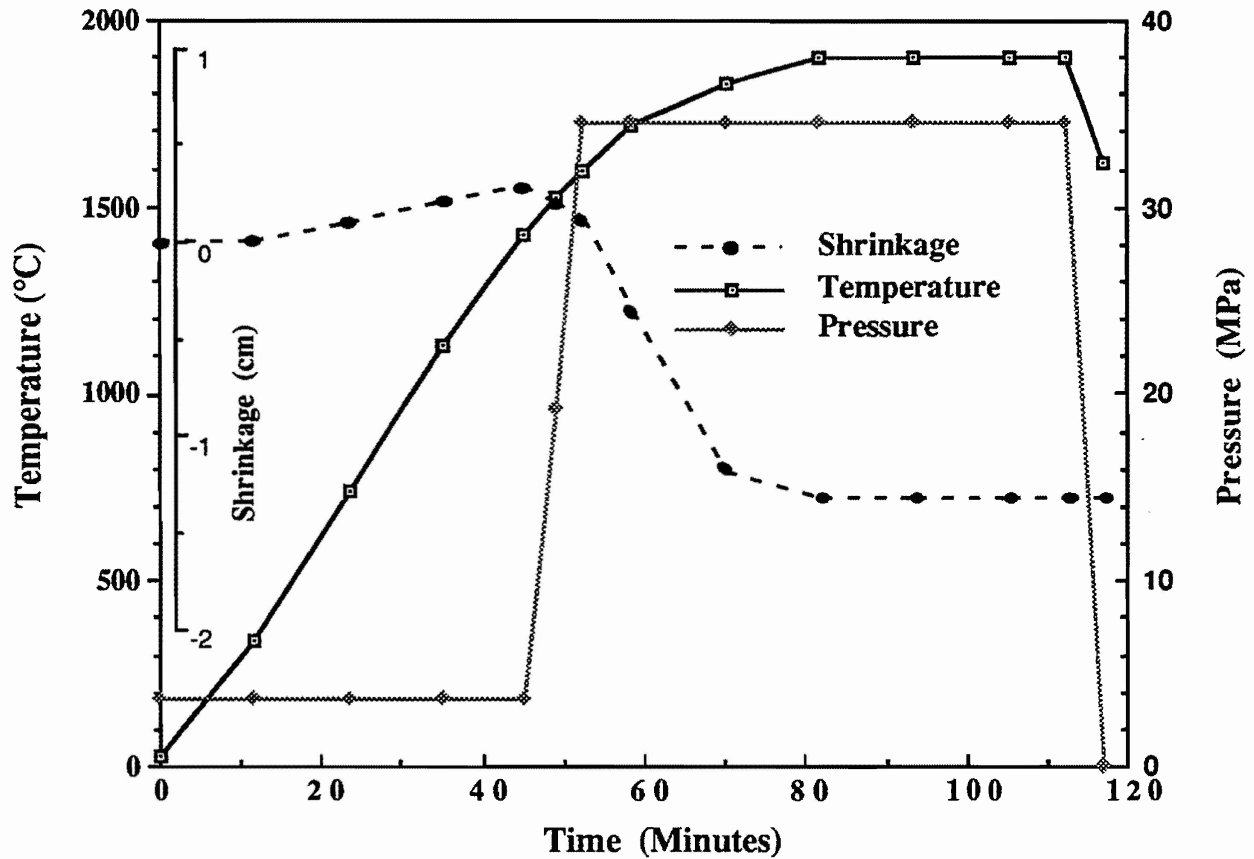


Fig. 2. Actual 1900°C hot-press run for Sumitomo and Denka AlN powders, showing heating and pressure schedules and observed shrinkage behavior for 12.5 gram pellets in a 2.2 cm die.

The pressure assisted densification of aluminum nitride was observed to be related to the ultimate particle size and distribution, and purity of the five powders. In figure 3, percent theoretical density is shown as a function of the hot-pressing temperature for each powder.

Hot-pressing was extremely effective in densifying all of the five aluminum nitride powders. However, the minimum temperature required to obtain complete densification increased with increasing particle size. The two carbothermal powders were essentially dense at 1700°C, while the broad distribution of the nitrated aluminum powders and the higher average particle size required the use of higher hot-pressing temperatures to achieve equivalent

densities. Despite being coarser than the Sumitomo powder, the Dow powder was slightly more active. The Dow powder achieved ~99% T.D. as low as 1600°C. The higher impurity content of the Dow powder, 570 ppm Ca, is most likely responsible for this improved densification behavior. The ART powder which had the highest average particle size, was not able to achieve full density at 2000°C.

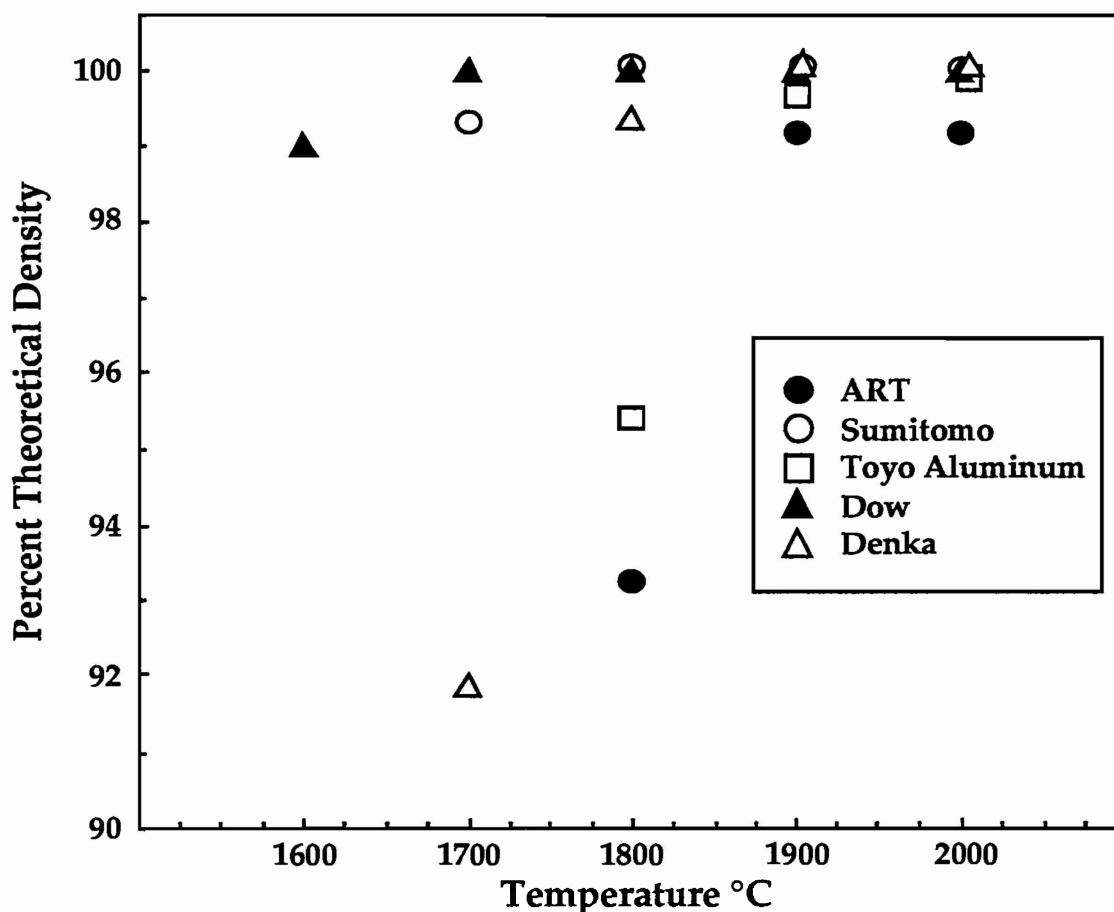


Fig. 3. Hot-pressed densities for the five aluminum nitride powders as a function of temperature.

While density is critical to the mechanical and ballistic performance of aluminum nitride ceramics, grain size may also play a role. Therefore, the effect of hot-pressing temperature on the average grain size of the five powders was examined. Average grain size was estimated using a modification of ASTM standard, E112-84, and straight line intercept methods with a computer interfaced digitizing pad. To meet the requirements of the ASTM standard, a magnification of 2000 times and typically 2 or 3 fields were necessary. For the

line intercept method, a minimum of 50 and more typically, 100 grains were measured. The results of this study are shown in figure 4. As expected, grain size increased with increasing temperature, but the growth was not exaggerated even at 2000°C.

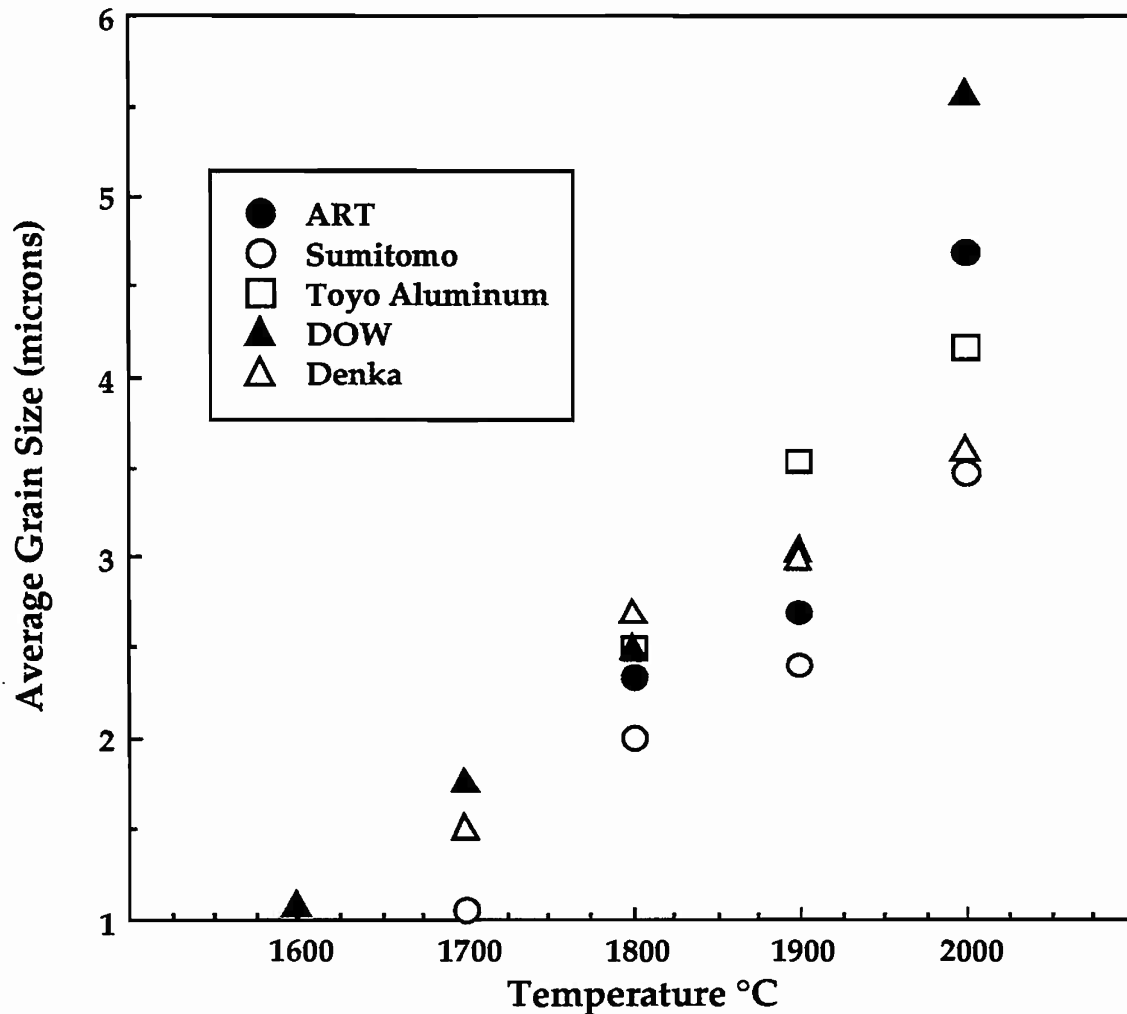


Fig. 4. Average grain size for the five hot-pressed aluminum nitride powders as a function of temperature.

A major objective of this baseline study was to determine if there were any performance differences observed which resulted from the unique characteristics of these five powders. With this goal in mind, it was important to minimize the potential for other effects, such as grain size and density, to dominate and hence control the mechanical and ballistic properties.

Based on this assumption and using the results of the hot-pressing study, the conditions for scale-up, described in Table II, were chosen to optimize density while maintaining roughly an equivalent average grain size for each powder. Except for the carbothermal materials, the temperature selected was dictated by the highest achievable density. The densification window was significantly large for Dow and Sumitomo AlN, that the ultimate grain size became the determining factor in selecting the specific hot-pressing conditions. The targeted density and grain size values were ~100% of theoretical density and 2 to 4 microns respectively.

Table II
Optimized Hot-Pressing Conditions for Ballistic Targets

POWDER	ART	Sumitomo	TOYO AL	DOW	DENKA
Temp. °C	1950	1850	1950	1800	1900
Time (min)	60	40	60	30	60

Powders used for this phase were taken from the 25 kg lots which were ordered at the start of the contract. As shown in Table III, the properties of these materials were very similar to the original AlN powders described earlier in Table I. Seven tiles were hot-pressed of each powder. Ballistic tests at SwRI required 10.2 cm (4") diameter tiles and at least two areal densities. Therefore, 4.6 cm (1.8") and 3.1 cm (1.2") thick tiles (three of each size), corresponding to areal densities of 15 and 10 g/cm², were pressed from each AlN powder. In addition, a 7.6 cm (3") square tile by 1.5 cm (0.6") thick, which was used for determining mechanical properties, was also hot-pressed from each material. In all cases, new carbon-carbon composite hoops were used to support the graphite dies. The 19 cm (7.5") O.D. x 11.4 cm (4.5") I.D. x 15.2 cm (6") high, graphite fiber reinforced cylinders provided the needed strength and dimensions to produce the large tiles for this program. The heating schedules were similar to the earlier runs, but the applied pressure was lower at 24.1 MPa (3500 psi).

Table III
Characteristics of AlN Powder Used in Preparing Ballistic Targets

POWDER	ART	Sumitomo	TOYO AL	DOW	DENKA
GRADE	A200	ANH-10	F	ARMOR	AP-10
LOT #	28467	H18102	8F.020	890629-48	10PF8612
TYPE	N	C	N	C	N
SIZE (μm)	3.15	0.9	2.36	1.68	1.8
SEM values					
High (μm)	12	0.6	6	1	3
Low (μm)	0.2	0.1	0.2	0.2	0.1
Mean (μm)	4.0	0.3	1.5	0.4	1.0
BET (m^2/g)	2.2	4.9	2.6	2.97	4.1
O (wt. %)	1.35	1.19	1.69	1.15	1.80
C (wt. %)	0.09	0.19	0.09	0.13	0.20
Fe (ppm)	662	<5	46	26	141
Si (ppm)	251	23	236	176	125
Ca (ppm)	10	35	14	444	6
Cr (ppm)	9	<5	<5	16	5

2.1.3 PHYSICAL AND MECHANICAL PROPERTIES

Specimens for measuring the physical and mechanical characteristics of the five AlN hot-pressed materials were prepared from 7.6 cm x 7.6 cm x 1.5 cm billets. These tiles were hot-pressed using the same conditions, Table II, as employed for producing the larger ballistic specimens. It was assumed then that the properties of these billets would be representative of the ballistic samples.

Photomicrographs of the hot-pressed powders are shown in figure 7 and reveal that the two carbothermal materials have noticeably finer microstructures than the nitrided materials. ART and Toyo Aluminum had comparable microstructures and were somewhat coarser than the DENKA product. While some differences in grain size are apparent, all five powders were manufactured to a very high density. The five materials had densities,

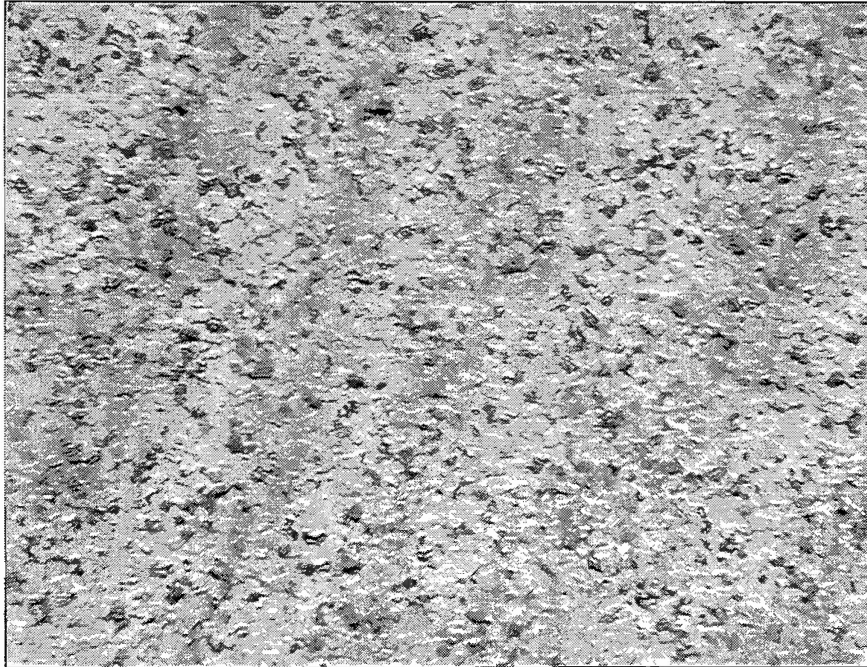
measured by immersion using archimedes principle, which were greater than 99% of theoretical. Based on these observations, the hot-press temperatures for the carbothermal powders needed to be increased in order to obtain more similar microstructures for all of the aluminum nitrides, while still maintaining the desired high density. Since the grain size differences appear to be less than a factor of 2 or 3, any performance advantage a particular powder would have should not be grain size related. This is particularly true since none of the materials have microstructures which are close to the critical grain size where the mechanical and ballistic performance degrades rapidly.¹¹

Oxygen and carbon levels for the hot-pressed pieces were measured with LECO^Y carbon determinator IR212 and TC136 oxygen/nitrogen determinator after crushing in a diamond embedded steel mortar to -100 mesh. These values were consistent with the powder values. Oxygen content slightly decreased during hot-pressing, while the carbon levels were unchanged or showed a modest increase. This result is expected from the heavily reducing carbon environment present when using graphite dies and a graphite furnace. Interestingly, the hot-pressed products were all different shades of gray. The Dow samples were the darkest materials, while the ART billets were the lightest. The Sumitomo powder resulted in a product which was a mixture of light and dark regions. None of these observations appear to be associated with the bulk chemistry of the powders or parts and an in depth analysis of this phenomenon was not pursued.

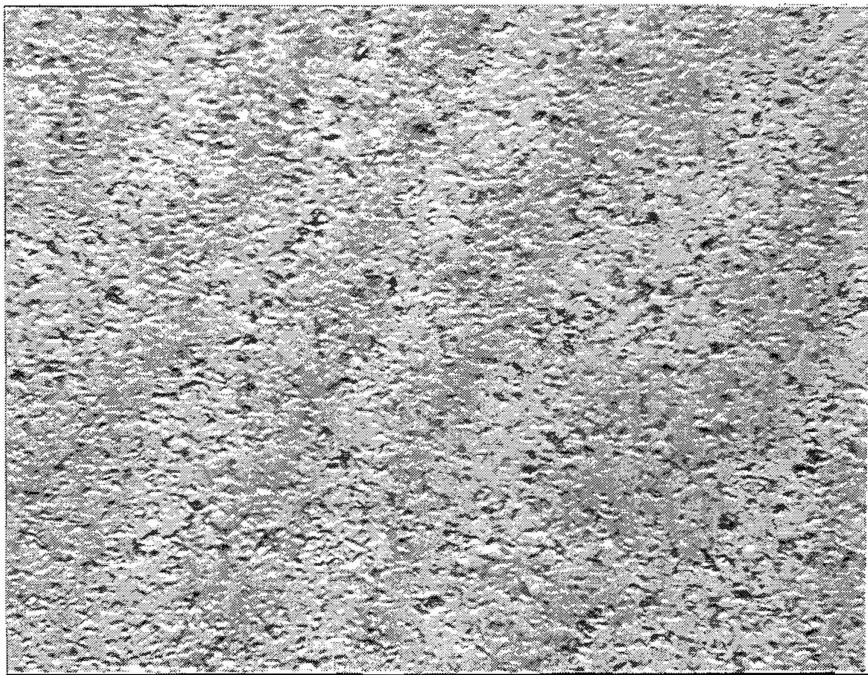
^Y LECO Corporation, St. Joseph, MI

Fig. 5. Photomicrographs of the hot-pressed aluminum nitride billets used for mechanical evaluation and representative of the ballistic specimens.

A. Carbothermal Aluminum Nitride

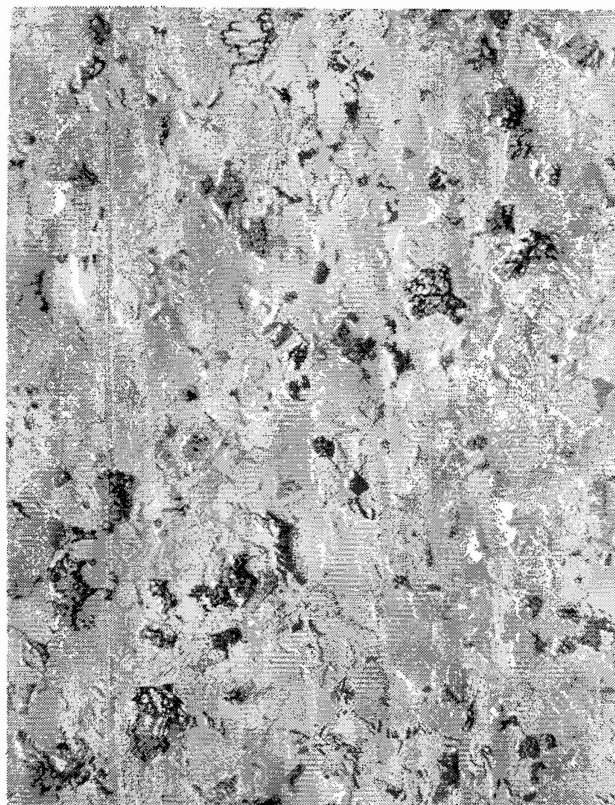


DOW (1000x)

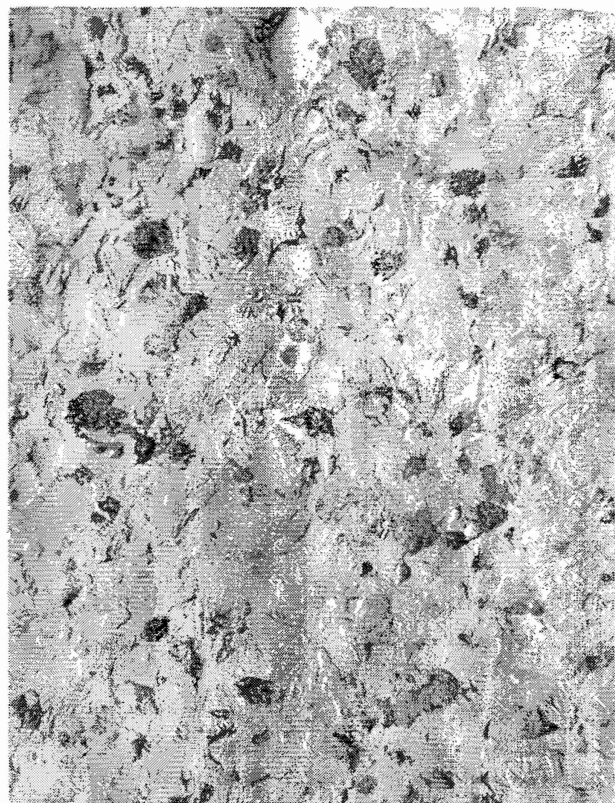


Sumitomo (1000x)

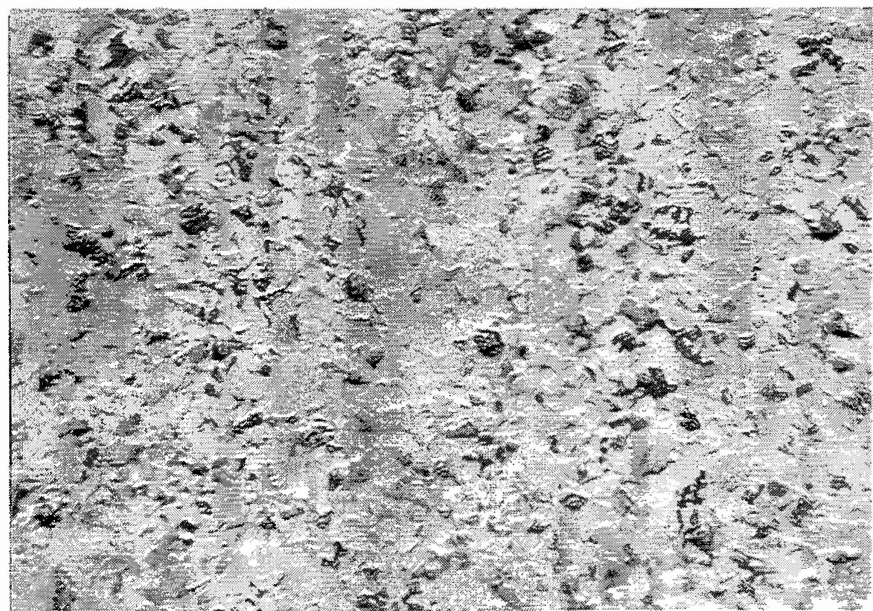
Fig. 5. B. Nitrided Aluminum Materials



ART (1000x)



Toyo Al (1000x)



DENKA (1000x)

The measured values for the two physical parameters, density and grain size, and the respective carbon and oxygen contents are detailed in Table IV.

Table IV
Physical Parameters of Hot-Pressed Aluminum Nitride Billets

POWDER	ART	Sumitomo	TOYO AL	DOW	DENKA
GRADE	A200	ANH-10	F	ARMOR	AP-10
LOT #	28467	H18102	8F.020	890629-48	10PF8612
Density (g/cm ³)	3.227	3.250	3.237	3.238	3.241
% T.D.	99.0	99.7	99.3	99.3	99.4
Grain Size(μm)	4.1±1.9	2.0±0.8	3.7±1.3	2.3±1.0	3.0±1.2
Oxygen (wt. %)	1.2	1.5	1.3	1.0	1.0
Carbon (wt. %)	0.042	0.024	0.029	0.067	0.104

Specimens for the various mechanical tests were machined out of the five hot-pressed square tiles. The 4-pt. bend tests utilized MIL-STD-1942B, except for the non-reticulated supports. At least twelve of the 3 mm x 4 mm x 45 mm bars were tested for each material. The crosshead speed was 0.054 cm/min. Average flexural strength and Weibull modulus was determined for all five powders. The sonic properties of two bend bars from each powder set, were measured using the pulse-echo method.¹² Microhardness was measured with a Vickers diamond indenter and a load of 9.8 N (1000 grams) using a Tukon Model 300 hardness tester. Averages of at least ten randomly positioned indentations were measured.

Two types of compression data were generated during this study. The method for measuring the static compressive strength of ceramics which was developed at MTL (US Army Materials Technology Laboratory)¹³ was utilized for analyzing these hot-pressed materials. Two dumbbell shaped specimens, with an overall length of 3 cm (1.2"), a diameter of 1 cm (0.4") and a reduced section of 0.5 cm (0.2"), were tested for each powder.

An examination of the mechanical characteristics of the hot-pressed aluminum nitride parts revealed some interesting observations. The average values measured for the aluminum nitride powders studied during this phase of the contract are detailed in Table V. The number of specimens used to determine the average strength values and corresponding Weibull modulus

are listed next to the recorded values. The sonic properties, modulus, poisson's ratio and sound speeds, were nearly identical for all of the five AlN powders.

Table V
Mechanical Properties of Hot-Pressed AlN

POWDER	ART	Sumitomo	TOYO AL	DOW	DENKA
Hardness (GPa)	11.0 ± 0.4	11.6 ± 0.4	11.0 ± 0.4	11.2 ± 0.6	10.8 ± 0.3
Flexure (MPa)	320 ± 46	310 ± 41	377 ± 25	326 ± 44	351 ± 35
Weibull	7.1 (15)	7.1 (11)	15.1 (12)	7.0 (11)	9.2 (9)
Compressive (GPa)	4.1 (3)	3.9 (1)	4.5 (4)	3.8 (1)	3.9 (2)
Modulus (GPa)	314	322	318	321	320
Poisson's Ratio	.240	.236	.239	.237	.239
Long.(km/sec)	10.72	10.76	10.74	10.75	10.79
Shear (km/sec)	6.27	6.33	6.29	6.32	6.32

* Values in parentheses represent the number of samples used to determine that parameter.

The nitrided materials as a group were stronger, both in compression and flexure, than the carbothermal materials. Toyo Aluminum's powder produced the material with the highest compressive and flexure strength. The measured difference between the high and low strength materials was nearly 20%. While there were insufficient flexure data points for generating good statistics (a minimum of 30 bars is usually required), the Weibull plots did produce numbers with high correlation coefficients for all of the samples. From the standard deviations, these differences are significant and reflect the intrinsic properties of the five studied powders. Potential anomalies as a result of orientation effects should be minimal since these aluminum nitrides are largely isotropic and all specimens were cut from the hot-pressed billets in a similar manner. Several of the flexure samples did fail at stress levels significantly less than the mean. However, based on the examination of the fracture surfaces and critical flaw sites, these samples were excluded when determining the average strengths and Weibull moduli. They were not representative of the material.

Due to problems associated with machining the small dumbbell shaped specimens, there were only a limited number of samples available for compression testing. However, the differences observed were again significant. All of the data for the two highest compressive strength materials, ART and Toyo Aluminum, were greater than the carbothermal products. The carbothermal powders were found however, to produce harder ceramics than the nitrated products, but this difference was substantially smaller ($\leq 7\%$).

Dynamic compressive strength measurements used small right cylinders, 0.63 cm (0.25") dia. x 1.27 cm (0.5") high, were prepared by first coring out blanks from the hot-pressed billets with a diamond drill and then machining to the needed tolerances and finish. At least five specimens from each AlN powder were sent to J. Lankford, SwRI, for both static and dynamic compression testing. The static tests were performed with a standard Instron testing frame, while a Hopkinson pressure bar¹⁴, figure 6, was utilized for the high ($10^3/\text{sec}$) and moderate strain rate compression testing.

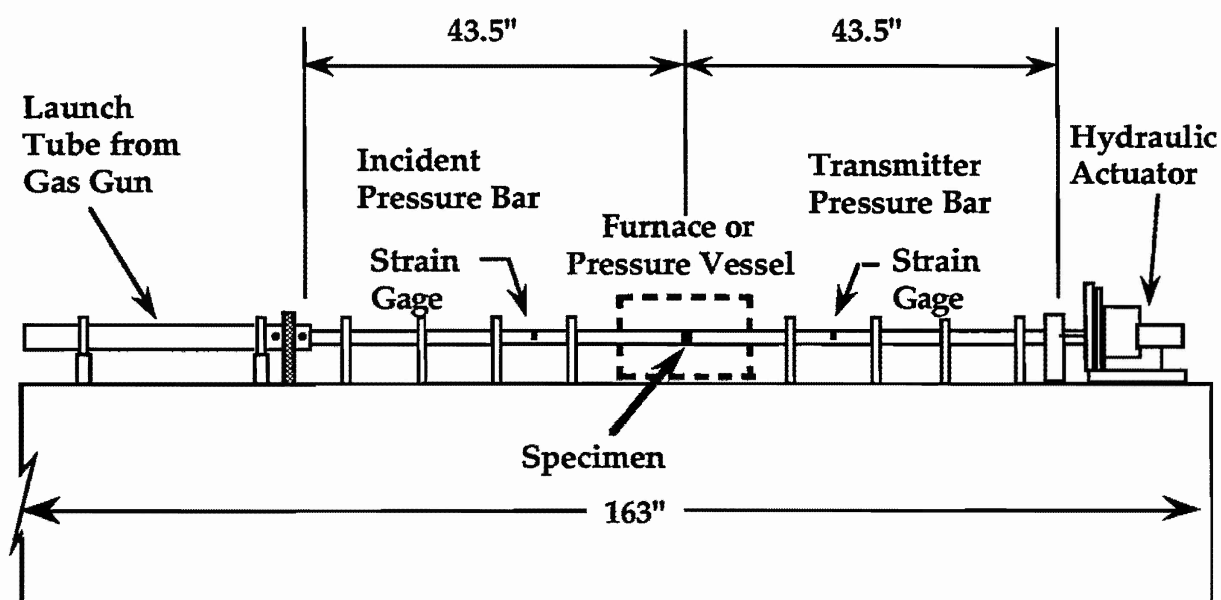


Fig. 6. Split Hopkinson Pressure Bar (SHPB) used at Southwest Research Institute to measure high strain rate compressive strength of AlN ceramics. This equipment also allows testing at elevated temperatures or pressures.

The pressure bar data and results from the quasi-static tests are plotted as a function of strain rate in figure 7. Except for the ART material, only one data

point was measured under each condition. The quasi-static data are consistent with the compression data obtained at Dow with the nitrided powders having higher strengths than the carbothermal products. However, the actual values were about 25% lower than the internally generated data.

While strength increased with increasing strain rate in all cases, the strength advantage which the nitrided materials had under quasi-static conditions, decreased dramatically at the highest strain rate. For monolithic ceramics, it has been found that at strain rates $> 10^2/\text{sec}$, the stress/strain rate dependence increases dramatically and follows a power law with an exponent of $1/3$.¹⁶ At the lower strain rate levels ($< 10^2/\text{sec}$), the compressive strength of ceramics is only modestly affected by strain rate.

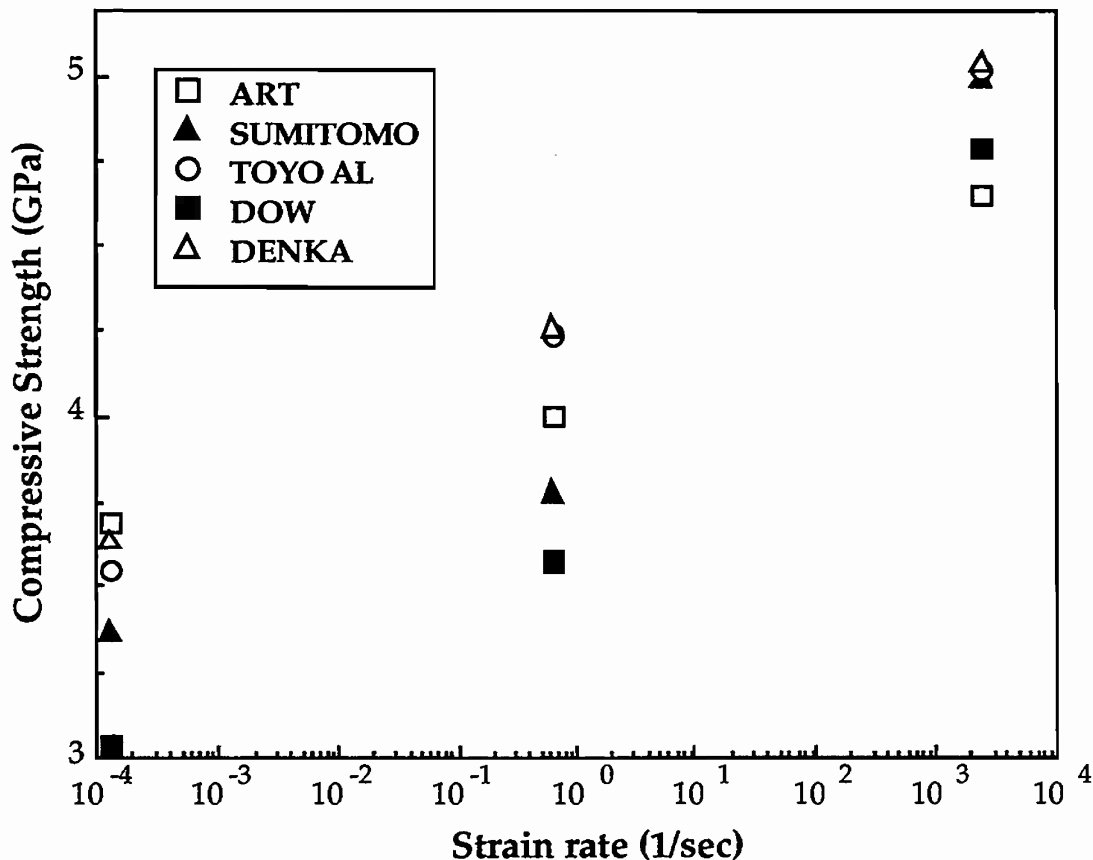


Fig. 7. Compressive Strength of the five hot-pressed aluminum nitride powders as a function of strain rate. Data generated by J. Lankford at SwRI.

During this study, each data point represents a single experiment, so there was insufficient information available particularly in the 10^2 - $10^4/\text{sec}$ strain

rate range to verify whether AlN followed this trend. However, three of the samples do show a significant deviation from linearity at the highest strain rate, suggesting a change in the material's response. In addition, for the highest strain rate data set, the five powders followed a trend of increasing strength with strain rate. This could be a reflection of the power law effect and indicate the sensitivity of strain rate on the measured compressive strength. These observations could also suggest that any differences in material characteristics are less significant when compared to the strain rate effect for these hot-pressed aluminum nitride products.

2.1.4 BALLISTIC STUDIES

Twenty machined AlN tiles were prepared for ballistic testing. The samples were coded according to size and powder type. The codes and dimensions of the tiles are described in Table VI. These dimensions represent the largest value measured for a given tile. The areal densities were all within 2% of each other and the desired 10 and 15 g/cm².

Ballistic testing was performed at Southwest Research Institute(SwRI) by B. Morris under the direction of C. Anderson. Residual penetration into 4340 steel, which was hardened to R_c 27, was the figure of merit used during these tests. 4340 bar stock (203 mm diameter) was machined out to accommodate the ceramic tiles. The dimensions of the cut-out were 0.25 mm larger than the ceramics. Epoxy was used to fix the tile in the holder and take up any remaining air space. The tile was aligned flush with the steel stock, which was 180 mm or 230 mm long. The majority of the tests used a 30 mm smooth bore gun. The barrel length was either 3.66 or 1.83 m. The projectiles were tungsten alloy long rods with length to diameter (L/D) ratios of 10 and 15. The projectiles had a hemispherical nose with diameters of 8.18 and 7.16 mm, and an average mass of 73.2 and 74.0 grams, respectively.

Using methodology developed by the US Army Materials Technology Laboratory (MTL),^{7,15} baseline data for penetration into steel was generated for each type of projectile as a function of yaw and velocity. Normalized expressions were generated for each type of projectile by dividing the penetration by the projectile length. These expressions were used to compute

Table VI
Ceramic Targets for LRP D.O.P. Testing

CODE	Powder	Thickness (cm)	Diameter (cm)	Mass (grams)	Density (g/cm ³)	Areal (g/cm ²)
A1801	ART	4.62	10.04	1166.8	3.240	14.97
A1802	ART	4.62	10.04	1165.3	3.243	14.98
B1803	Sumitomo	4.61	10.06	1175.6	3.214	14.80
B1804	Sumitomo	4.57	10.05	1165.5	3.267	14.93
C1805	Toyo Al	4.62	10.03	1165.1	3.243	14.98
C1806	Toyo Al	4.61	10.06	1172.3	3.253	15.00
E1807	DENKA	4.63	10.08	1183.7	3.253	15.07
E1808	DENKA	4.63	10.06	1178.9	3.257	15.09
D1809	DOW	4.63	10.06	1181.6	3.264	15.12
D1810	DOW	4.63	10.05	1178.8	3.263	15.12
A1211	ART	3.08	10.01	762.3	3.212	9.90
A1212	ART	3.07	10.01	761.6	3.220	9.88
B1213	Sumitomo	3.07	9.98	763.2	3.238	9.95
B1214	Sumitomo	3.08	10.01	767.3	3.237	9.96
C1215	Toyo Al	3.07	10.02	767.9	3.240	9.94
C1216	Toyo Al	3.06	10.01	760.7	3.232	9.88
E1217	DENKA	3.07	10.03	768.6	3.231	9.93
E1218	DENKA	3.07	10.03	769.2	3.235	9.93
D1219	DOW	3.02	9.98	749.8	3.263	9.85
D1220	DOW	3.02	9.95	745.9	3.264	9.87

the ceramic performance improvement compared to the baseline steel. In addition, data were generated for Coors AD90 alumina at 1500 m/sec. This material had been studied previously by MTL and was used as a second confirmation of the validity of the test as well as a comparison for the experimental ceramics. Flash x-rays were used to measure the velocity and total yaw. The depth of penetration was measured on the x-rays of cut target slabs from the top of the crater lip. The height of the crater was then subtracted from this measurement to determine the penetration depth. The preferred method is to measure the back of the steel slab to the point of maximum penetration. However, because of the variability in the thickness of the steel target holders this was not possible. The depth of penetration test is schematically represented in figure 8.

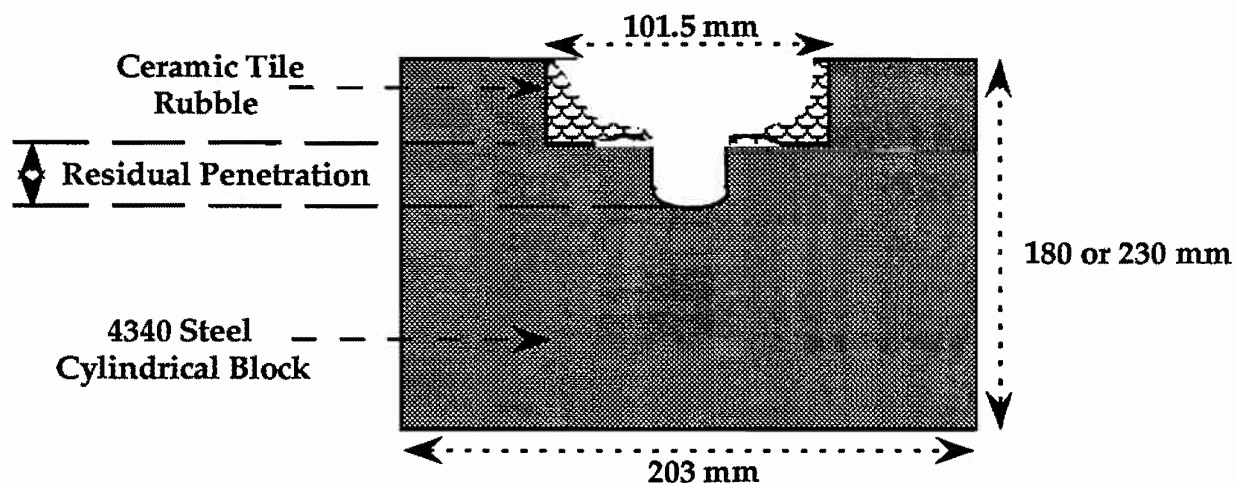


Fig. 8. Schematic of ballistic test performed at SwRI showing the residual penetration measurement.

Proper interpretation of the aluminum nitride ballistic data generated at SwRI, requires first an examination of the steel and alumina baseline data. Penetration of the tungsten projectiles into 4340 steel is shown in figure 9. The higher L/D threat is substantially more lethal, resulting in higher penetration. Projectile yaw had significant shot to shot variability and it needs to be taken into consideration when evaluating these ballistic results. Ideally, the total yaw should be as small as possible, but most ballistic labs consider values less than 2° to be acceptable. During their analysis of the data (see section C of Appendix), SwRI included all of the values shown in figure 9. However, since the data were used to determine the baseline for subsequent tests, it was not appropriate to include the $L/D = 10$ results which had a higher than acceptable yaw. In Figure 10, the penetration results are replotted without the high yaw values as a function of projectile velocity. This modification led to an improved correlation coefficient and more accurately reflected the baseline penetration into the steel. Using the SwRI fit would lead to a comparative value which would be 3.5% under the actual ceramic performance.

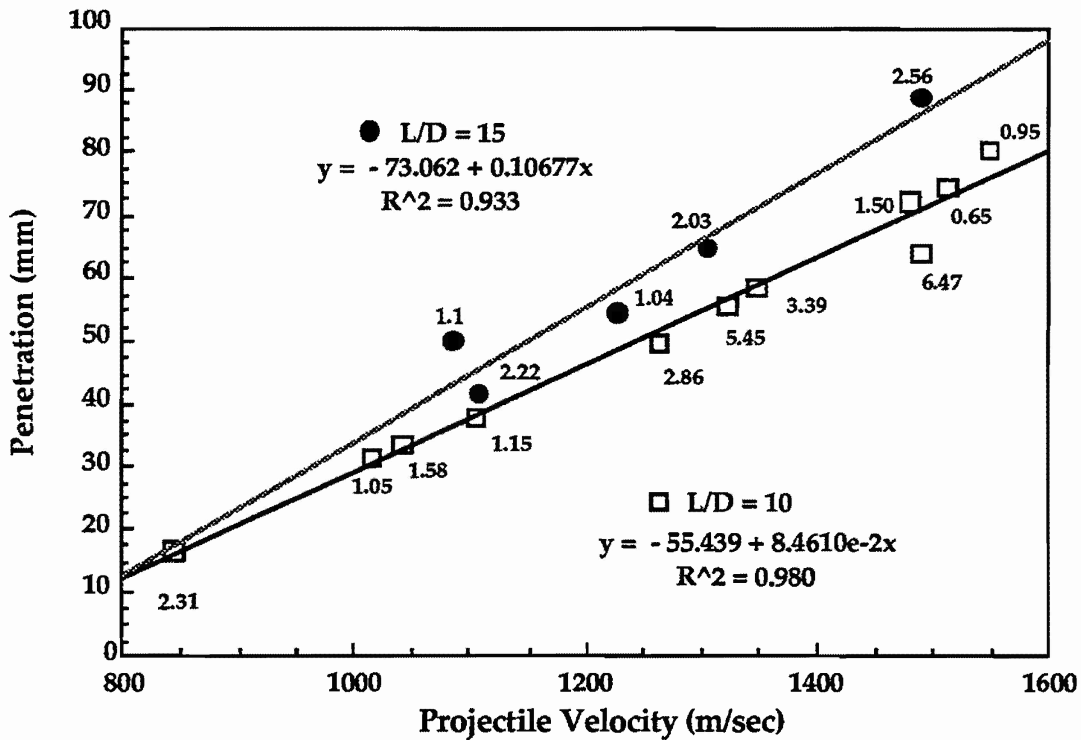


Fig. 9. Penetration data for two tungsten alloy projectiles into 4340 steel, hardened to $R_c 27$, as a function of projectile velocity. The total yaw of the projectile for each shot is also shown.

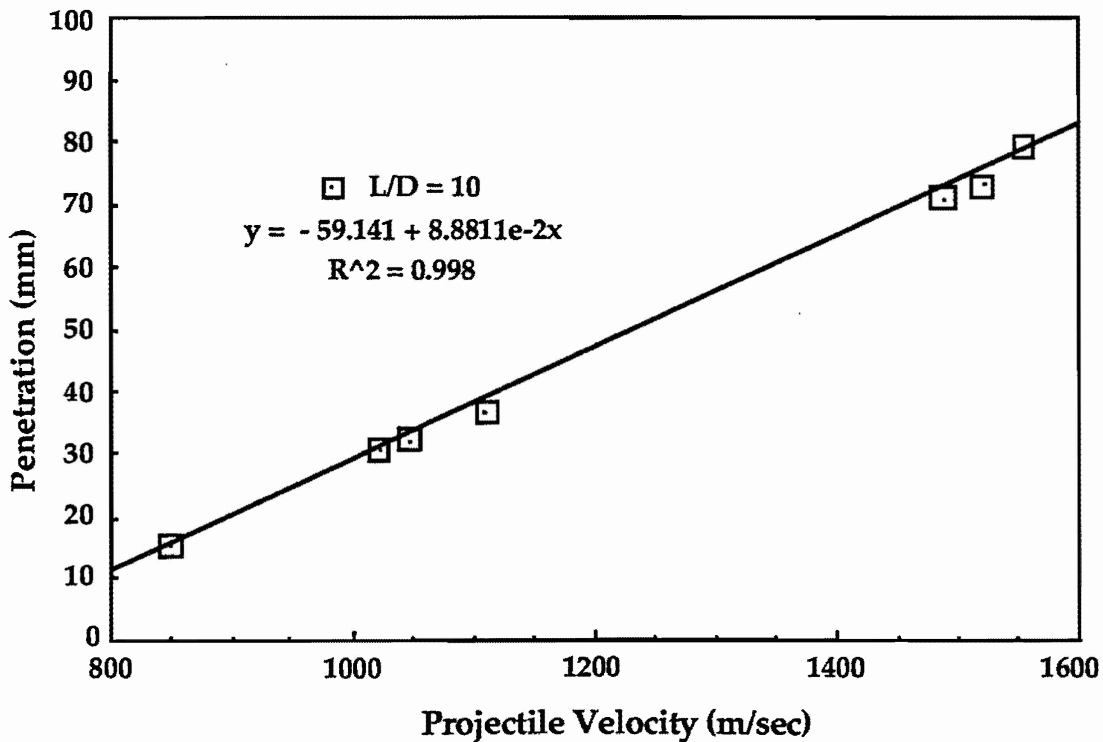


Fig. 10. Penetration data for tungsten alloy $L/D = 10$ projectile into 4340 steel, as a function of projectile velocity, without the high yaw (>2.5) data points.

The major objective of the SwRI program was to compare and evaluate the ballistic performance of the ceramic materials being developed under BTI funding. The methodology selected for the ballistic testing was carefully scrutinized. Therefore, it was important from SwRI's prospective, that data be generated on an accepted ceramic with an existing data base.¹⁵ Coors alumina, AD90, was chosen for this purpose. AD90 was evaluated against both projectiles at two different areal densities (two shots at each condition). Hence, a total of eight alumina targets were studied.

Since the standard analysis used for depth of penetration ballistic data requires several areal densities to be tested for each threat and this was beyond the scope of the BTI armor contracts. SwRI developed a specific criteria, scaled penetration reduction (SPR), for comparing the performance of the various ceramics. The advantage of utilizing this parameter is that it provides a means of evaluating materials with different areal densities with a limited number of shots. In addition, the velocities do not need to be identical. This would be especially important to a facility with a less than consistent ballistic range. The physical significance of this measurement, however, is unknown and a comparison to the more typically reported, mass efficiency would be difficult. SPR is calculated by first determining what the penetration capability for the same velocity of that shot would be into steel alone; then, the actual depth of penetration into the steel is measured and the difference recorded. That difference, which is the penetration reduction as a result of the ceramic, is then divided by the areal density of the ceramic to obtain the final result. The units for this parameter are mm/g/cm². The alumina and aluminum nitride ballistic results for both tungsten projectiles, L/D = 10 and L/D = 15, are given in Tables VII and VIII, respectively. Except for one ART tile (A1801), the thin AlN tiles (areal density of 10) were tested against the L/D = 10 threat, while the thicker samples were (areal density of 15) shot with the L/D = 15 projectile.

Table VII
D.O.P. Ballistic Results for LRP, L/D = 10

ID #	CERAMIC	A.D.	VEL.	YAW	D.O.P.	CAP.	RED.	SPR
9	AD90	9.93	1484	5.81	43.2	72.2	29.0	2.92
10	AD90	9.91	1513	3.15	48.1	74.7	26.6	2.69
2	AD90	14.96	1498	0.43	38.6	73.4	34.8	2.33
6	AD90	14.91	1500	0.44	36.1	73.6	37.5	2.51
A1211	ART	9.90	1502	1.07	39.4	73.8	34.4	3.47
A1212	ART	9.88	1504	0.66	42.6	73.9	31.3	3.17
A1801	ART	14.98	1499	5.56	12.0	73.5	61.5	4.11
B1213	Sumitomo	9.85	1499	0.43	36.1	73.5	37.4	3.80
B1214	Sumitomo	9.96	1506	2.34	41.1	74.1	33.0	3.31
C1215	Toyo Al	9.94	1491	0.43	39.1	72.8	33.7	3.39
C1216	Toyo Al	9.88	1499	1.52	39.3	73.5	34.2	3.46
E1217	DENKA	9.93	1506	1.20	37.9	74.1	36.2	3.65
E1218	DENKA	9.93	1482	2.26	29.1	72.0	42.9	4.32
D1219	DOW	9.85	1457	1.52	36.7	68.4	31.7	3.22
D1220	DOW	9.87	1505	1.35	41.8	74.0	32.2	3.26

D.O.P. is depth of penetration (mm) into the steel, CAP. is the penetration capability (mm) of this threat into steel alone at the shot velocity, RED. is the penetration reduction (mm) as a result of the ceramic being present, and SPR is the scaled penetration reduction parameter.

Table VIII
D.O.P. Ballistic Results for LRP, L/D = 15

ID #	CERAMIC	A.D.	VEL.	YAW	D.O.P.	CAP.	RED.	SPR
11	AD90	9.90	1508	2.57	58.8	88.1	29.3	2.96
14	AD90	9.90	1500	3.38	59.1	87.2	28.1	2.84
3	AD90	14.94	1493	3.89	50.1	86.4	36.3	2.43
4	AD90	14.91	1513	3.27	53.2	88.5	35.3	2.37
A1802	ART	14.97	1512	5.67	29.7	88.4	58.7	3.92
B1803	Sumitomo	14.80	1504	4.11	35.5	87.5	52.0	3.51
B1804	Sumitomo	14.93	1499	1.60	42.4	87.0	44.6	2.99
C1805	Toyo Al	14.98	1503§	-	43.3	87.4	44.1	2.94
C1806	Toyo Al	15.00	1510	2.33	41.9	88.2	46.3	3.09
E1807	DENKA	15.07	1482	3.67	33.7	85.2	51.5	3.42
E1808	DENKA	15.09	1511	5.47	31.0	88.3	57.3	3.80
D1809	DOW	15.12	1503§	3.21	41.3	87.4	46.1	3.05

§ Velocity was estimated from powder charge and average velocities.

D.O.P. is depth of penetration (mm) into the steel, CAP. is the penetration capability (mm) of this threat into steel alone at the shot velocity, RED. is the penetration reduction (mm) as a result of the ceramic being present, and SPR is the scaled penetration reduction parameter.

For the $L/D = 10$ tests, the yaw was appropriately low for most of the shots. Also, the average shot to shot variability was less than 10%. The advantage aluminum nitride offers over alumina was relatively clear overall. The distinction between the single, thick AlN tile and the two alumina tests at a comparable areal density is especially vivid. The D.O.P. was reduced by a factor of 3, which led to a nearly 80% increase in the scaled penetration reduction (SPR) factor.

Launching the $L/D = 15$ projectile was apparently much more difficult for SwRI, since the yaw values are consistently higher than the $L/D = 10$ tests. The samples with the best ballistic performance also had the highest yaw. In addition, the velocities for two of the tests were not measured. Estimated values were used instead. Because of these difficulties, the significance of these results are uncertain. However, the DENKA powder did produce tiles which gave the best overall ballistic performance against both threats. While the calculated efficiency difference between the highest and lowest samples was ~15 - 20%, the actual differences may be substantially less due to the yaw effect.

In general, relative to the steel backing material, alumina and aluminum nitride were more effective in defeating the $L/D = 10$ threat than the $L/D = 15$ projectile. This observation is vividly displayed in figure 11. The results also suggest that the efficiency of alumina ceramics to defeat either tungsten projectile decreased with increasing thickness. The scaled penetration reduction factor was 15% lower for the tiles with an areal density of 15 compared to the thinner tiles. This was not the case for the only aluminum nitride example which was shot with the same threat at two areal densities.

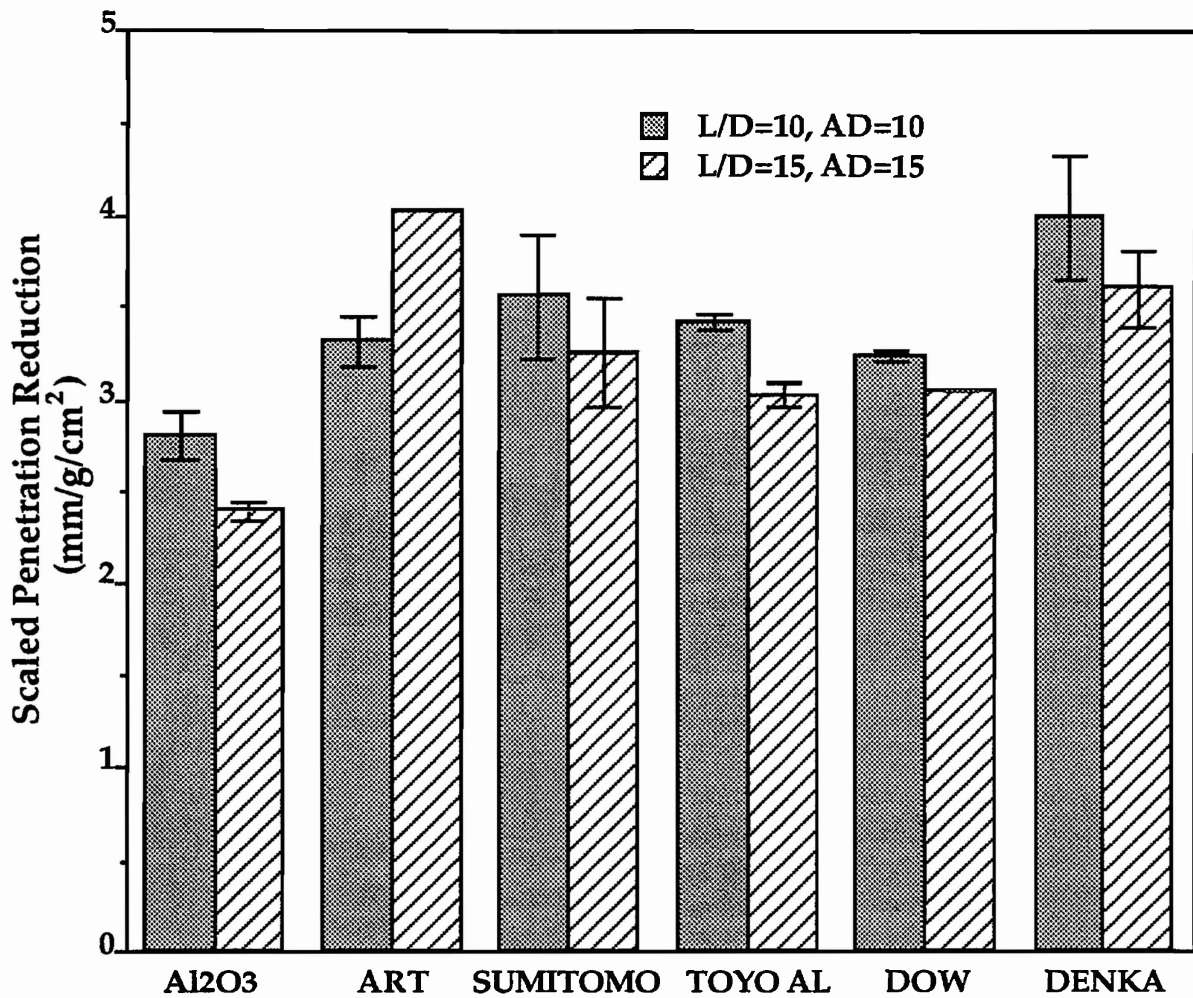


Fig. 11. Average Scaled Penetration Reduction (SPR) values for alumina and aluminum nitride for data for two tungsten alloy projectiles, $L/D = 10$ and 15 , and two areal densities, 10 and 15 g/cm^2 .

The advantage of the SPR factor compared to the standard D.O.P. method of data analysis can be seen in figure 12, where the problems associated with trying to extrapolate to zero penetration with limited data points are illustrated. Because of the extensive extrapolation, the validity of that method for these results is very questionable. As a basis for material comparison, all of the five AlN powders were grouped together in that plot and considered as typical AlN performance.

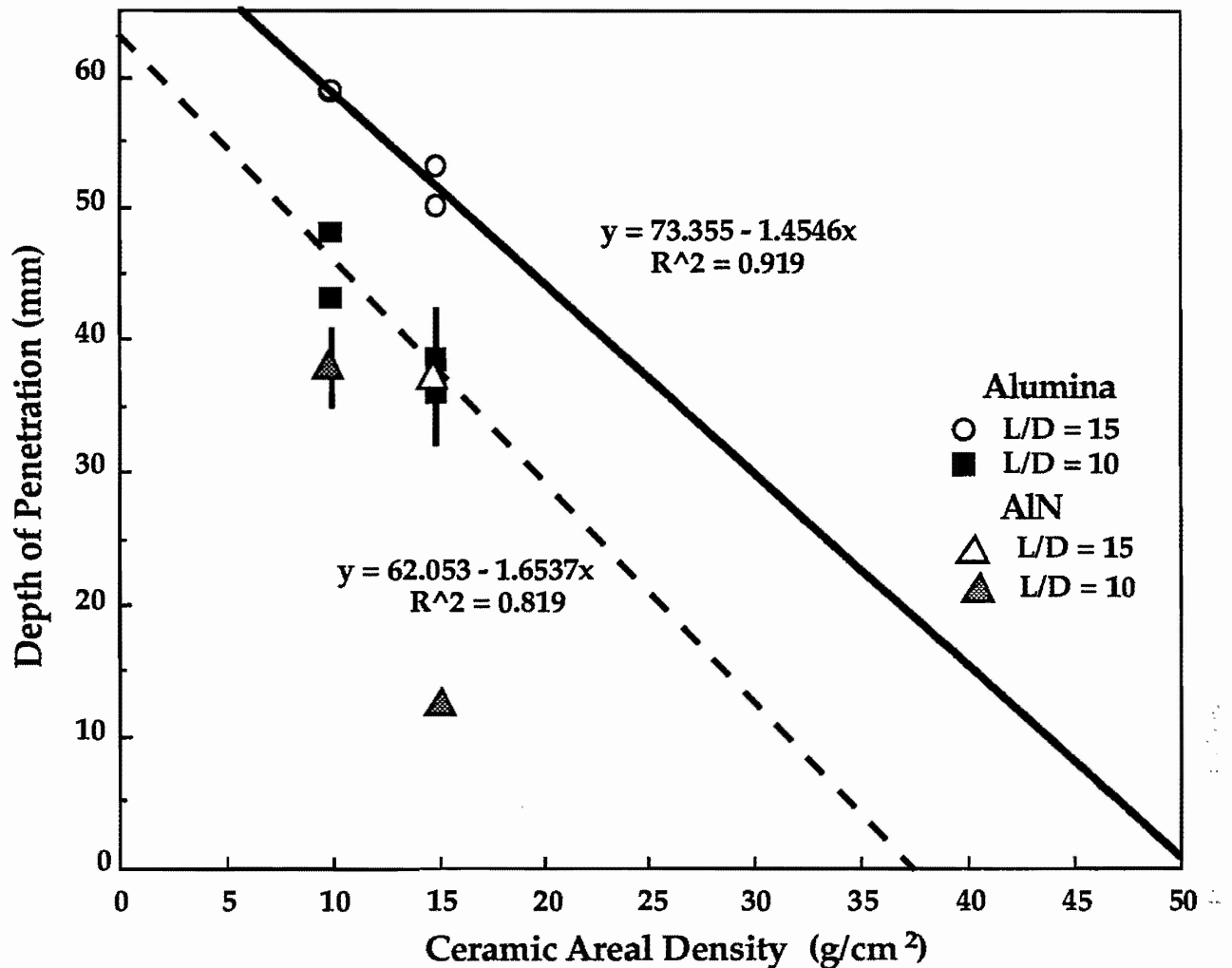


Fig. 12 Ceramic Depth of Penetration (D.O.P.) data for two tungsten alloy projectiles into hardened 4340 steel as a function the ceramic areal density.

2.1.5 DISCUSSION

The objectives of this hot-press study were to determine the critical powder specifications for aluminum nitride and to establish baseline data from which sintered products could then be compared. Five aluminum nitride powders were chosen for this study and each was produced by a different manufacturer. Represented by these five materials were the two major manufacturing methods, the carbothermal reduction of alumina and the direct nitridation of aluminum metal. Distinctions between the powders also existed with regards to purity, particle size and particle distribution. Fundamental issues which need to be considered include: whether there are

any inherent differences between the two classes of AlN powders; does grain size influence performance; does the level of the major contaminants in AlN, carbon and oxygen, have an effect; what role do metallic impurities play in the AlN's response to high strain rate conditions; and can high strain rate testing help predict the ballistic performance of aluminum nitride.

During this study, the nitrided aluminum powders tended to have a higher average grain size than the carbothermally produced materials. Since the Dow and Sumitomo powders had a smaller particle size initially, the grain size difference observed, which was only a factor of two, was not unexpected. The particle size difference, while typical for many of the current commercially available AlN powders, is not believed to be inherent to the two specific manufacturing methods. However, as a material class, the nitrided AlN samples had a higher quasi-static compression strength than the carbothermal materials. This trend was consistent for both sets of compression measurements. Compressive failure, unlike tensile or flexure, does not depend on crack initiation of the worst flaw in the body. Failure occurs due to the coalescing of microcracks which developed with increasing applied load. The microstructure of the material, which determines the characteristic and distribution of the inherent flaws, plays a critical role in controlling the ultimate compressive strength. Since grain boundaries are often crack initiation sites, strength typically increases with decreasing grain size.¹⁷

However, in this study the samples with the higher grain size, the three nitrided aluminum products, also had the higher strength. This may suggest that the inherent flaws are more associated with the chemistry rather than the size of grain boundaries. While it is not known whether there is a chemical difference at the grain boundaries of these five AlN materials, since the nitrided products are in general not as pure, especially compared to Sumitomo, it would appear this should be a minor effect. Crack initiation sites may also be associated with some other microstructural phenomenon. Resolving this question requires additional testing and analysis. To identify the crack initiation sites, the specimen must be loaded near but below the fracture load, and then examined using electron microscopy techniques. This

analysis may provide some valuable insights into the response of AlN materials under compressive loading conditions.

The higher hardness and modulus of the carbothermal materials are most likely a result of the finer microstructures and higher densities. While these physical characteristics were only slightly different between the two classes of AlN, the sensitivity of the microhardness and sonic modulus measurements could easily reflect that difference.

While the limited number and questionable quality of the data generated are a major concern, there was a 20% difference in the observed ballistic performance. Since more shots were fired with the $L/D = 10$ threat and the yaw was significantly lower than the $L/D = 15$ data, the discussion will focus on the shorter threat. DENKA was the highest performing AlN material. Sumitomo was about 10% lower and was followed closely by Toyo Aluminum. ART and Dow were similar and nearly 5% below the Toyo material. From this order of performance, there was no clear distinction between the two powder manufacturing processes. Within a group, there were also no obvious trends. The only clear difference between the Sumitomo material and the Dow product is the calcium content and the possibility of a chemical effect on ballistic performance has already been suggested from lower caliber results on sintered products.¹⁸ ART, the lowest performing nitrided aluminum material, also has the highest impurity levels, with the major component being iron rather than calcium. DENKA was intermediate based on purity, but was finer than either of the other two metal derived products. Grain size could be a secondary effect, but based on the modest differences present, it appears unlikely.

Based on these results, it would also be difficult to recommend AlN powder specifications. Particle size and distribution influences densification and the minimum size needed for a particular density can be determined. Oxygen (1 - 2%) and carbon (0.05 - 0.2%) levels in the range tested do not appear to be critical. Impurity levels near 500 ppm could present a problem, while <200 ppm of Fe or Si should not.

In a previous study,¹⁸ it was determined that there no physical or mechanical property measurement which could be used to accurately predict the ballistic performance of aluminum nitride. However, in this study it appears that the high strain rate pressure bar results closely mimic the ballistic results. The compressive strengths were grouped into two sets. Dow and ART were about 5% lower in strength than the other three materials. DENKA had the highest strength of that group but the difference was very small. Since the pressure bar experiments consisted of only single data points, further work in this area is clearly warranted. With cautious optimism, pressure bar tests could be extremely useful in screening ballistic materials.

While one can question the quality of these or any other ballistic test results, this study clearly illustrates that ballistic values can differ substantially for aluminum nitride materials and more work is required to understand aluminum nitride's unique ballistic characteristics.

2.2 Sintered Aluminum Nitride

The objective of this research effort was to develop a technology base for processing aluminum nitride using economical ceramic forming methods and then study the ballistic characteristics of these sintered products. One goal of this program was to utilize the differences in the selected AlN powders to gain fundamental insights into the densification of AlN ceramics.

Obtaining an understanding of the relationships between the formulation, fabrication, binder removal, and sintering phases of process was another goal of this study. Formulated aluminum nitride powders were prepared by spray drying, dry pressing was used to form the ceramic greenware, and final densification was achieved by pressureless sintering. Traditional sintering variables such as sintering aid level, time, temperature, atmosphere and environment were investigated as well. Failed components will be used to illustrate the difficulties encountered during the processing of large AlN components. Adjustments in the burnout and sintering cycles needed to produce crack free bodies will be discussed. The results of extensive physical, mechanical and ballistic evaluations will also be detailed.

2.2.1 SINTERING SCREENING STUDY

The statistically designed powder screening study was intended to elucidate the interrelationships between aluminum nitride powder quality, sintering aid levels and the sintering parameters of time, temperature, atmosphere and environment. The five AlN powders, which were utilized in the hot-pressing study and described earlier (Table I), were also used in these sintering experiments. Several compounds have been shown to be effective as sintering aids for aluminum nitride.¹⁹ For electronic applications, yttrium and calcium based compounds have received the most attention and three, yttrium oxide, yttrium fluoride and calcium carbonate, were examined during this work. Two additional rare earth oxides, cerium oxide and lanthanum oxide were also studied. These raw materials not only cover a broad price range, but also have different melting temperatures and wetting characteristics. These latter properties are particularly important since aluminum nitride densifies by a liquid phase sintering mechanism. These five sintering additives were studied at two levels, 0.5 and 5.0 volume percent. The relative cost and the lowest potential liquidus temperature for each system is detailed in Table IX.

The remaining sintering parameters were also examined at two levels or conditions. The sintering temperature was either 1750°C or 2000°C and the hold at that temperature was 30 minutes or 4 hours. The furnace atmosphere was nitrogen or a nitrogen/5% hydrogen mixture and either a graphite or boron nitride crucible was used to vary the sintering environment.

Table IX
Sintering Aids Studied in Screening Experiment

Sintering Aid	Y ₂ O ₃ [§]	CeO ₂ [§]	La ₂ O ₃ [§]	CaO*	YF ₃ [¶]
Grade/Purity	5600/99.99	5310/96.0	5200/99.99	USP	99.9
Lot	1734	U-1203	990	948410	32,606-2
Relative Price	200	20	35	1	740
Lowest T _m	1760°C	1670°C	1830°C	1360°C	1142°C

[§]MOLYCORP, Louviers, CO; *Added as CaCO₃, J.T. Baker, Phillipsburg, NJ; [¶]Aldrich Chemical, Milwaukee, WI.

Since this study consisted of both qualitative (powder, sintering aid, atmosphere and environment) and quantitative (temperature, sintering time and sintering aid level) parameters, a D-optimal design strategy was employed.²⁰⁻²² With only 150 design points, all main effects and two-factor interactions were obtainable. 200 additional specimens were sintered including design center points, samples without sintering aids, and duplicates to check experimental error. Percent theoretical density was the only dependent variable used in the analysis.

Preparation of greenware involved first preparing the binder solution which consisted of a mixture of ECB⁼ and PEG⁺⁺ in ethanol. While the binder solution was homogenizing, the sintering aid was dispersed with fish oil^{**} in ethanol and mixed with AlN media for 1 hour in a 250 ml polyethylene jar. Binder solution equivalent to 7.5 wt. % on an AlN powder basis was then blended with the sintering aid slurry. Finally, the AlN powder (50 g) was added and mixed for 1 hour. The slurry was poured out onto trays and air dried overnight. The dried powder was then crushed and sieved through a 100

⁼ Experimental Ceramic Binder, XUS 40303.00, Dow Chemical, Midland, MI

⁺⁺ PolyGlycol, The Dow Chemical Company, Midland, MI

^{**} Spencer Kellogg KELLOX Z3 Fish Oil, NL Chemicals, Hightstown, NJ

mesh screen. Pellets, 2.2 cm in diameter, were dry pressed at 69 MPa and then isopressed at 276 MPa. The 6 gram pellets were heated in air to 550°C and held for 1 hour. The greenware was then weighed and dimensions taken in order to calculate green density. After the graphite or boron nitride 10 cm crucible was lined with a powder mixture of AlN and BN, the samples were then placed on the powder bed, the crucibles were covered and then fired in a graphite resistance heated furnace.[◇] An initial heating rate of 25°C/min. was used. At 1200°C, the heating rate was reduced to 10°C/min. and maintained at that rate until the desired sintering temperature was reached. While other physical parameters were measured, only percent theoretical density was analyzed in the experimental model. The density results for the 150 samples included in the design and their replica points are shown in figure 13.

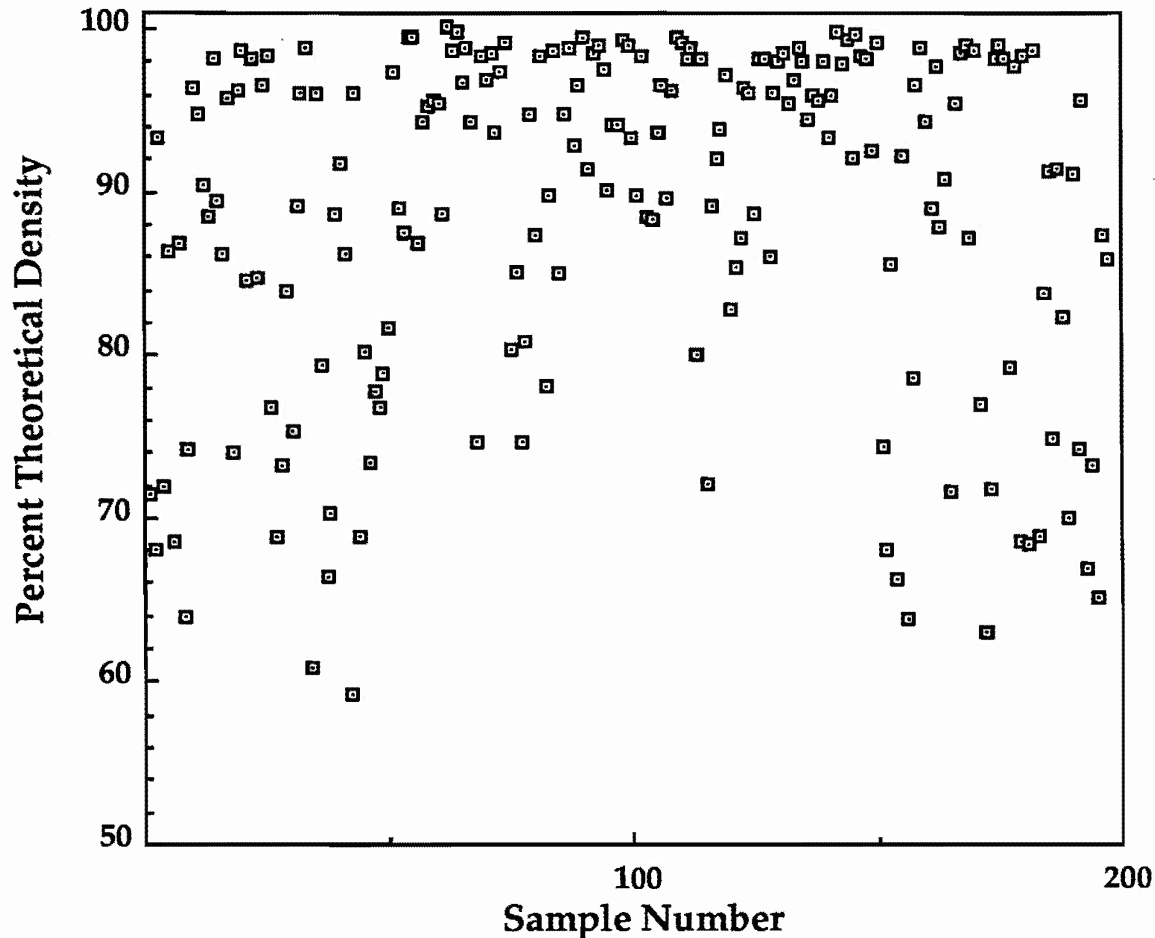


Fig. 13. Percent theoretical density of sintered samples used in designed screening study.

[◇] Model 1000-4560, Thermal Technology, Astro Division, Santa Barbara, CA

These results were analyzed using Experimental Design Analysis of Variance (ANOVA). In this seven variable study, a fixed effects model was used and both main effects and two factor interactions were examined. The parameters which were most statistically significant (largest impact on densification) in the ranges studied were temperature, environment, powder, the interaction between environment and atmosphere, and the interaction between powder and environment. These results are described in Table X.

Table X
Statistical Results of Powder Screening Study

Design Variable	Degrees of Freedom	F-Value	Critical Significance Level
Temperature	1	26.06	.0001
Environment	1	19.16	.0001
Powder	4	10.32	.0001
Envir./Atm.	1	14.89	.0003
Temp./Time	1	12.03	.0009
Powder/Envir.	4	5.24	.0010

Model Std. Dev. = 5.63, Coef. of Var. = 6.2%, Replicate Data Coef. of Var. = 3.3%

These results are graphically represented in figures 14 and 15, where the means of the significant main effect and two-factor interaction terms are shown. The overall density results of the five powders appears to follow closely with the average particle size and distribution. The finer and more uniform carbothermal powders had the highest density means. However, the nature of the environment also had a dramatic impact on the densification of two powders in particular. As seen in figure 15, the sintering of ART and Dow containing samples was clearly inhibited by the reducing conditions of carbon environment and hydrogen containing atmosphere. This development may be the result of the proportionately lower oxygen contents of these two materials. This suggests then that there is a minimum surface oxide required on AlN powders to react with the sintering aids and provide the needed liquid phase which enables densification. The reducing conditions may be removing the surface oxide before the interaction with the sintering aid can take place or the formed liquid may be volatilizing before significant densification has occurred.

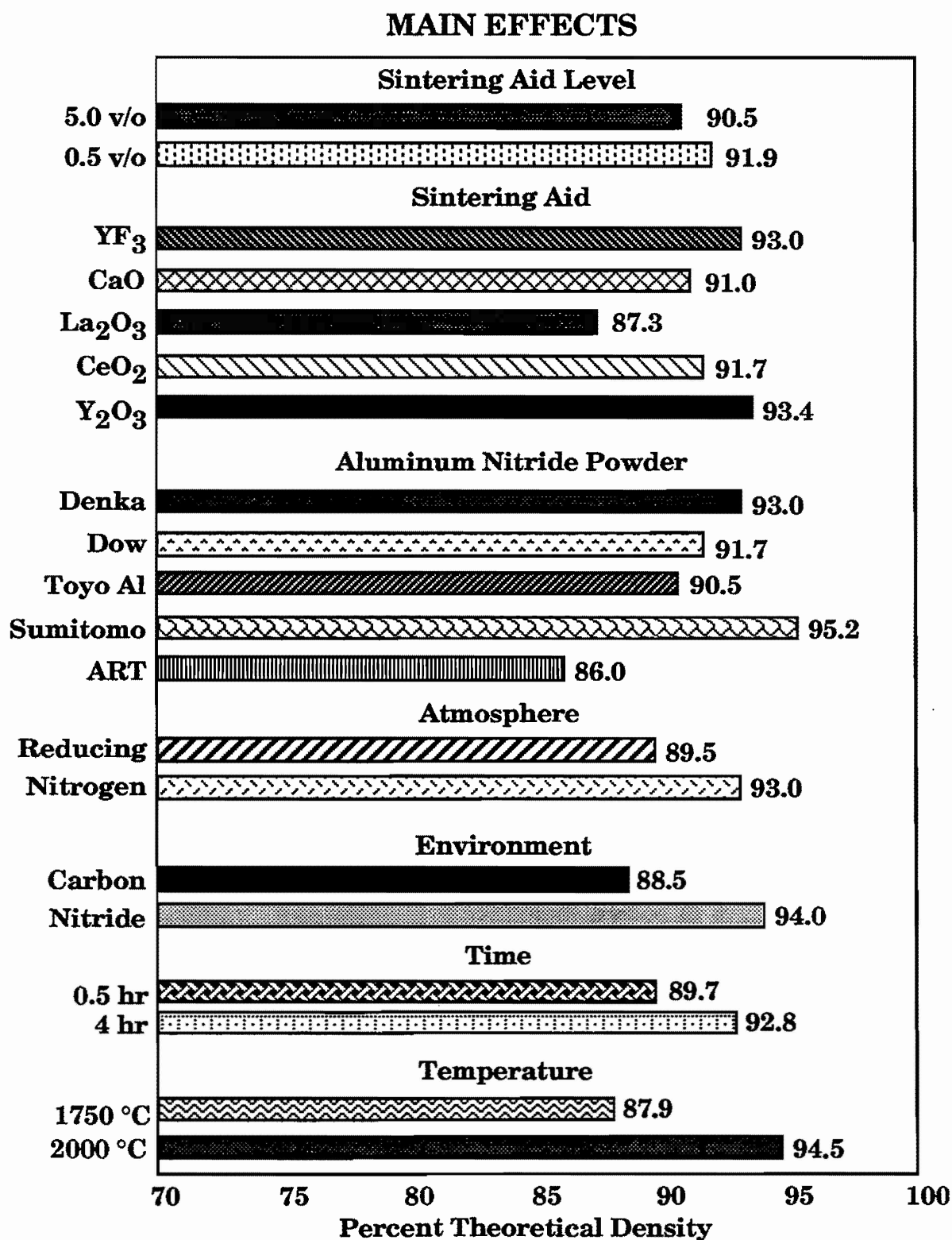


Fig. 14. Bar charts showing percent theoretical density means of main effects for aluminum nitride sintering screening study.

Because of the strong influence of ceramic density on ballistic performance, a primary interest of this research program was to evaluate the ballistic performance of high density (>98% T.D.) aluminum nitride products. As part of this screening study, 41 out of 150 samples had a density >98% T.D. The cell frequencies of this subset were determined for the 6 studied parameters. As seen in figure 16, all powders were represented in this high density group, but the most active powder, Sumitomo ANH-10, clearly offered the most options for achieving high density ceramics. As expected, the two yttrium containing compounds were the most effective sintering aids. The number of variations available to obtain dense parts has allowed the selection of AlN materials with unique physical and chemical characteristics to be evaluated.

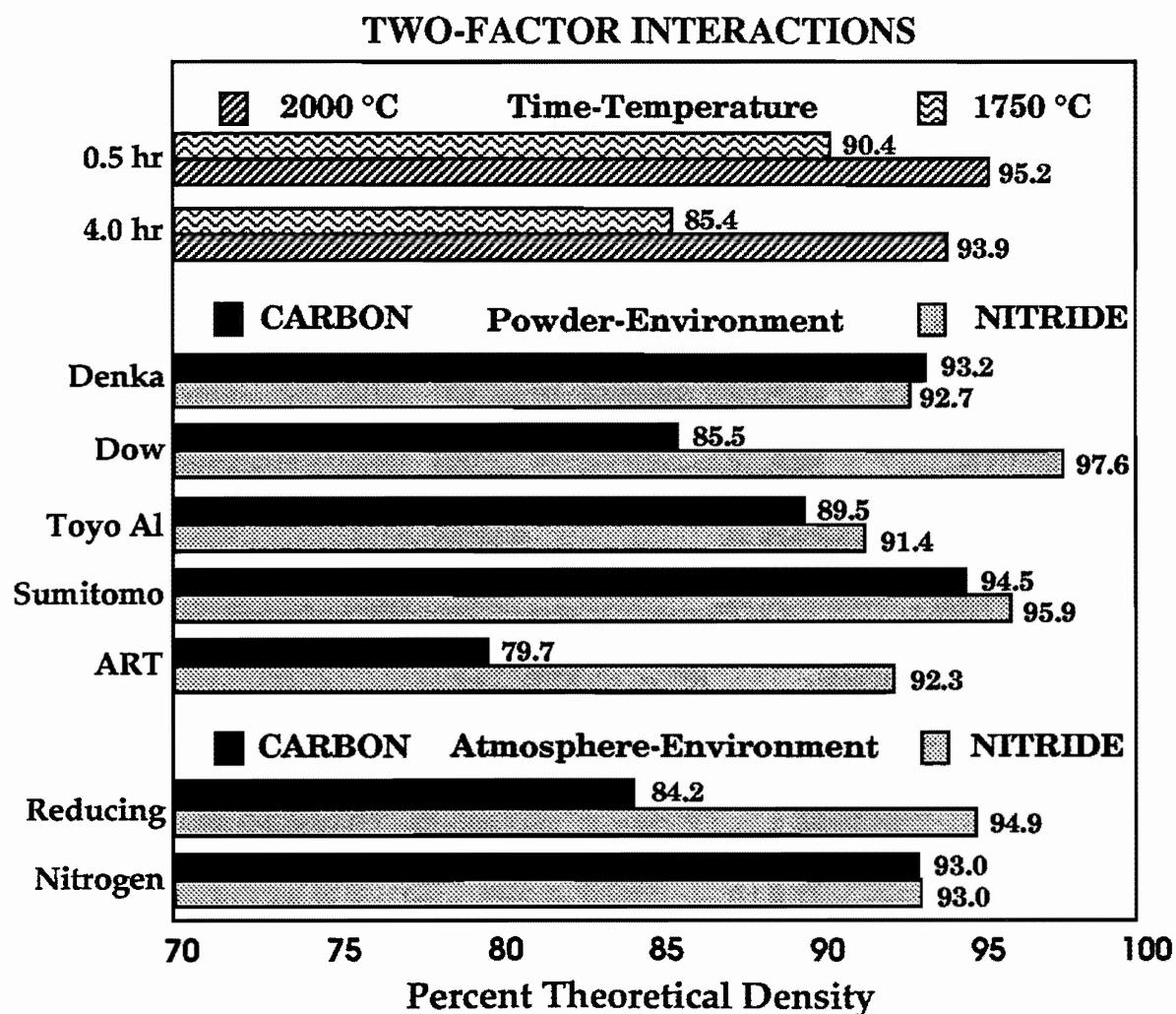


Fig. 15. Percent theoretical density means of significant two-factor interaction terms as determined by Standard Analysis of Variance (ANOVA)

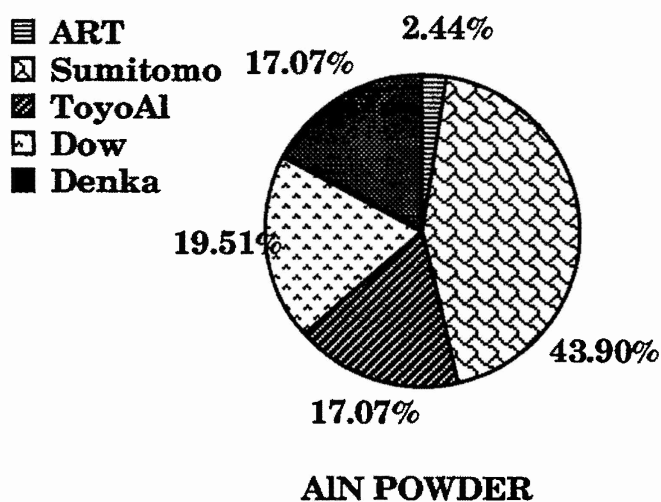
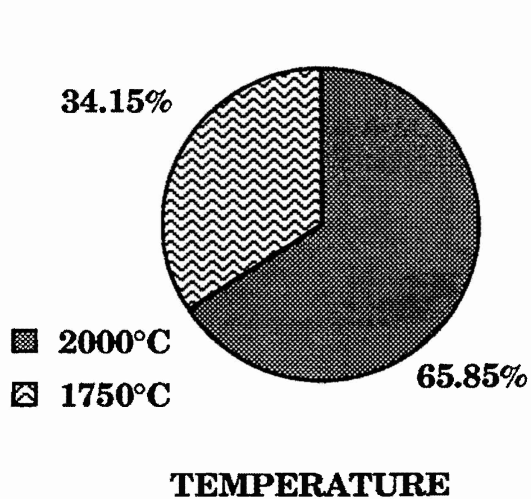
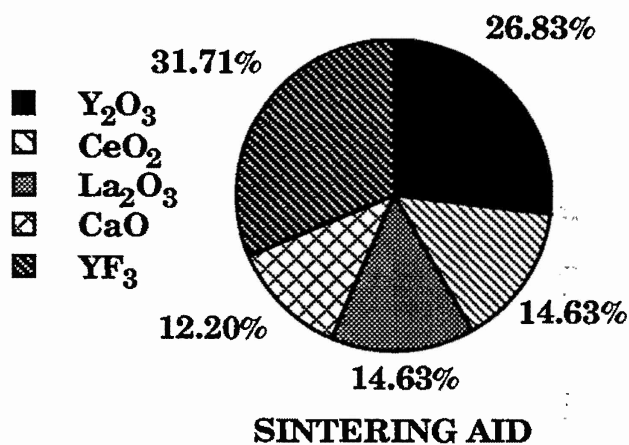
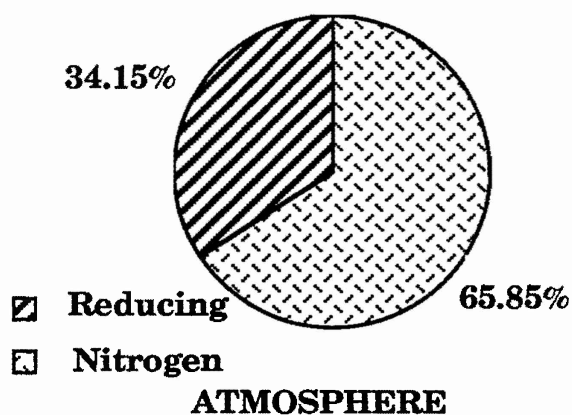
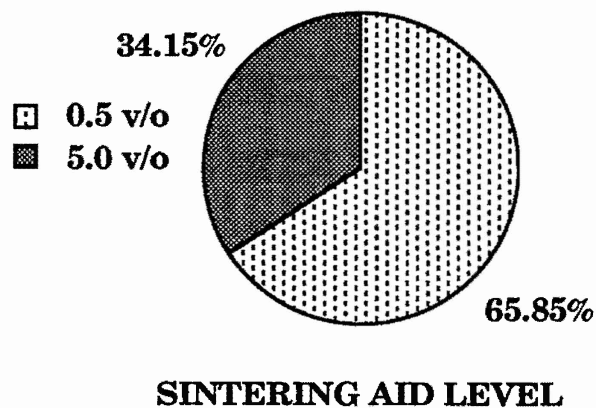
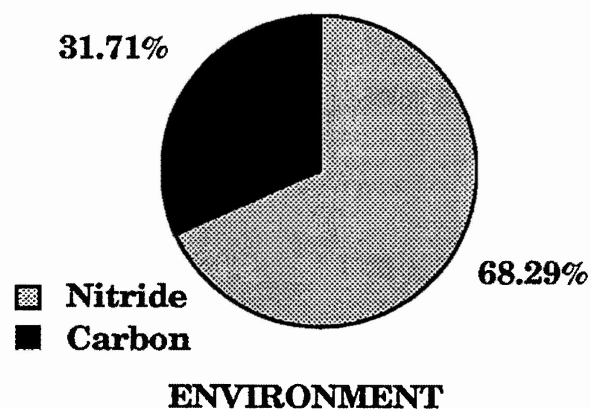


Fig. 16. Frequency pie charts of the 6 studied sintering parameters for the 41 sintered AlN samples which achieved high density (>98% T.D.).

2.2.2 PROCESS OPTIMIZATION

This study consisted of a series of experiments which examined the key components of the dry press/sinter process illustrated in figure 16. In addition to studying the effect of powder characteristics on sinterability, the effect of pressing pressure on green and fired densities was studied, binder system variations were examined, and the binder burnout and sintering steps were optimized for large parts. The binder system used in these studies consisted of mixtures of ECB[¥] and PEG,[^] polyethylene glycol, in ethanol. Extensive use of statistically designed experiments minimized the number of data points required while maximizing the amount of information obtained during this program.

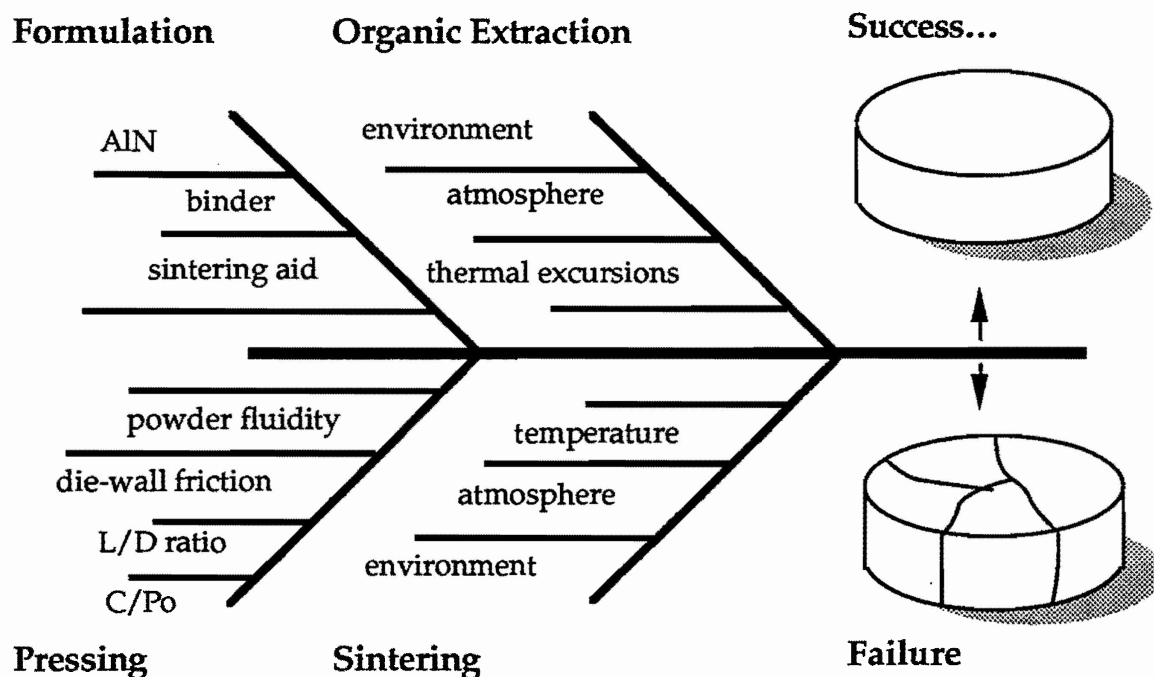


Fig. 17. Schematic of process to fabricate large aluminum nitride parts, showing key parameters for each step.

A factorial experimental design²³ strategy was utilized to determine the statistical significance of key processing parameters on green and fired

[¥] Experimental Ceramic Binder, XUS 40303.00, Dow Chemical, Midland, MI

[^] PolyGlycol, The Dow Chemical Company, Midland, MI

densities. Predictive green and fired density models based on binder - ceramic mixtures, spray-dry parameters, dry pressing pressure, and sintering temperature were established for a carbothermal powder (Dow Lot 890629-48) and a nitrided metal powder (DENKA Lot 10PF8620). The 2 kg aluminum nitride batches were prepared with 3 weight percent yttrium oxide using a Niro portable spray-dryer[¶]. The binder levels ranged from 4 to 10 wt. % and the solids loading was 30 to 50 % on a weight basis. The ECB/PEG ratios varied from 1:2 to 2:1 and the spray dryer outlet temperature was also a variable. Flowability, tap density and pour density were measured for the 22 AlN formulations. Flowability was similar for both powders and was determined by the size distribution of the spray dried product which was mostly affected by the solvent concentration and the slip feed rates. Analysis of the density response variables indicated that except for the ceramic powder, the effect of the spray-dry and slip parameters was not statistically significant. Denka AlN had substantially better packing characteristics than the carbothermally produced Dow powder. This observation also carried over into the green density measurements where there was a consistent 15% density difference over the entire tested pressure region. This is dramatically illustrated in figure 18, where the density of the samples from the nitrided aluminum powder are clearly higher than the carbothermal samples under equivalent conditions. The statistical model for the green density results is outlined in Table XI. The correlation factors and confidence levels for the green density model were extremely high. Of the processing parameters studied, forming pressure clearly dominated the green density results. While reducing the binder level may lead to slightly higher green densities, it had no influence on the final measured densities and as will be discussed later, this decrease could lead to lower green strengths.

[¶] 36" Type HT portable spray dryer, Niro Atomizer Inc., Columbia, MD

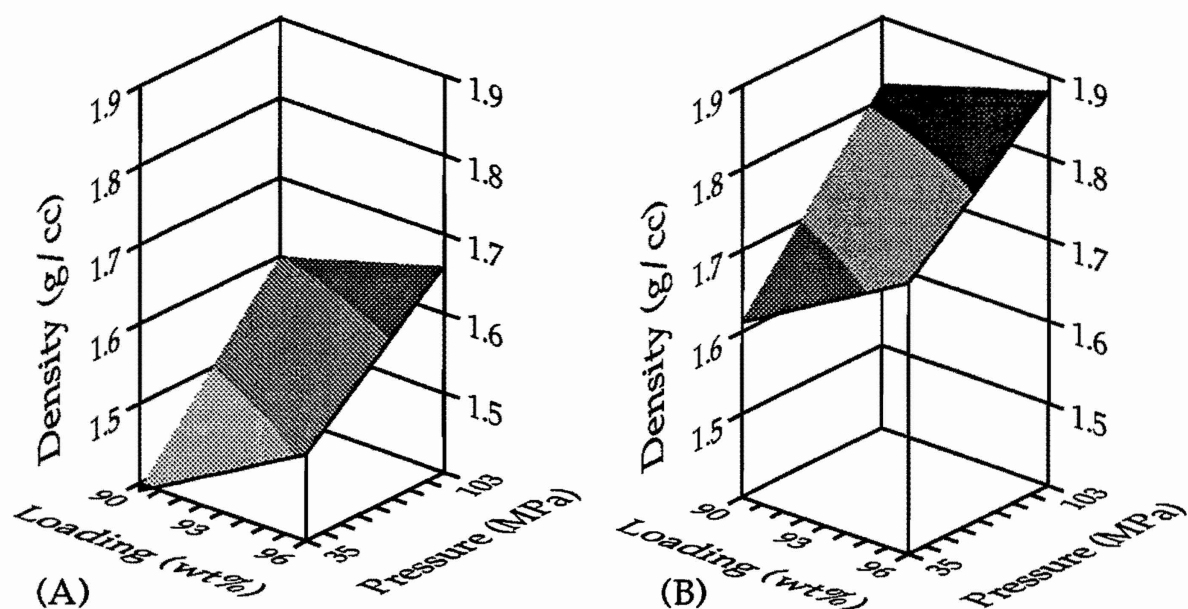


Fig. 18. Predictive models for green density of a carbothermal AlN powder (A) and a nitrided AlN powder (B).

Table XI
Process Screening Study: Green Density Results

Design Variable	Variable Range	Degrees of Freedom	F-Value	Critical Significance Level	Model Coefficients
Powder	Dow (-1) Denka (1)	1	710	.0001	0.111
Pressure (MPa)	35 (-1) 103 (1)	1	425	.0001	0.090
Binder Level Wt. %	10 (-1) 4 (1)	1	117	.0001	0.045
Binder ECB/PEG Ratio	0.5 (-1) 2.0 (1)	1	16	.0001	-0.017

Model Std. Dev. = 0.04, Coef. of Var. = 2.4%, Intercept = 1.678

For the sintered density models, temperature was the dominant factor in determining the final ceramic density. A three dimensional plot of fired density, temperature and pressure is shown in figure 19. Enhanced sinterability of the carbothermal powder at the lower temperatures is again a

reflection of the more narrow particle size distribution. Even though these two powders had the same surface area ($4 \text{ m}^2/\text{g}$), the larger particles ($>2 \mu\text{m}$) in the nitrided material resulted in lower fired densities in the $1750\text{-}1900^\circ\text{C}$ temperature regime. This observation is especially significant when one considers the green density advantage that the nitrided material had initially. Above 1900°C , both powders achieved essentially full density.

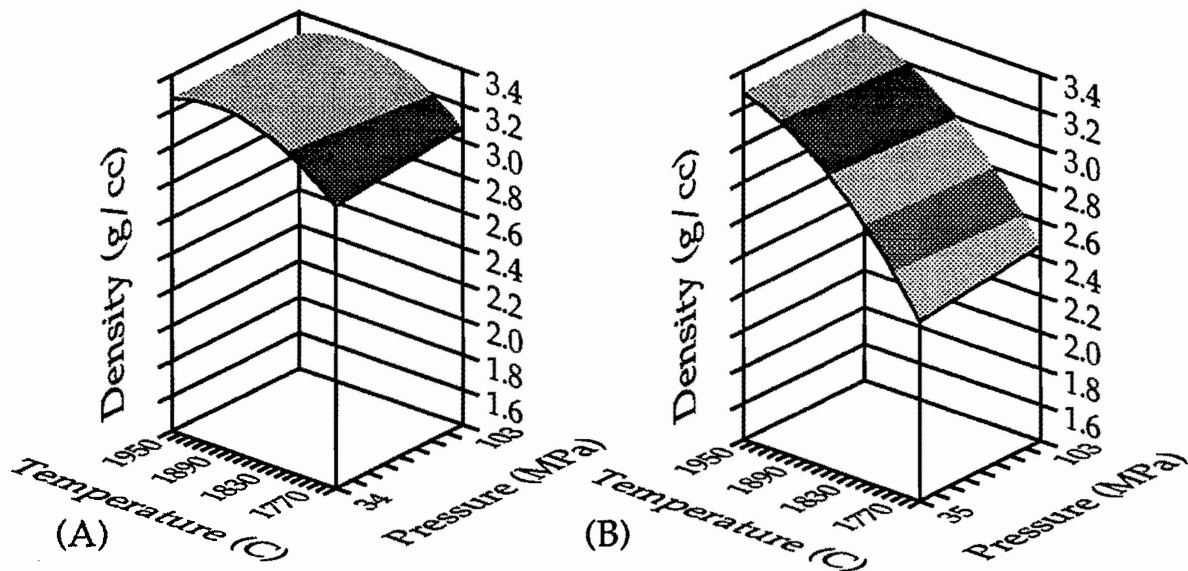


Fig. 19. Predictive models for fired density for a carbothermal AlN powder (A) and a nitrided AlN powder (B).

The fired density results for the significant effects are given in Table XII. As in the green density case, the correlation factors and confidence levels for the generated equations for this series of experiments was extremely high. While these specific models apply only to the two powders tested, the observed packing and sintering differences have been typical of these two types of synthesized AlN powders. Slight modifications to these equations would be required if these results were to be extended to other aluminum nitride materials.

Table XII
Process Screening Study Results for Fired Density

Design Variable	Parameter Range	Degrees of Freedom	F-Value	Critical Significance Level	Model Coefficients
Temperature °C	1750(-1) 1950(1)	1	788	.0001	0.247
Powder	Dow (-1) Denka(1)	1	334	.0001	-0.148
Temp.* Powder		1	308	.0001	0.155
Temp.* Temp		1	39.7	.0001	-0.151
Pressure MPa	35(-1) 103(1)	1	39.7	.0001	0.054
Temp.* Press.		1	27.3	.0001	-0.048

Model Std. Dev. = 0.07, Coef. of Var. = 2.3%, Intercept = 3.186

The effects of ceramic - binder interactions on several response variables were examined, with a single AlN source, using a statistical mixture design.²⁴ The ECB/PEG ratio, the molecular weight of the PEG used and the total level of binder added were all varied during this parallel but independent effort.

The statistical mixture experimental design examined the parameters associated with the ECB/PEG ceramic binder system and their impact on green strength, green density and fired density. By treating the ECB/PEG/AlN combinations like a ternary phase system, contour plots, figures 20 and 21, were generated for two of the response variables as a function of a composition and PEG molecular weight.

As expected, the green strength increased as the binder level increased, especially for the higher molecular weight PEG samples. However, if green strength is not a concern, then the lowest molecular weight PEG has the greatest potential with regards to manufacturing robustness. Increases in residual carbon are suspected to be the cause for the decrease in fired density with increased binder levels for the higher molecular weight PEG.

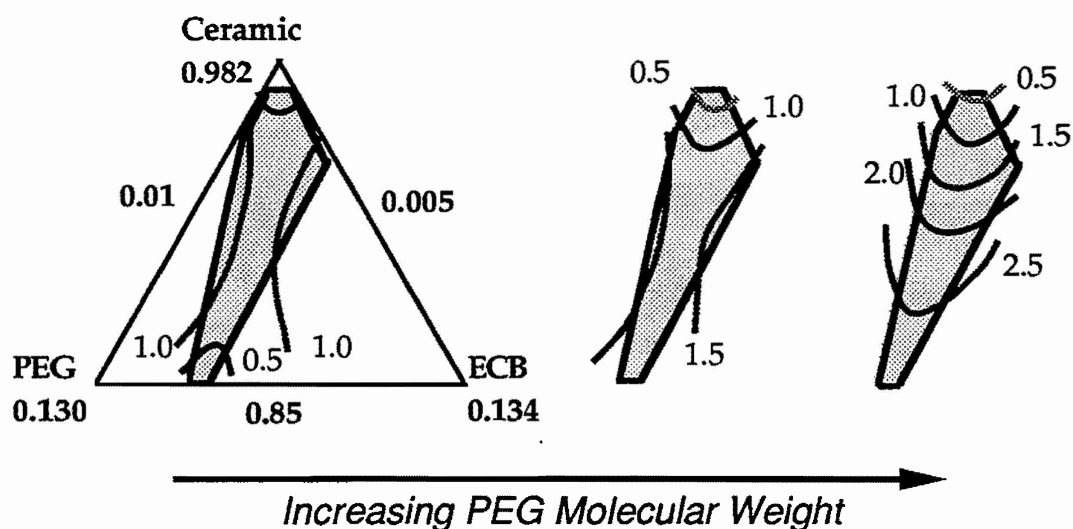


Fig. 20. Effect of PEG molecular weight and binder-ceramic composition on the biaxial flexure strength²⁵ of a compact. The compositions for the AlN, ECB, and PEG are in weight fractions. The six-sided shaded area is the compositional region examined during this study. Line contours represent constant strength values in MPa.

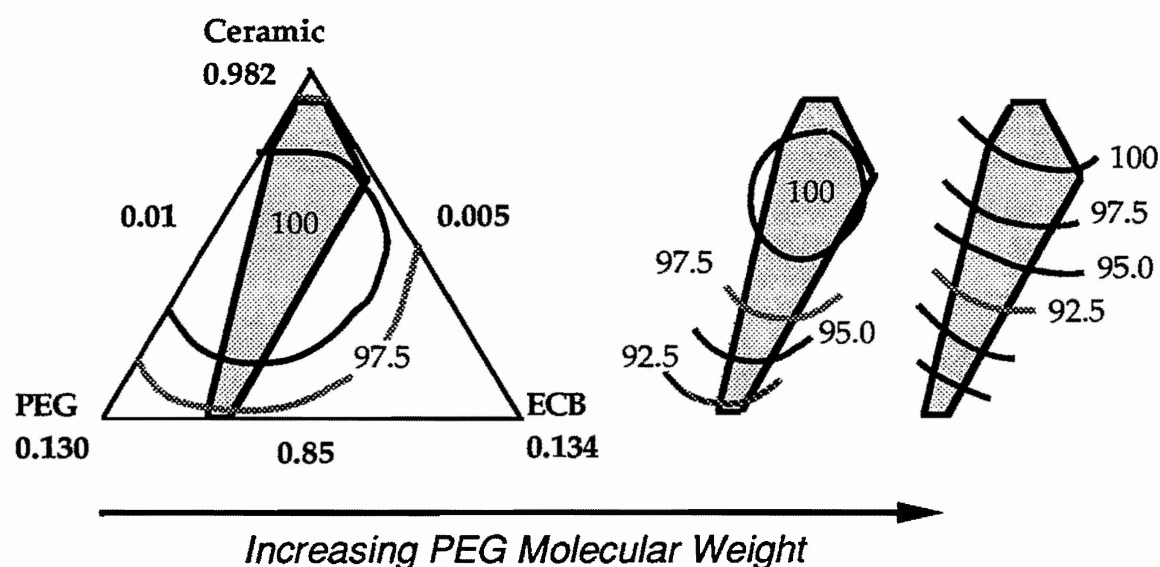


Fig. 21. Effect of PEG molecular weight and binder-ceramic composition on the densification of AlN. Line contours represent constant density regions in % of theoretical.

The burnout and sintering optimization for the large aluminum nitride parts also utilized spray-dried powders containing 3 w/o yttria. The binder system used had an ECB/PEG ratio of 1:2 and on a ceramic solids basis, was 6.5 wt.%.

In addition to establishing schedules for binder removal and sintering, the pressing procedure also needed to be optimized. Since a standard, single acting 12.7 cm (5 in) diameter steel die was used in a 100 ton press, the degrees of freedom available to ensure uniform density greenware were very limited. This limitation did not seem to be a problem during these initial phases of scale-up. During pressing, the load was applied gradually to the maximum pressure of 65 MPa (9500 psi), held for several minutes, then the pressure was slowly removed. The parts were removed using at a constant displacement rate. Several green tiles with sizes up to 6.4 cm (2.5 in) thick were fabricated with Dow powder using the standard 3 w/o yttria formulation. These tiles were used to develop appropriate burnout and sintering schedules. As the tile I/D (thickness/diameter) ratio increased, there was a corresponding decrease in the calculated green density. The decrease was less than 4% over the tested range. This observation is summarized in Table XIII.

Table XIII
Tile Thickness Effect on Green Density

Thickness cm	I/D cm/cm	Mass grams	Linear Density g/cm **	Green Density g/cm³ **
1.24	0.10	286	230.6	1.82
2.48	0.20	572	229.7	1.81
3.82	0.30	858	224.6	1.77
5.12	0.40	1143	223.2	1.76
6.45	0.51	1429	221.6	1.75

** Density values include binder.

For small laboratory samples, the burnout step is not a area for much concern. However, as the size of the aluminum nitride greenware increases, the burnout process becomes increasingly more critical. For an AlN formulation, with 6.5 wt.% of the 1:2 ECB/PEG binder, the weight losses in air and nitrogen are shown in figure 22. In nitrogen, the organic loss is directly a result of binder pyrolysis. While in air, oxidative decoupling occurs, so the decomposition products are different and the weight loss begins at much lower temperatures. For large parts, a slow, controlled weight loss is required to maintain part integrity. From the TGA results, a constant weight loss schedule can be approximated for any tile mass. This was more easily

accomplished when a nitrogen atmosphere was used due to the more controlled pyrolysis. For the nitrogen runs, a three step program was used to achieve the constant weight loss conditions. In air, the oxidative decoupling of the binder is an exothermic reaction, therefore it was impossible to tightly control the rate of weight loss due to the absence of external cooling on the binder furnace. A six step heating schedule was employed for any aired burned out samples. Because of this, binder removal in nitrogen was preferred to obtain large flaw free greenware. However, a noticeable carbon gradient, as seen in figure 23, was often observed with thicker tiles which impacted their sinterability. The carbon level is clearly higher in the mid-section of the part than on the outside.

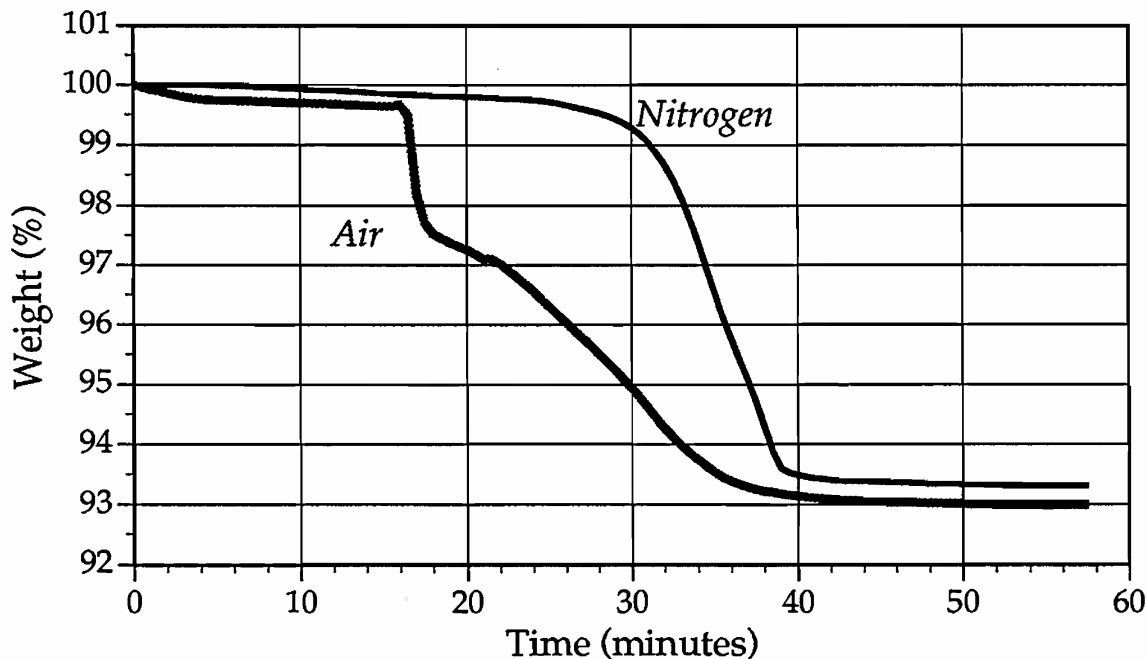


Fig. 22. Weight loss of aluminum nitride greenware, with a 1:2 ECB/PEG binder formulation, using a heating rate of 10°C/min from R.T. to 600°C .

The chemistry gradient was successfully eliminated by subjecting the part to an oxidative environment after the nitrogen pyrolysis. This procedure not only eliminated the carbon distribution problem, it also improved the oxygen profile compared to an equivalent air burned out part.

While this approach to determining burnout schedules was a good first approximation, there are obvious shape and size factors which mass alone can not take into account. A furnace with capabilities to measure the weight losses

of large ceramic parts was designed and constructed in our laboratory to better understand this important issue. In addition to being able to monitor the weight change as a function of time and temperature, a feedback system was installed to allow total weight loss control. While this apparatus did not directly impact this contract, it was found to be invaluable during the successful transfer of this technology to the market development plant.

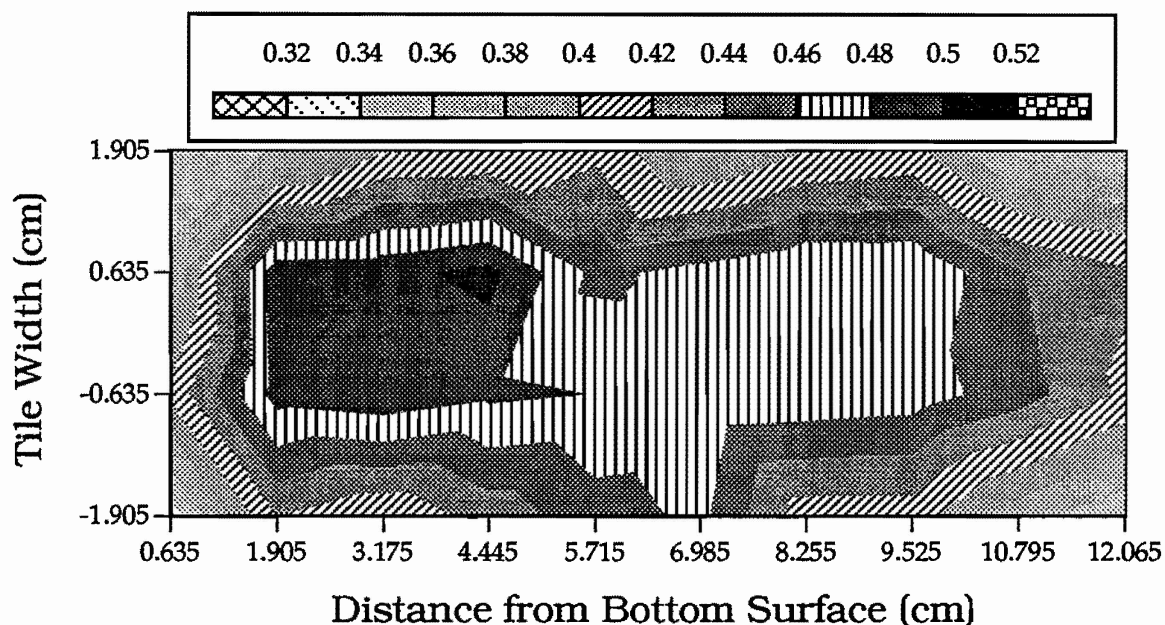


Fig. 23. Carbon distribution of a green AlN tile, 12.7 cm x 12.7 cm x 5 cm, after being burned out in nitrogen using a constant rate profile up to 650°C.

When processing ceramics with minimum cross-sections as large as 5 cm, binder removal is only one of the difficulties which must be overcome. Figure 24 shows another consequence associated with fabricating thick ceramic parts. Since aluminum nitride is a high thermal conductivity material, one would anticipate that thermal shock would not be a severe concern during the fabrication process. Unfortunately, this has been observed to be true only after densification has taken place. The greenware is relatively weak and a poor thermal conductor, so thermal shock from heating too quickly during the sintering step (figure 24A) and from rapid cooling after binder burnout should be avoided. Initial heating rates were reduced from 30°C/min to 10°C/min and in the temperature range where densification occurs, the ramp rates were lowered from 10°C/min to 2.5 °C/min. This reduction proved to be very

successful. The verification of which is reflected in the high density 10 cm dia. x 5 cm tall AlN disk (figure 24B), fabricated using low-cost technology based on dry-pressing and pressureless sintering.

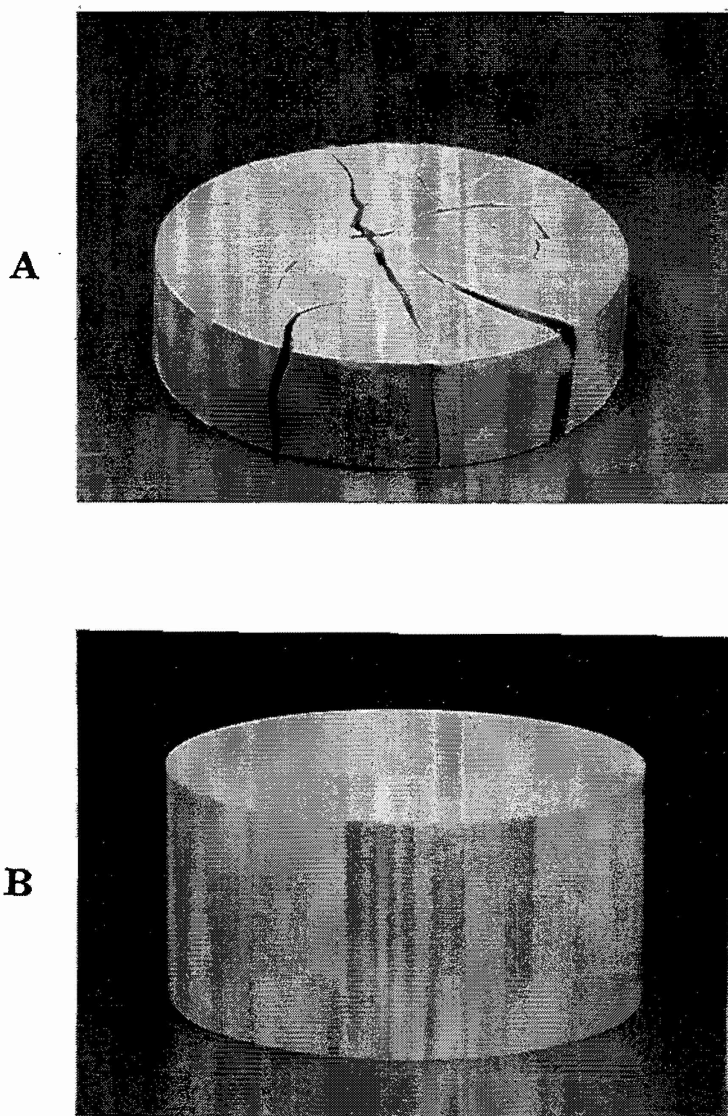


Fig. 24. Sintered aluminum nitride cylinders showing A) thermal shock failure due to rapid heating during sintering and B) a successful demonstration of processing technology.

2.2.3 PREPARATION OF SINTERED TARGETS

Originally, two sets of samples were prepared for ballistic testing. The first set, which was prepared for light caliber tests, consisted of 21 AlN compositions. These tiles had a fired diameter of ~8 cm and a thickness of 0.8 cm. The selection criteria used for this set will be detailed later, however the results of the sintering screening study played a dominant role in that process. The second set was prepared for LRP tests after an assessment of the light caliber ballistic results. These targets used tiles which were 10 cm in diameter and either 3 or 4.5 cm thick. Five of the previous 21 compositions were scaled-up to the larger sizes. During the last phase of this contract, several additional samples were prepared for SLAP D.O.P. targets. These compositions and diameters were the same as the LRP samples, but the thickness was only 0.9 cm thick.

Previously,¹⁸ it has been shown that ballistic performance did not correlate well with routine mechanical and physical measurements. Ballistic testing was therefore necessary to accurately assess the relative performance of AlN ceramics. However, the cost of LRP testing made it unrealistic to test a large sampling of materials to determine an optimum AlN composition. Therefore, it was decided that less expensive, light caliber testing with steel projectiles would be used for screening purposes. In selecting the compositions for preliminary evaluation, several criteria had to be met. The first requirement was that all compositions chosen should be capable of achieving high density. The ultimate outcome would determine any effect of grain size, sintering aid and level, or powder quality on ballistic performance. Therefore, it was desirable that all powders and sintering aids were examined. Statistically designed experiments have been extremely useful in screening parameters and developing optimum processing conditions. However, for this task, this methodology was not suitable because of the rigid boundary conditions. By using coupled or grouped samples, it was rationalized that the program objectives could be achieved by testing the 21 compositions listed in Table XIV. Because of the density requirement, the two coarse AlN powders, ART and Toyo Al, were primarily evaluated at a higher temperature and sintering aid level. Since La_2O_3 and CaO were most effective in aiding densification at the lower values, only materials with 0.5 v/o of these sintering aids were explored.

Grain size effects could be determined from an analysis of 3 sample sets (1,2), (5,6), and (17,18). Samples (8,9 and 10), (11, 12 and 19), and (6,7 and 16) would establish if there is any AlN powder influence on ballistic performance. The influence of sintering aid chemistry would be identified primarily from sample sets (9, 12 and 22), (8 and 11), and (15, 17 and 19). Samples (14, 15 and 16) should provide insights into the effect of sintering aid level.

Table XIV
Selected Sintered AlN Samples for Ballistic Evaluation

Batch #	Powder	Sinter Aid	Level	Temp °C	Hold Time	Crucible	Heating Rates
1	Sumitomo	CeO ₂	5 v/o	1830	1 hr	BN	50/2.5
2	Sumitomo	CeO ₂	5 v/o	1940	3 hr	Carbon	30/2.5
3	Denka	CeO ₂	5 v/o	1830	1 hr	BN	50/2.5
4	Toyo F	CeO ₂	5 v/o	1830	1 hr	BN	50/2.5
5	Toyo F	Y ₂ O ₃	5 v/o	1960	3 hr	Carbon	30/2.5
6	Toyo F	Y ₂ O ₃	5 v/o	1830	1 hr	BN	30/2.5
7	ART	Y ₂ O ₃	5 v/o	1900	1 hr	BN	10/2.5
8	Sumitomo	CaO	0.5 v/o	1960	0.5 hr	Carbon	10/2.5
9	Denka	CaO	0.5 v/o	1870	1 hr	BN	10/2.5
10	Toyo F	CaO	0.5 v/o	1870	1 hr	BN	10/2.5
11	Sumitomo	La ₂ O ₃	0.5 v/o	1750	3 hr	BN	10/2.5
12	Denka	La ₂ O ₃	0.5 v/o	1870	1 hr	BN	10/2.5
13	ART	YF ₃	0.5 v/o	1970	4 hr	BN	10/2.5
14	Dow			1830	1 hr	BN	10/2.5
15	Dow	Y ₂ O ₃	0.5 v/o	1830	1 hr	BN	10/2.5
16	Dow	Y ₂ O ₃	5 v/o	1830	1 hr	BN	10/2.5
17	Dow	CeO ₂	0.5 v/o	1750	0.5 hr	BN	10/2.5
18	Dow	CeO ₂	0.5 v/o	1970	4 hr	BN	10/2.5
19	Dow	La ₂ O ₃	0.5 v/o	1870	1 hr	BN	10/2.5
20	Dow	YF ₃	5 v/o	1830	1 hr	BN	10/2.5
22	Denka	CeO ₂	0.5 v/o	1870	1 hr	BN	10/2.5

These batches were prepared in 3000 gram lots (AlN powder basis). First a binder solution of ethanol, PG E3350 and ECB (2:1 ratio, 6.7 % by wt. AlN) was

prepared by milling for 24 hr. Then, fish oil (0.5%) and the sintering aid was added to 2250 grams of ethanol in a 7 gallon alumina lined ball mill with Al_2O_3 media. After a brief milling period to ensure appropriate mixing, the AlN powder was added and milled for 2 hours. At this time, the binder solution was added and milling was continued for 5 hours. The ceramic slurry was then spray dried in the Niro solvent dryer described earlier. All of the mixes were prepared within a month time period. The batch numbers reflect the preparation order which was adjusted to minimize clean-up between runs. Compositions with similar sintering aids were done during the same cycle, with the finest powder being spray dried first. The spray dryer and collection areas were completely cleaned and flushed out when the sintering aid was changed. Product yields and particle characteristics are shown in Table XV.

Table XV
Spray Dried AlN Product for Ballistic Screen

Batch #	Powder/ Sinter Aid	Product (g)	Fines (g)	Total Yield %	Size (μm)	Flow Rate (g/sec)	Tap (g/cc) Density
1/2	Sumi/ CeO_2	4897	828	83.7	98	0.23	0.70
3	Denka/ CeO_2	2454	341	81.7	77	0.60	1.05
4	Toyo F/ CeO_2	1204	1592	81.7	77	0.54	1.08
5/6	Toyo F/ Y_2O_3	5091	1251	91.0	96	0.48	1.13
7	ART/ Y_2O_3	2344	391	78.5	77	0.00	1.11
8	Sumi/ CaO	1876	419	70.8	77	0.30	0.71
9	Denka/ CaO	2118	297	74.4	77	0.53	1.00
10	Toyo F/ CaO	2174	356	78.0	116	0.49	1.11
11	Sumi/ La_2O_3	2041	612	81.7	77	0.18	0.77
12	Denka/ La_2O_3	2230	404	81.1	77	0.54	1.11
13	ART/ YF_3	2184	321	83.0	77		1.14
14	Dow	1979	456	81.2	63	0.44	1.03
15	Dow/ Y_2O_3	2181	406	85.5	77	0.40	1.03
16	Dow/ Y_2O_3	2358	391	84.1	77	0.48	1.05
17/18	Dow/ CeO_2	3766	613	72.5	77	0.32	1.11
19	Dow/ La_2O_3	1895	223	69.9	77	0.28	1.10
20	Dow/ YF_3	2242	301	79.6	77	0.62	1.05
22	Denka/ CeO_2	2158	394	84.5	77	0.51	1.10

Based on the median size, flow rates and tap density values, it is very clear that this spray dry formulation is not optimized. For dry press applications, all of these parameters should be substantially higher. In particular, the finest powder overall, Sumitomo ANH-10, had the poorest flow characteristics and particle packing density. The relatively low solids loading (15%) was largely responsible for most of the product being less than 100 μm . The three nitrided aluminum powders had the best product characteristics for dry pressing ceramic greenware, as expected from their original particle size distributions.

Ten tiles of each composition were dry pressed at 104 MPa (15,000 psi) in a 10 cm (4 inch) steel die using ~160 grams of powder. For binder removal, a fused quartz sample holder was manufactured. This holder was designed so that the tile could set vertically, allowing for good airflow around the tiles and complete binder removal. A forced air convective oven[#] was used for binder removal. The heating schedule started with a ramp rate of ~2°C/min to 550°C, followed by a 5 hour hold at 550°C and ended with a cooling rate ~2°C/min. If the furnace was not allowed to cool below 100°C prior to opening the oven, fracture of the greenware was likely due to thermal shock. After measuring the physical dimensions of the tiles, the samples were stacked in either a graphite or boron nitride crucible. The use of boron nitride powder between the tiles eliminated any sticking problems which could occur during sintering. The heating rates and sintering temperatures for each sample set were listed in Table XIV. The switch to the slower ramp rate occurred at 1500°C. A graphite resistance heated furnace was used throughout this project.* The heating rates used for the first few batches were the same as those used previously during the screening study. Heating rates were reduced substantially due to poor tile yields from thermal shock failures during the heat-up phase of the sintering cycle. Reducing the rates down to 10°C/min and 2.5°C/min respectively, eliminated this source of failure.

Table XVI summarizes the sintering results for these 21 sets of samples. Except for some early samples where there were burnout and sintering problems, tile uniformity and consistency was excellent. During the runs which used a

[#] Model CW-8880F, Blue M, Blue Island, IL

* Model 121212G, Thermal Technology, Brew Division, Concord, NH

graphite crucible, the top and often the bottom tiles were severely distorted due to an inhibition of the sintering process on the surfaces exposed to the graphite. Consistent with earlier observations, green densities for the compositions containing powders synthesized by a nitrided aluminum process were significantly higher than the materials prepared with Dow or Sumitomo powders and accordingly shrinkages were substantially higher for these two powders as well. In general, the fired densities were lower than anticipated even though higher temperatures and longer times were generally used than that required to achieve full density during the preliminary sintering studies.

Table XVI
Average Values for Sintered AlN Tile Sets

Batch #	Powder/ Sinter Aid	Green Density	Weight Loss (%)	Shrinkage Radial(%)	Fired Density	% T.D.
1	Sumi/CeO ₂	1.697±.004	0.53±.02	20.9±0.1	3.363±.001	98.91±.03
2	Sumi/CeO ₂	1.677±.005	1.28±.09	20.6±0.1	3.311±.006	97.38±.18
3	Denka/CeO ₂	1.874±.010	0.73±.37	18.4±0.1	3.359±.002	98.79±.05
4	Toyo F/CeO ₂	1.983±.006	0.36±.01	16.7±0.1	3.354±.004	98.59±.15
5	Toyo F/Y ₂ O ₃	1.984±.018	0.61±.27	15.5±0.2	3.313±.006	98.73±.19
6	Toyo F/Y ₂ O ₃	1.979±.011	0.39±.04	16.1±0.1	3.344±.012	99.65±.36
7	ART/Y ₂ O ₃	1.915±.008	0.22±.03	17.2±0.1	3.345±.003	99.66±.08
8	Sumi/CaO	1.606±.007	0.77±.19	20.8±0.1	3.217±.006	98.68±.17
9	Denka/CaO	1.860±.009	0.54±.19	17.1±0.1	3.223±.021	98.87±.65
10	Toyo F/CaO	1.940±.006	0.53±.22	16.0±0.1	3.204±.020	98.27±.60
11	Sumi/La ₂ O ₃	1.610±.011	0.54±.04	21.3±0.1	3.266±.001	99.68±.02
12	Denka/La ₂ O ₃	1.848±.027	0.66±.05	17.6±0.2	3.211±.020	98.02±.61
13	ART/YF ₃	1.883±.010	0.70±.07	16.6±0.1	3.191±.002	97.75±.06
14	Dow	1.696±.013	0.36±.02	19.3±0.1	3.187±.001	97.77±.03
15	Dow/Y ₂ O ₃	1.692±.014	0.41±.02	19.5±0.2	3.253±.002	99.52±.05
16	Dow/Y ₂ O ₃	1.729±.008	0.35±.02	19.7±0.1	3.316±.005	98.81±.16
17	Dow/CeO ₂	1.707±.002	0.33±.01	19.3±0.1	3.206±.002	97.74±.07
18	Dow/CeO ₂	1.718±.007	0.93±.08	19.1±0.2	3.222±.009	98.23±.27
19	Dow/La ₂ O ₃	1.708±.014	0.50±.20	19.7±0.1	3.239±.001	98.86±.04
20	Dow/YF ₃			18.7±0.1	3.188±.011	96.68±.33
22	Denka/CeO ₂	1.887±.011	0.54±.03	17.0±0.1	3.182±.002	97.01±.05

Using insights gained during the production of the thin tiles and the light caliber ballistic results which will be detailed later, five formulations were selected for scale-up. The compositions chosen were equivalent to batch numbers 9, 11, 12, 14, and 17. Only the higher surface area powders were utilized for this series of samples because of the need to minimize the sintering aid level. Examination of calcium oxide, cerium oxide and lanthanum oxide as sintering aids continued through this phase of the program as well. The characteristics of the powders used for this task are listed in Table XVII. These lots were very similar to the powders used previously. One difference worth noting was that the calcium content of the Dow powders had been lower with each lot received.

Table XVII
AlN Powder Used in Preparing Large Sintered Tiles

POWDER	Sumitomo	DOW	DOW	DENKA
GRADE	ANH-10	ARMOR	ARMOR	AP-10
LOT #	H18102	890629-48	890927-72	10PF8625
TYPE	Carbothermal	Carbothermal	Carbothermal	Nitrided Al
SIZE (μm)	1.19	1.68	1.98	1.81
SEM values				
High (μm)	0.6	1	1.4	3
Low (μm)	0.1	0.2	0.3	0.1
Mean (μm)	0.3	0.4	0.5	1.0
BET (m²/g)	4.6	2.97	3.09	3.64
O (wt. %)	1.19	1.15	1.23	1.54
C (wt. %)	0.04	0.13	0.19	0.10
Fe (ppm)	< 5	26	68	133
Si (ppm)	23	176	186	126
Ca (ppm)	35	444	158	<10
Cr (ppm)	< 5	16	< 5	< 5

10 kg batches were prepared using the same mixing and spray dry procedures outlined earlier. Prior to pressing the large (12.7 cm dia.) tiles, small pellets were pressed, burned-out (air, nitrogen and nitrogen/air) and sintered (1775°C and 1900°C) to qualify these formulated products. Using green density and shrinkage factors, weights and expected tile thicknesses for the large pressed AlN tiles were determined. Greenware from carbothermal powders required less material because to achieve the same fired thickness, the diameters will

be smaller due to a higher shrinkage and hence overall the tile would be lighter. Initially, three tiles at the two thicknesses were pressed for compositions 25 through 28. One tile of each size was prepared from batch 29 due to a shortage of powder and only large tiles were pressed for the later batches. However, because of load limitations of the uniaxial press, the planned thicknesses could not be achieved. A comparison of expected and actual thicknesses for the scaled up compositions are shown in Table XVIII. A pressing pressure of only 69 MPa could be achieved instead of 104 MPa which was used previously when preparing the 10 cm tiles. The lower pressure reduced the average green density by ~ 5% for all of the formulations. There was less than 1% density improvement for the 4.5 cm thick tiles compared to the thicker ones. A spray lubricant* was used to reduced die wall friction. The pressing cycle consisted of a two minute ramp, a 15 sec. dwell and a one minute release sequence. In an attempt to improve greenware strength and uniformity, tiles prepared from batches 30 through 35 were isopressed at 207 MPa, after uniaxial pressing.

Table XVIII
Selected Sintered AlN Samples for LRP Testing

Batch #	Powder	Sinter Aid	Level	Tile Size (cm)		Green Density		Sinter Temp.
				Expected	Actual	Small	Large	
25(14)	Dow			6.39	6.78	1.63	1.62	1925°C
26(17)	Dow	CeO ₂	0.5 v/o	6.41	6.83	1.64	1.62	1800°C
27(9)	Denka	CaO	0.5 v/o	6.09	6.38	1.78	1.79	1925°C
28(12)	Denka	La ₂ O ₃	0.5 v/o	6.27	6.58	1.76	1.76	1925°C
29(11)	Sumi	La ₂ O ₃	0.5 v/o	6.43	6.72	1.56	1.55	1775°C
30(14)	Dow				6.35	• •	1.88	1925°C
31(17)	Dow	CeO ₂	0.5 v/o		6.39	• •	1.88	***
32	Dow	CeO ₂	2.0 v/o		6.48	• •	1.83	***
33	Dow	La ₂ O ₃	0.5 v/o		6.27	• •	1.87	1800°C
34(12)	Denka	La ₂ O ₃	0.5 v/o		6.27	• •	2.06	1925°C
35(9)	Denka	CaO	0.5 v/o		6.03	• •	2.05	1925°C

• • Tiles isopressed at 207 MPa, *** Tiles failed during Burnout.

* CRAMOLIN R-5, Craig Laboratories, Escondido, CA

All of these tiles were burned out using a constant weight loss schedule. A flowing nitrogen atmosphere was used throughout the binder removal process, since it was felt that the evolution of gases could be more easily controlled in that environment. Based on the preliminary trial runs for the first five batches, the burnout atmosphere was switched from nitrogen to air during the 4 hr hold period at 550°C for batches 25, 27, and 28, and 30 to 35. By reducing the carbon levels in the greenware, this change effectively increased the oxide levels available for aiding densification. The burn out schedules were calculated using a weight loss rate of 0.09 g/min while imposing a maximum heating rate limit of 2°C/min. A representative schedule for a large (1498 g) tile is shown below:

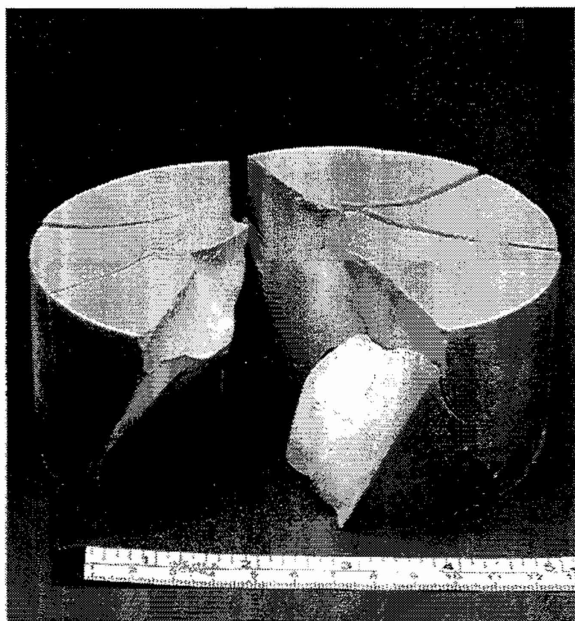
25°C to 338°C in 2.61 hr (2°C/min) Nitrogen
338°C to 428°C in 16.13 hr (0.09°C/min) Nitrogen
428°C to 550°C in 1.02 hr (2°C/min) Nitrogen
hold at 550°C for 4 hr Air
Cooling from 550°C to 50°C in ≥ 8 hr ($<2^\circ\text{C}/\text{min}$)

Tile yields after the binder removal step were only 50% for most compositions and most of the failures occurred with the larger tiles. Isopressing, which had a dramatic effect on the green density of the pressed tiles, did not appear to impact the burnout process. Tiles from batches 31, 32 and most of 33 failed during this step, while tiles from batches 30, 34 and 35 survived including the controls which were only uniaxially pressed. Some of the observed problems could have been attributed to powder and/or chemistry factors. Despite some obvious inconsistencies in the data, inherent weakness from low and nonuniform green density still appears to have been the major cause of greenware failure.

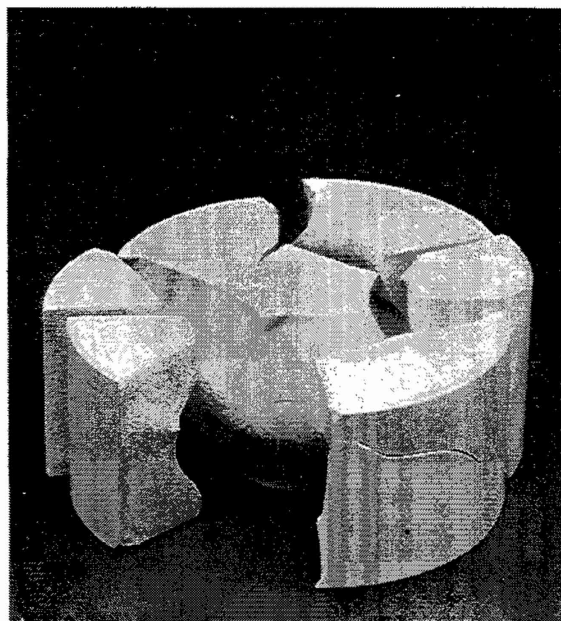
Process yields during the sintering step were also disappointing, but achieving high density parts was not determined to present any problem. The tiles were first placed in a covered boron nitride box. Sintering schedules which were found to be suitable for the standard 3 w/o yttria formulation, consisted of an initial heating rate of 10°C/min. to 1200°C, then 2.5°C/min. to the sintering temperature. After holding at the sintering temperature for one to three hours, the furnace was cooled down using a rate of 2.5°C/min. However, because of early cracking problems, which appeared to develop before the onset of densification, the heating rate was reduced to 2.5°C/min. during the entire heating and cooling cycle. In retrospect, the faster schedules were probably appropriate for these parts since the failures could be attributed to other factors.

Figure 25 shows some of the typical failures which occurred during sintering. The presence of chemical gradients in large parts, which was alluded to earlier, appears to have led to differential shrinkage during sintering and ultimately a cracked part (figure 25A). This failure occurred exclusively in tiles from batch 26. This composition was burned out in nitrogen only and apparently higher carbon levels (lower oxygen) in the center of the tile inhibited the sintering process to create sufficient tensile stresses on the surface to crack the parts. The major tile failure however was due to density gradients which, when subjected to thermal stresses, eventually led to cracked components. The position of the cracks was consistent with probable pressure contours which have been shown to exist for uniaxially pressed parts with an I/D ratio of 0.5.²⁶ In the extreme case (figure 25B), the outer sections completely separated, leaving a flattened ellipsoidal core. This fracture pattern was similar to some of the earlier failures which occurred during binder removal. The less severe examples had thin hairline surface cracks primarily on the perimeter of the large disks. Internal bloating was also observed primarily with tiles from batch 35 which were isopressed. There was no cracking evident with these tiles, but lower than expected densities and some distortion on the top and bottom surfaces suggested the unanticipated bloating problem. Cutting a batch 35 tile in half, vividly revealed the internal fissures (figure 25C). The control, which was not isopressed, for batch 35 was high density (3.22 g/cm³) and there was no indication of large internal voids. Isopressing, clearly improved the parts green density, but that improvement had little impact on either product yield or fired density.

Overall, 18 out of 62 tiles were sintered intact. Successful parts with densities >98 % T.D. came from batches 25, 27, 28, 29, 34 and 35. Tiles prepared from batches 29 and 34 had the best overall visual quality, with regard to flatness, color uniformity and surface finish. Samples for ballistic testing were selected from these tiles. The difficulties encountered in obtaining high quality sintered AlN during this contract have largely been avoided in Dow's ceramic armor development facility. Automated pressing equipment with higher load capabilities, consistent powder characteristics and more effective I/D ratios (larger tile sizes) have all contributed to the successful transfer of this low-cost, dry-press, sinter fabrication technology.



A



B

C

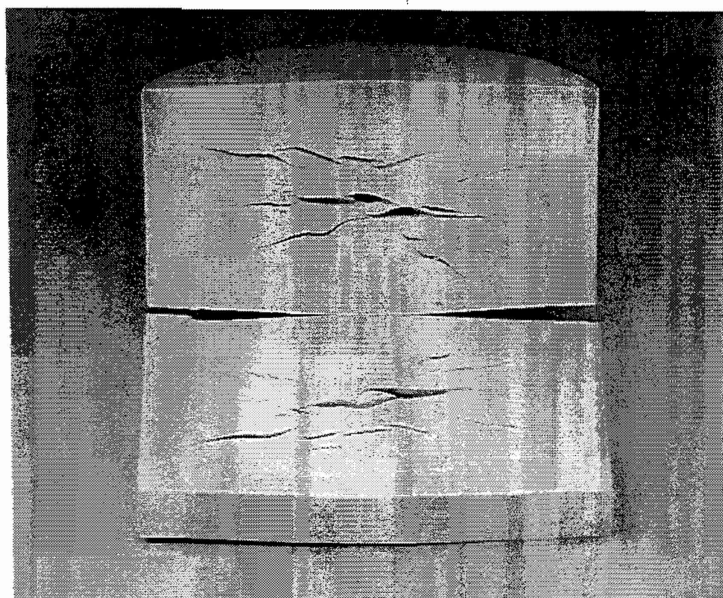


Fig. 25. Typical failures observed in fabricating large AlN tiles. A) Chemical nonuniformities led to differential shrinkage during sintering; B) Pressure gradients during dry pressing led to characteristic failure during sintering and C) Elevated temperature gas evolution led to tile distortion and internal bloating.

2.2.4 PHYSICAL AND MECHANICAL PROPERTIES

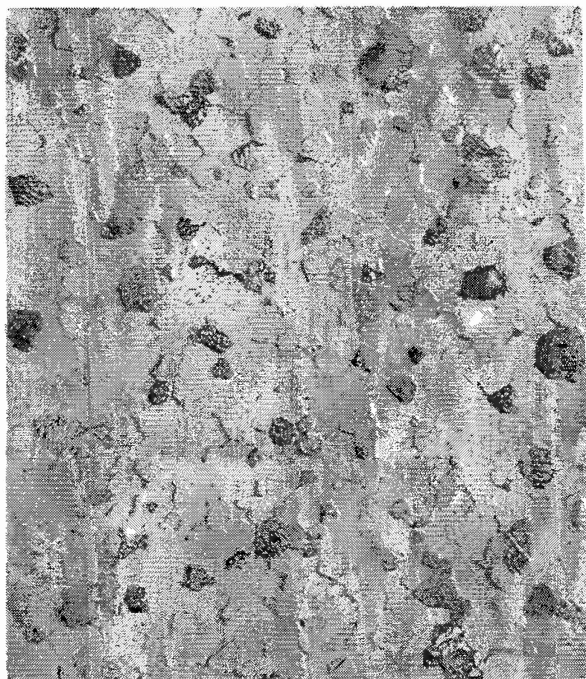
The physical and chemical characteristics for the 21 sintered aluminum nitride formulations are detailed in Table XIX. Methods employed for determining weight percent oxygen and carbon, grain size, and density were described earlier in section 2.1.3. Oxygen values reflected the level of sintering aid addition, while carbon values were relatively constant. For the X-ray diffraction specimens, sintered tiles were crushed to -45 mesh with a Plattner's diamond impregnated steel mortar and pestle set. Diffraction patterns were obtained from 20° to 70° 2θ for each composition using Cu K α radiation. Secondary phases were identified with computer interfaced peak searching software. The compounds identified reflect the chemistry of both the starting AlN powder and the specific sintering aid, as well as the sintering environment. The influence of the more reducing graphite crucible, which was used when sintering samples from batches 2 and 5 is reflected in both higher carbon and lower oxygen contents and also by the presence of oxynitrides and oxide phases which are deficient in alumina. This chemistry difference led to somewhat lower densities when compared to their equivalent counterparts, batches 1 and 6 respectively, which were sintered in BN. Since densification of aluminum nitride proceeds through a liquid phase sintering mechanism, the presence of low melting phases, which were primarily aluminates, is essential. X-ray diffraction results confirmed how the sintering aids studied during this contract reacted with the oxide surface layer on AlN powders to affect densification.

Based on the grain size measurements, batches (1, 2), (5, 6), and (17, 18) should provide excellent insights into the effect grain size has on ballistic performance. Photographs of etched polished sections, figure 26, vividly show the comparison between two of these paired sets of materials. There was a factor of 3 to 4 difference in grain size for these sample pairs. As expected from the size of the starting powders, the lowest average grain size was achieved with both carbothermally produced powders. In the temperature range employed, the resultant microstructure did not appear to be sintering aid dependent, and was clearly controlled by the sintering time and temperature.

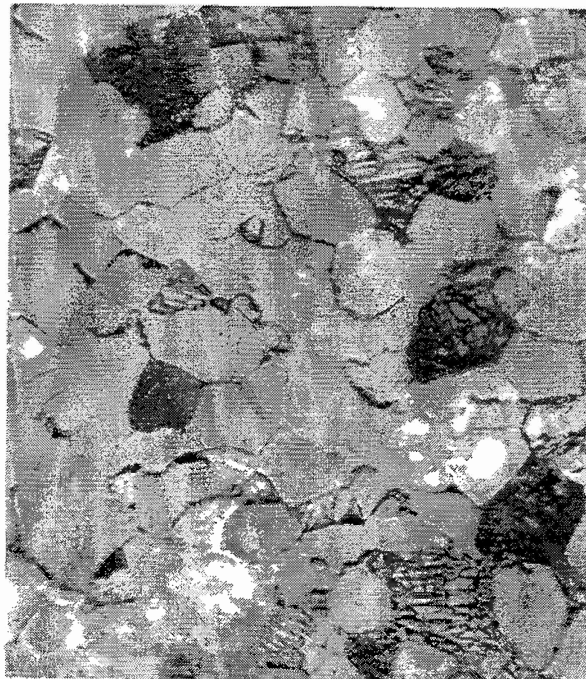
Table XIX
Physical and Chemical Properties of Selected Sintered AlN Samples

Batch #	Sinter Aid/Level	Density g/cm ³ (%)	Phases - X-Ray Diffraction [§]	Gr. Size μ m	Oxygen wt %	Carbon wt %
1	CeO ₂ /5.0	3.363(98.9)	CeAlO ₃ /Al ₂ O ₃	4.2±1.2	2.75	0.02
2	CeO ₂ /5.0	3.311(97.4)	Ce ₃ O ₃ N/CeAlO ₃ /CeO ₂	11.0±4.0	2.09	0.29
3	CeO ₂ /5.0	3.359(98.8)	CeAlO ₃ /Al ₂ O ₃	4.6±1.5	3.29	0.05
4	CeO ₂ /5.0	3.354(98.6)	CeAlO ₃ /Al ₂ O ₃	5.1±1.8	3.26	0.02
5	Y ₂ O ₃ /5.0	3.313(98.7)	Y ₂ O ₃ /Al ₂ Y ₄ O ₉ /Al ₁₀ N ₈ O ₃	14.0±5.3	2.57	0.46
6	Y ₂ O ₃ /5.0	3.344(99.7)	AlYO ₃ /Al ₂ Y ₄ O ₉	4.5±1.8	3.44	0.03
7	Y ₂ O ₃ /5.0	3.345(99.7)	AlYO ₃ /Al ₂ Y ₄ O ₉ /Al ₂ O ₃	5.4±1.8	3.69	0.05
8	CaO/0.5	3.217(98.7)	CaAl ₁₂ O ₁₉ /CaAl ₄ O ₇	6.1±2.0	1.07	0.09
9	CaO/0.5	3.223(98.9)	CaAl ₁₂ O ₁₉ /CaAl ₄ O ₇	5.5±1.7	2.35	0.07
10	CaO/0.5	3.204(98.3)	CaAl ₁₂ O ₁₉ /CaAl ₄ O ₇	7.1±2.5	2.28	0.05
11	La ₂ O ₃ /0.5	3.266(99.7)	LaAlO ₃ /LaAl ₁₁ O ₁₈	2.6±1.0	1.85	0.01
12	La ₂ O ₃ /0.5	3.211(98.0)	LaAlO ₃ /LaAl ₁₁ O ₁₈	4.9±1.5	2.12	0.47
13	YF ₃ /0.5	3.191(97.8)	AlYO ₃	10.2±4.3	1.59	0.04
14		3.187(97.8)	Al ₁₀ N ₈ O ₃ /Al ₂ O ₃	4.5±1.7	1.36	0.09
15	Y ₂ O ₃ /0.5	3.253(99.5)	Al ₅ Y ₃ O ₁₂	3.8±1.4	1.63	0.07
16	Y ₂ O ₃ /5.0	3.316(98.8)	Al ₂ Y ₄ O ₉ /AlYO ₃	3.6±1.3	3.05	0.04
17	CeO ₂ /0.5	3.206(97.7)	Al ₂ O ₃ /CeAlO ₃	2.9±1.0	1.66	0.08
18	CeO ₂ /0.5	3.222(98.2)	CeAlO ₃ /Al ₂ O ₃	12.8±5.1	1.27	0.09
19	La ₂ O ₃ /0.5	3.239(98.9)	LaAlO ₃ /LaAl ₁₁ O ₁₈	5.7±2.4	1.74	0.12
20	YF ₃ /5.0	3.188(96.7)	Y/Al ₅ Y ₃ O ₁₂ /YF ₃	3.9±1.6	1.44	0.09
22	CeO ₂ /0.5	3.182(97.0)	Al ₁₀ N ₈ O ₃ /Al ₂ O ₃ /AlBO ₃	4.9±1.8	2.14	0.04

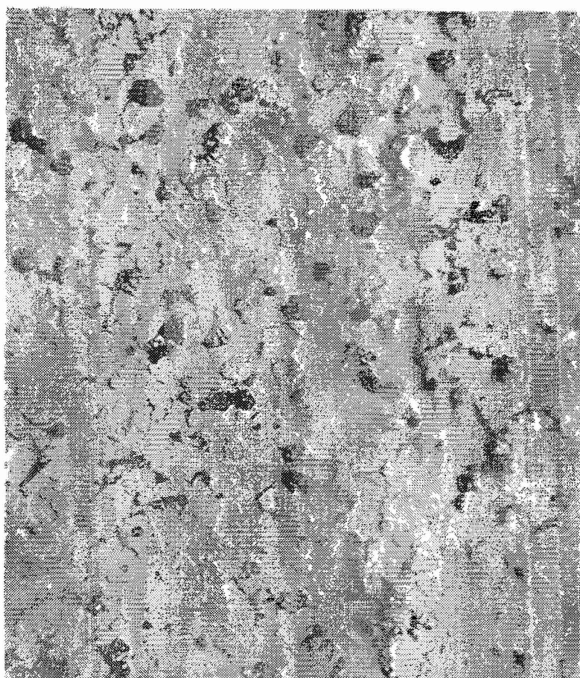
[§] Crystalline phases identified in addition to AlN. Compounds listed in decreasing order of peak intensity.



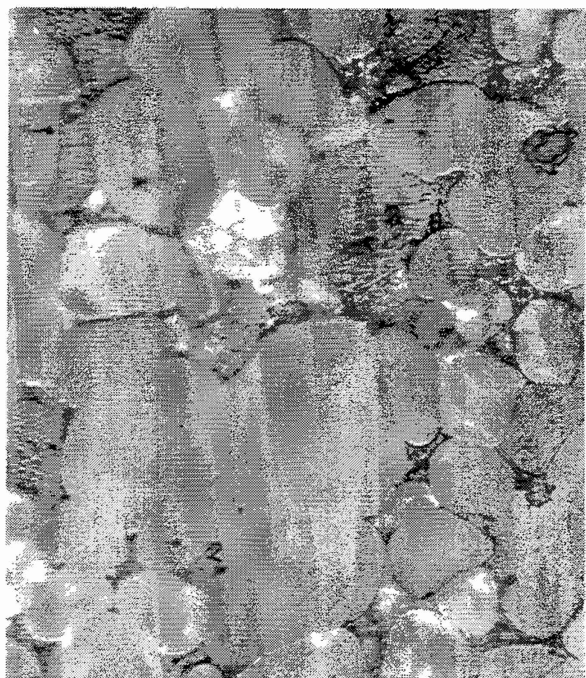
BATCH 1



BATCH 2



BATCH 6



BATCH 5

Fig. 26. Photomicrographs of etched polished sections showing dramatic grain size differences among paired AlN batches with 5 % CeO₂ (1, 2) and 5% Y₂O₃ (5, 6). All photomicrographs at 1000x magnification.

Mechanical evaluation of these tiles included microhardness, flexure strength, compressive strength (static and dynamic), and sonic properties. While the intent was to have two complete tiles of each composition for testing, processing losses often limited the amount of material available for analysis. Mechanical characterization of these compositions is detailed in Table XX. Microhardness numbers were determined from polished sections using a Vickers diamond indenter at a load of 9.8 N. Since a materials hardness is adversely affected by even low levels of porosity and the presence of grain boundary phases, measured values for the sintered compositions were all lower than those measured for the hot-pressed powders. Batch 14, which contained no sintering aid, had the highest average hardness. Samples with higher levels of sintering aid generally had lower hardness numbers and the lowest values were obtained from compositions which contained YF_3 .

Flexure strengths were determined with as few as 3 bars and with as many as 31 using MIL std 1942B. Strength values for the sintered aluminum nitride were comparable with those for the hot-pressed materials. Factors which had the greatest influence on the average fracture strength were grain size and the presence of YF_3 and to a lesser extent CaO . Strength numbers were 30 to 40% lower for those compositions. Tiles prepared with a high surface area powder (Dow, Denka or Sumitomo) and containing 0.5 v/o ceria or lanthana had the highest measured values at ~350 MPa.

Compressive strength data was generated by J. Lankford, SwRI using equipment and procedures outlined earlier. These were single data points tested at three distinct strain rate regimes using small right cylinders (0.64 cm dia. x 1.27 cm long). In general, the compressive strength increased with strain rate, but the biggest increase was observed when the samples were tested under dynamic loading conditions. There also appeared to be a direct correlation between the quasi-static and dynamic compressive strength values. The linear correlation coefficient was 0.83 at a significance level of 0.0001. The agreement was particularly strong at the high and low strength values as shown in figure 27, where the relative ranking for these materials is plotted for the two compressive strength measurements. It could then be inferred that the microstructural characteristics which control the dynamic and quasi-

static compressive strengths appear to be very similar for these AlN compositions.

Table XX
Mechanical Characterization of Selected AlN Compositions

Batch #	Density g/cm ³ (%)	Gr. Size μm	Hardness GPa	Flex Strength MPa (# of Bars)	Compressive Strength MPa (Strain Rate 1/sec)		
					(.0004)	(0.6)	(2500)
1	3.363(98.9)	4.2 \pm 1.2	9.5 \pm 0.3	340 \pm 24 (9)	3111	3314	4320
2	3.311(97.4)	11.0 \pm 4.0	8.7 \pm 0.6	204 \pm 53 (9)	2636	2794	3765
3	3.359(98.8)	4.6 \pm 1.5	9.8 \pm 0.4	322 \pm 32 (11)	2971	3429	4298
4	3.354(98.6)	5.1 \pm 1.8	9.7 \pm 0.7	322 \pm 19 (4)	2772	3449	4306
5	3.313(98.7)	14.0 \pm 5.3	8.1 \pm 1.5	267 \pm 40 (3)	2128	1911	3128
6	3.344(99.7)	4.5 \pm 1.8	8.9 \pm 0.9	317 \pm 48 (26)	2857	3198	4270
7	3.345(99.7)	5.4 \pm 1.8	9.6 \pm 0.5	304 \pm 25 (7)	3397	3400	4209
8	3.217(98.7)	6.1 \pm 2.0	9.4 \pm 0.7	279 \pm 28 (6)	3486	3688	4683
9	3.223(98.9)	5.5 \pm 1.7	9.7 \pm 0.5	268 \pm 23 (31)	2918	3397	4185
10	3.204(98.3)	7.1 \pm 2.5	9.5 \pm 0.3	293 \pm 13 (22)	2846	2968	4116
11	3.266(99.7)	2.6 \pm 1.0	9.8 \pm 0.4	342 \pm 46 (7)	3448	3719	4921
12	3.211(98.0)	4.9 \pm 1.5	9.9 \pm 1.0	355 \pm 21 (19)	2442	3623	4573
13	3.191(97.8)	10.2 \pm 4.3	9.2 \pm 0.7	201 \pm 08 (15)	2339	2640	3710
14	3.187(97.8)	4.5 \pm 1.7	10.5 \pm 0.7	333 \pm 33 (6)	3317	3103	4613
15	3.253(99.5)	3.8 \pm 1.4	9.6 \pm 0.4	299 \pm 27 (10)	2988	3298	4309
16	3.316(98.8)	3.6 \pm 1.3	8.8 \pm 0.4	334 \pm 48 (8)	3071	3293	4101
17	3.206(97.7)	2.9 \pm 1.0	9.5 \pm 0.4	353 \pm 36 (24)	3149	3408	4412
18	3.222(98.2)	12.8 \pm 5.1	9.5 \pm 0.6	256 \pm 14 (7)	2464	2539	3895
19	3.239(98.9)	5.7 \pm 2.4	9.4 \pm 0.4	348 \pm 28 (22)	3246		4482
20	3.188(96.7)	3.9 \pm 1.6	7.0 \pm 0.5	214 \pm 34 (20)	1741		2911
22	3.182(97.0)	4.9 \pm 1.8	9.5 \pm 0.4	301 \pm 13 (16)	2800		4065
Std	3.266(98.7)	2.6 \pm 1.0	9.4 \pm 0.3	327 \pm 35 (9)			

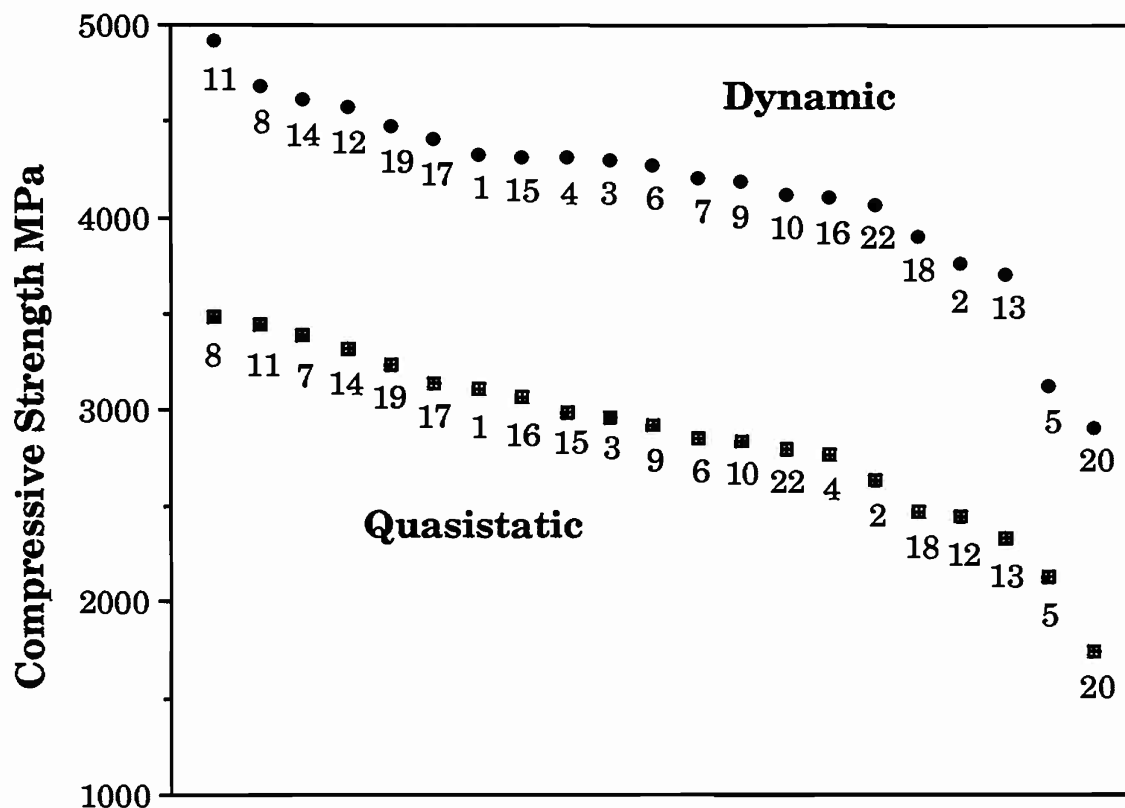


Fig. 27. Ranked compressive strength of 21 aluminum nitride compositions. Batch numbers are indicated below the data points.

Sonic properties, sound speeds, modulus and Poisson's ratio, were measured by the pulse-echo technique using flexure bar specimens from each composition. Reported values were an average of a minimum of ten measurements. These results are summarized in Table XXI. As expected, percent theoretical density had the largest effect on the elastic modulus. Sintering aid and level also appeared to have some impact. Poisson's ratio was not influenced by any of the measured microstructural or chemical differences identified for these materials.

Through the extensive evaluation of these materials, it has been demonstrated that high quality AlN ceramics can be manufactured using low cost raw materials. Higher surface area powders provide more processing flexibility by requiring lower sintering aid levels to achieve densification which allow for higher mechanical performance. Ceria and lanthana have been shown to be

cost effective alternatives to the higher priced yttrium based compounds. There appears to be a critical grain size where a significant decrease in mechanical performance occurs. The use of YF_3 substantially decreased the properties of sintered aluminum nitride ceramics.

Table XXI
Sonic Properties of Sintered Aluminum Nitride

Batch #	Sinter Aid/Level	Density g/cm ³ (%)	Young's Modulus GPa	Poisson's Ratio	Sound Speeds Long. m/sec	Shear m/sec
1	CeO ₂ /5.0	3.363(98.9)	303	.240	10375	6068
2	CeO ₂ /5.0	3.311(97.4)	303	.234	10277	6053
3	CeO ₂ /5.0	3.359(98.8)	308	.244	10364	6031
4	CeO ₂ /5.0	3.354(98.6)	305	.242	10344	6038
5	Y ₂ O ₃ /5.0	3.313(98.7)	288	.245	10420	6058
6	Y ₂ O ₃ /5.0	3.344(99.7)	303	.236	10431	6127
7	Y ₂ O ₃ /5.0	3.345(99.7)	310	.240	10397	6084
8	CaO/0.5	3.217(98.7)	308	.241	10775	6296
9	CaO/0.5	3.223(98.9)	302	.238	10650	6247
10	CaO/0.5	3.204(98.3)	301	.239	10632	6223
11	La ₂ O ₃ /0.5	3.266(99.7)	318	.243	10718	6249
12	La ₂ O ₃ /0.5	3.211(98.0)	313	.240	10603	6200
13	YF ₃ /0.5	3.191(97.8)	304	.235	10547	6210
14		3.187(97.8)	306	.236	10665	6267
15	Y ₂ O ₃ /0.5	3.253(99.5)	314	.239	10655	6240
16	Y ₂ O ₃ /5.0	3.316(98.8)	303	.241	10484	6123
17	CeO ₂ /0.5	3.206(97.7)	310	.237	10692	6280
18	CeO ₂ /0.5	3.222(98.2)	312	.240	10689	6255
19	La ₂ O ₃ /0.5	3.239(98.9)	315	.239	10699	6264
20	YF ₃ /5.0	3.188(96.7)	270	.233	10033	5918
22	CeO ₂ /0.5	3.182(97.0)	299	.236	10459	6148
Std	Y ₂ O ₃ /3w/o	3.266(98.7)	317	.240	10662	6240

2.2.5 BALLISTIC STUDIES

Four types of ballistic tests were conducted during this phase of the contract. Targets were prepared for testing against several light caliber threats and the quarter scale, tungsten long rod penetrator (LRP). All ballistic tests were conducted at the University of Dayton Research Institute. The light caliber threats were used to screen the aluminum nitride compositions and help guide the selection of the LRP targets. Depth of penetration (D.O.P.) was the criteria used to evaluate the performance of these AlN compositions in three of four tests performed including the LRP shots. While ballistic limit data is preferred for designing armor, D.O.P. results have been shown to be effective as a means of evaluating ceramic materials.^{27,28}

2.2.5.1 Light Caliber Tests

Screening tests for the sintered aluminum nitride consisted of a ballistic limit determination with a .30 caliber AP simulant and D.O.P. measurements for a .50 caliber APDS bullet. The methodology developed by Wilkins in the early 60's for determining ballistic limit values for a ductile backed, ceramic faced armor has been used as a primary materials screening tool.²⁹ The target configuration is shown in figure 27. The use of this test allowed for a direct comparison with other ceramic materials and more importantly with the extensive aluminum nitride data base which had already been generated.¹⁸ All of the tiles were machined to a constant areal density of 2.5 g/cm^2 , then mounted onto the 6061-T6 aluminum backing plate with a thin adhesive bondline. Three concentric circles were painted onto the targets to enable some differentiation of ballistic fragments. Typically, six targets were prepared from each composition. Ballistic limit velocities were determined by averaging the highest partial and lowest complete penetrations. A maximum difference of 30 m/sec (100 fps) was the target range for these two values. Based on whether the previous shot was either a partial or complete penetration, the velocity was modified higher or lower by adjusting the powder charge. The results for this ballistic experiment are summarized in Table XXII. Included in this table is the relative efficiency (e_r) of these aluminum nitride compositions compared to the areal density of a boron carbide standard at a limit velocity of 823 m/s (2700 fps). Using this parameter, comparisons can be made with the existing data base. The measured relative efficiencies for

this aluminum nitride set were lower than previously reported values.¹⁸ A probable explanation of this result is the effect of tile size on the ballistic limit determination. In the previous study, 10 cm square tiles were tested compared to current 8.3 cm dia. disks. In addition, the boron carbide standard also had a lower, ~4%, measured ballistic limit, which was not taken into account during the calculation of e_r . Since the boron carbide tiles were from the same lot of material used previously, it is not expected that the consistency of the ceramic would be an issue. However, lot to lot variations in the aluminum backing material could have easily caused the observed discrepancy.

.30 Caliber Target

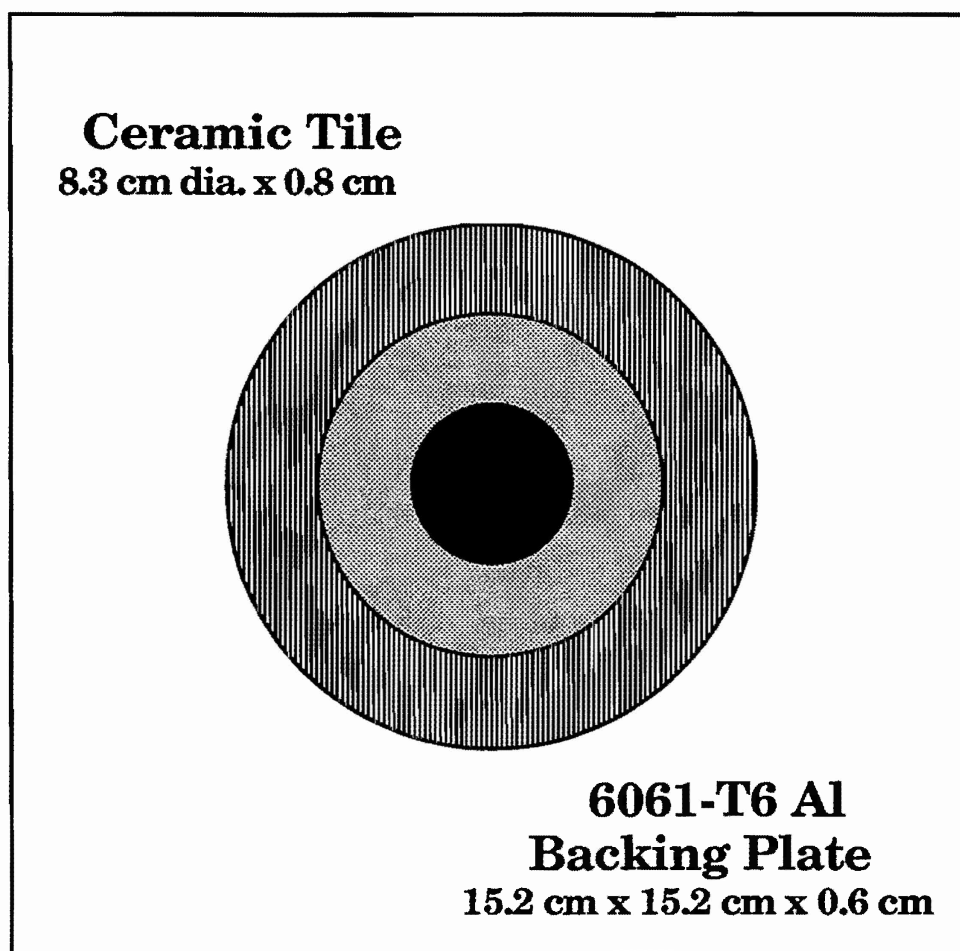


Fig. 28. Schematic of .30 caliber AP target. Unconfined ceramic mounted onto backing plate using a thin adhesive layer. Ceramic color coded to facilitate fragment analysis. Aluminum witness plate was mounted 2.5 cm behind target.

Table XXII
.30 Caliber AP Ballistic Limits for Sintered Aluminum Nitride

Batch #	Lowest Complete (m/sec)	Highest Partial (m/sec)	ΔV^{**} (m/sec)	V_{BL} (m/sec)	e_r
1	861	851	10	856	0.76
2	807	816	-9	811	0.72
3	844	842	3	843	0.75
4					
5	831	837	-6	834	0.75
6	853	845	8	849	0.76
7	834	844	-10	839	0.75
8	847	862	-16	855	0.77
9	865	851	14	858	0.77
10	831	842	-11	837	0.76
11	895	899	-5	897	0.82
12	853	843	10	848	0.76
13	826	832	-6	829	0.75
14	876	863	13	869	0.78
15	840	853	-13	846	0.75
16	809	826	-17	817	0.72
17	860	862	-2	861	0.77
18	635	633	2	634	0.47
19	851	854	-3	852	0.76
20	791	801	-10	796	0.69
22	841	841	0	841	0.76
Std	858	857	1	857	0.77

**** Negative numbers indicate zone of mixed results.**

Overall, the ballistic limit results were very similar. 16 out the 21 compositions tested had efficiency ratios between 0.75 and 0.78. There was one composition, batch 11, which had an e_r of 0.82 and was clearly superior to other

formulations. The lowest performing compositions had either a large average grain size, high levels of sintering aid, or contained yttrium fluoride. However, the dramatic reduction in e_r (0.47) for batch 18 was not expected even after considering the potential grain size effect.

Based on previous experiences with ballistic limit determinations, there was a concern that this technique would not be sensitive enough to differentiate the similar aluminum nitride compositions being studied during this phase of the contract. For this reason, targets were also prepared for depth of penetration (D.O.P.) measurements into thick, semi-infinite backing material.

AlN ceramics, having an areal density of 2.5 g/cm^2 , were mounted, unconfined to both faces of the 15.25 cm dia. x 30.5 cm long, aluminum cylinders. The targets were shot with a .50 caliber APDS bullet at a constant velocity of $857 \pm 4 \text{ m/sec}$ (2800 fps). Two tiles were tested of each composition. After testing, about 5 cm of the Al cylinder was cut off from each end for penetration depth determination by x-ray photography. The remaining aluminum block was refaced and used again for another series of shots.

The results of these tests are illustrated in figure 28, where the error bars represent the two measured values and the data points shown are the average of the two results. The measured penetration values ranged from 22 to 70 mm. Except for a few cases, the reproducibility of the penetration values for a given composition was not very good. Differences in penetration depths ranged from $<1 \text{ mm}$ to $>30 \text{ mm}$. However, most differences were between 4 and 10 mm and this represented a 10 - 40% variation. Because of this variability, it was difficult to make any judgments on the relative performance of these compositions with a high confidence level. There were some notable trends, however. Penetration depth increased with higher sinter aid levels and the poorest performing compositions (highest D.O.P. values) had microstructures with a large average grain size. As in the ballistic limit tests, batch 18 clearly had the lowest penetration resistance of the compositions tested. A comparison of penetration depths for batches 17 and 18 ($0.5\% \text{ CeO}_2$) showing the effect of grain size is vividly illustrated in figure 29.

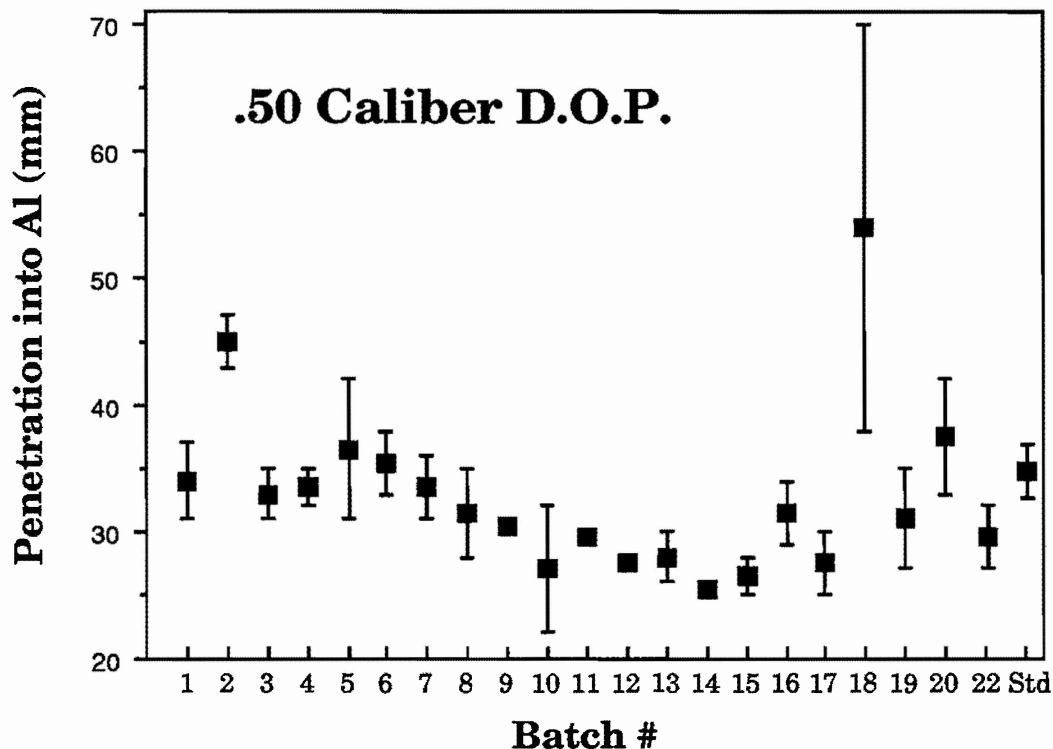


Fig. 29. Penetration results for .50 caliber APDS bullets shot at ~857 m/sec against aluminum nitride targets with an areal density of 2.5 g/cm² and backed by a semi-infinite aluminum cylinder.

Based on these light caliber ballistic tests, the achievement of maximum ballistic protection with aluminum nitride ceramics requires sintering aid levels to be minimized and sintering conditions controlled to avoid excessive grain growth. These requirements are most easily met by active AlN powders, such as the Dow, Denka or Sumitomo grades which have been evaluated during this contract. Within the ranges bounded by the AlN powders examined, powder purity does not seem to be a significant factor. In addition, except for the fluoride containing compositions, the chemistry of the grain boundary phase, which is controlled by the sintering aid used and the sintering conditions, does not appear to critically impact light caliber ballistic performance. A controversial issue within the armor community is whether D.O.P. type experiments adequately mirror armor system performance. In this particular case, there was not a one to one relationship between ballistic limit performance and penetration depth into a semi-infinite block. However, if results were divided into groups, such as high, low and average performers, then there was good agreement between these two testing methods.

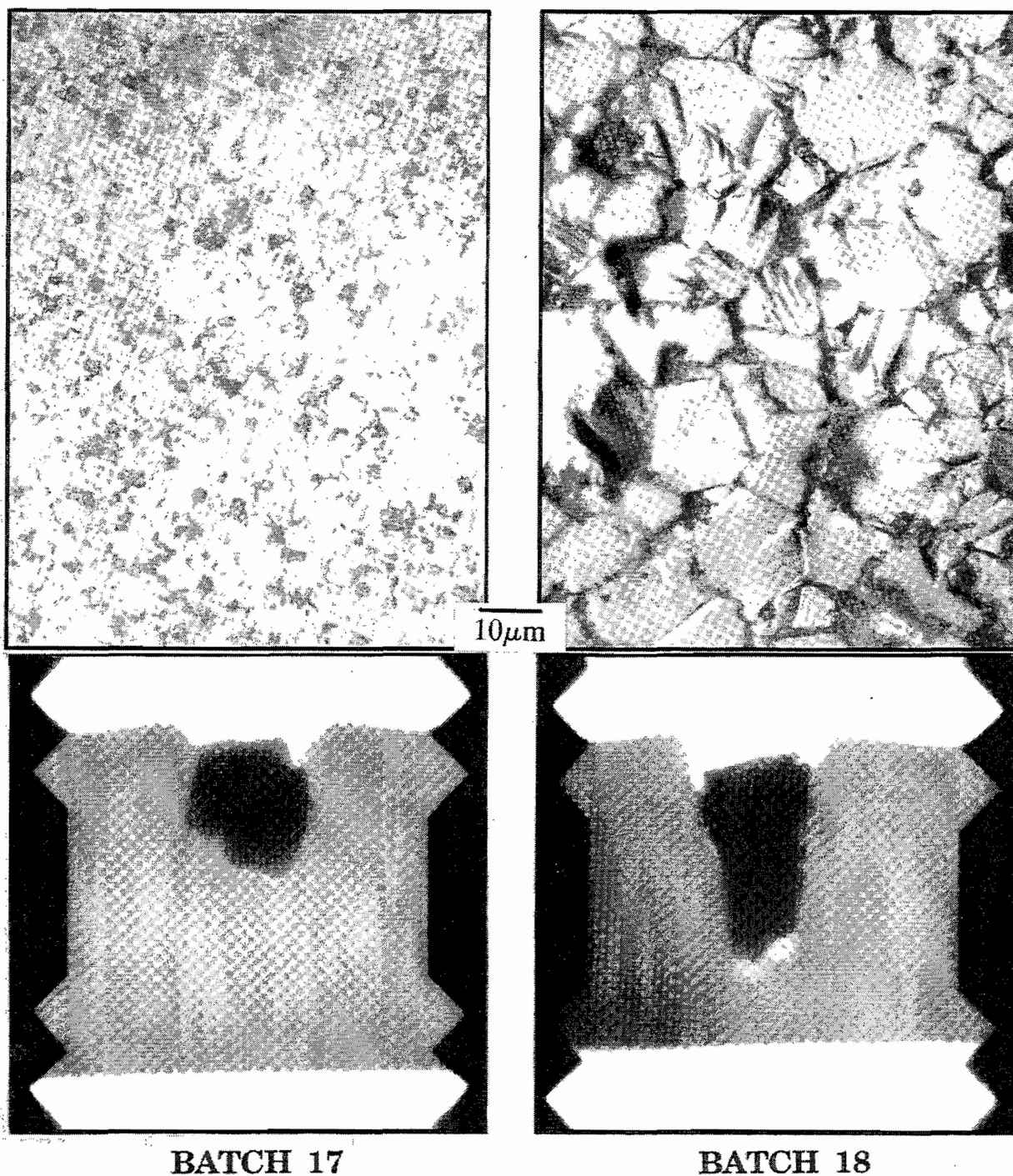


Fig. 30. X-ray photographs of .50 caliber targets showing penetration depths for two AlN materials of the same composition (0.5% CeO₂) but with noticeably different microstructures. The large grained material, batch 18, had a penetration of 38 mm, while the finer AlN, batch 17, had a value of 25 mm.

Previously, it was shown that the ballistic performance was related to the mode of fracture of the tile fragments and that the fracture mode changed with position from the impact zone.¹⁸ Fragments from targets which were tested near the ballistic limit were identified from the colored surface and examined with a scanning electron microscope (SEM). For this data set, fracture mode did not seem to correlate with performance and there were only a few examples where the mode of failure changed from transgranular near the impact region to intergranular away from the target area. The fracture mode was largely independent of position for most of these compositions. Except for the large grained materials (2, 5, 13 and 18), intergranular fracture was the dominate mechanism. Fracture surface examination is summarized in Table XXIII and representative microstructures are shown in figures 30 and 31.

Table XXIII
Microscopic Analysis of Ballistic Fragments

Batch #	Fracture Surfaces - Failure Mode
1	Mixed mode red & yellow zones, green largely intergranular
2	Center mainly transgranular, then intergranular dominates
3	Largely transgranular throughout
4	
5	Mostly transgranular with large pockets of second phase evident
6	Shift from mainly trans (red) to mainly intergranular (yellow)
7	Similar throughout, mixed mode, but largely intergranular
8	Intergranular throughout tile
9	Some transgranular, but largely intergranular throughout
10	primarily intergranular, but some trans throughout
11	Some limited trans , but intergranular clearly dominates
12	Primarily trans in red zone, shifting to mixed mode elsewhere
13	Exclusively transgranular
14	Mixed mode, shift from mostly trans (red) to mostly inter (yellow)
15	Some limited transgranular in red area
16	Intergranular throughout sample
17	Some limited transgranular, primarily in red zone
18	Primarily transgranular, some intergranular in yellow region
19	Transgranular (red) shifting to mixed mode (green and yellow)
20	Completely intergranular, thin continuous grain boundary phase
22	Primarily transgranular throughout
Std	Intergranular throughout sample

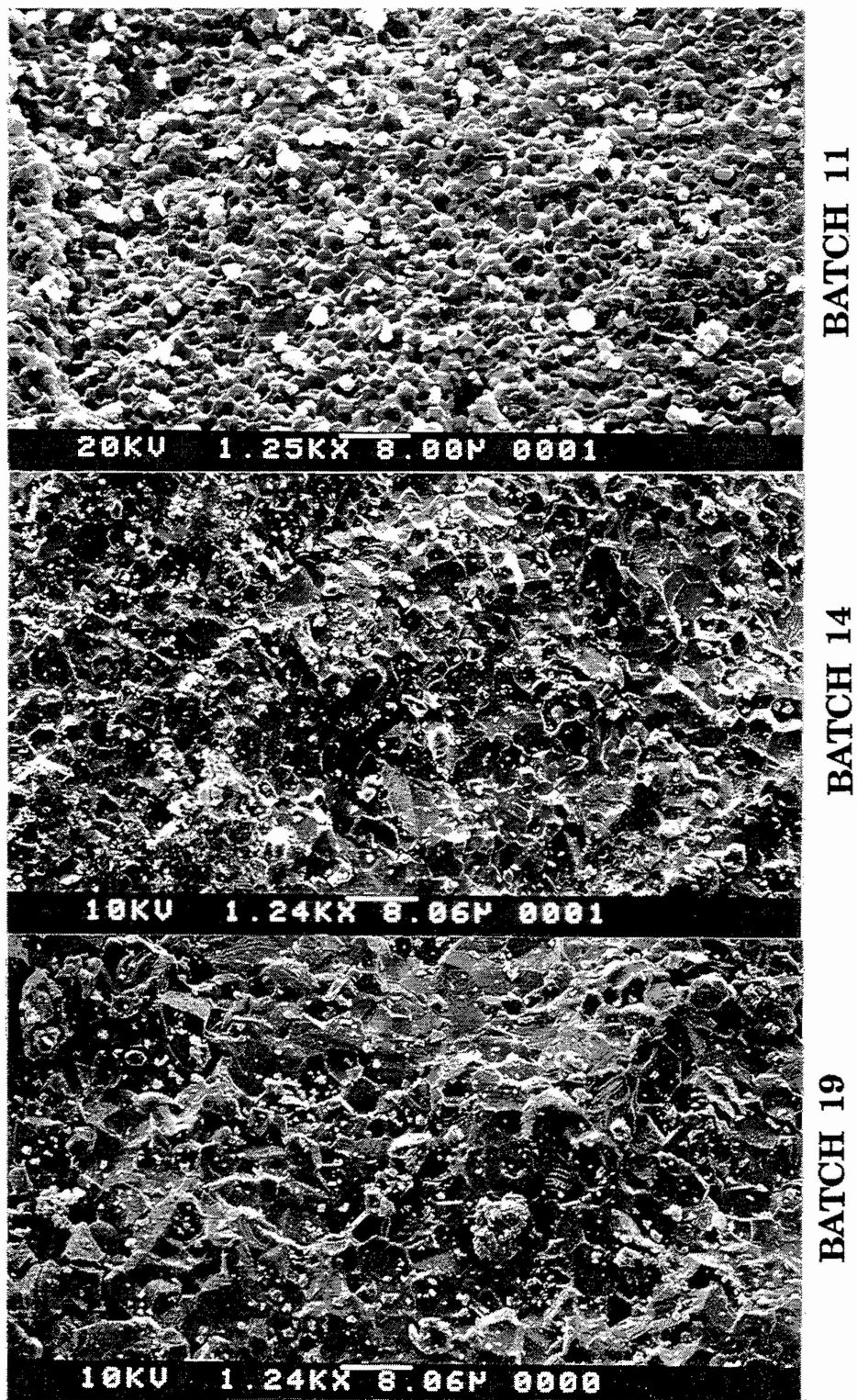


Fig. 31. SEM photomicrographs of fracture surfaces of .30 caliber ballistic rubble showing different fracture modes in impact area.

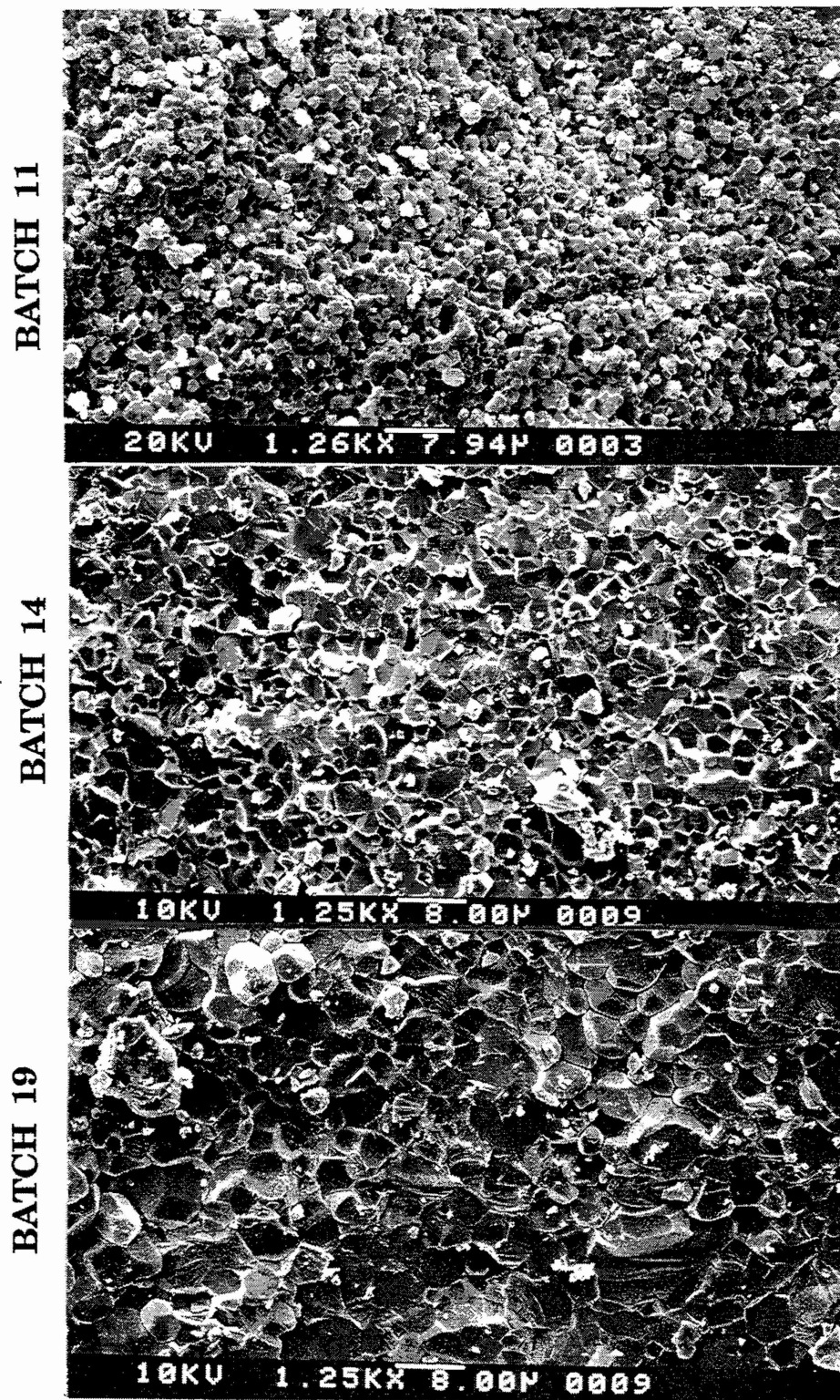


Fig. 32. Fracture surfaces of ballistic fragments taken from outer areas of tile.

2.2.5.2. LRP and SLAP D.O.P. Results

Ballistic performance, processability and potential manufacturing costs were the criteria used in selecting compositions for long rod penetrator (LRP) testing. The intent was to first test several compositions at an areal density of 10 g/cm² with the tungsten penetrator (L/D = 10), then based on those results, prepare one or two compositions with an areal density of 15 g/cm² for evaluation. Five formulations, batch numbers 9, 11, 12, 14, and 17, were chosen for this phase of the contract. Since materials with a moderate average grain size and lower sintering aid levels had better ballistic properties, only AlN powders which readily densified were considered for scale-up. Because of cost considerations, only non-yttrium based sintering aids which were previously examined were included. The compositions chosen had the best penetration resistance (≤ 31 mm) in the .50 caliber APDS D.O.P. tests and also had high ballistic limit values ($e_r \geq 0.76$) against the .30 caliber AP. Both 3 and 4.5 cm tiles were prepared for testing. The processing of these thick tiles was discussed in section 2.2.2.

During the latter stages of this contract, responsibility for LRP testing was transferred from SwRI to the University of Dayton Research Institute under the direction of Dr. S. Bless. While the primary objective of the program extension was to evaluate AlN/SiC composites there was some limited opportunity to test the thick, sintered AlN parts which were prepared during the earlier phases of this contract. Six shots with an L/D of 10 projectile were allocated for AlN testing. However, with additional support from Dow, a total of 12 targets were actually prepared and tested. The target configuration was nominally identical to that used during the SwRI shots (see figure 8), however the projectile used at UDRI was smaller at 65 grams (73 gram projectile was used at SwRI) and fired at a higher velocity (1550 versus 1500 m/s). The combination of a smaller projectile mass with higher velocities resulted in baseline penetration values into 4340 steel which were equivalent to those run at SwRI. Using this observation as a guide, comparisons with earlier HP AlN results can be considered. Two hot-pressed AlN tiles and AD90 alumina were also tested at UDRI to further verify the suitability of a direct comparison. The tile dimensions, shot specifications, and penetration results are shown in Table XXIV.

Table XXIV
Penetration Results for L/D = 10 LRP into Sintered Aluminum Nitride

Tile ID	Machined Density (g/cm³)	Areal Density (g/cm²)	SHOT #	Velocity (m/sec)	Total Yaw	D.O.P. (mm)	e_m	Residual Mass (g)
HPA	3.24(99.4)	15.01	1-210	1534		28.7	2.53	7.1
HPC	3.25(99.7)	15.02	1-216	1525		29.5	2.45	9.0
28B	3.21(98.0)	9.99	1-208	1541	0.4	40.9	2.89	18.7
34E	3.25(99.2)	9.95	1-217	1539	2.2	43.0	2.66	11.1
34A	3.26(99.5)	14.93	1-212	1530	2.9	33.8	2.26	8.1
34C	3.26(99.5)	14.95	1-218	1539		32.0	2.40	10.4
27H	3.23(99.1)	10.13	1-271	1535	1.1	42.0	2.73	10.0
35A	3.21(98.5)	9.95	1-209	1529	1.1	46.5	2.38	
35E	3.11(95.4)	14.88	1-272	1555	1.1	29.6	2.61	7.9
35F	3.16(96.9)	15.01	1-262	1505	1.0	27.3	2.48	6.6
29A	3.25(99.2)	9.99	1-211	1524	2.8	47.3	2.27	25.7
29B	3.25(99.2)	10.00	1-213	1529	0.6	40.0	2.88	20.6
AD90A	3.59	15.06	1-206	1532	1.3	44.0	1.72	
AD90B	3.59	15.03	1-207	1540	0.7	43.7	1.77	

$$e_m = (p_{ref} - p_c) \rho_{ref} / AD_c$$

The relative mass efficiency, e_m , is the ratio of the areal density of steel which was reduced (difference between reference penetration and actual penetration with ceramic insert) over the areal density of the ceramic in the target. Using this methodology, aluminum nitride was 2.5x more effective than 4340 steel at stopping this threat and ~40% better than AD90 alumina. Sintered aluminum nitride was found to be equivalent to hot-pressed AlN. The sintering aids which were evaluated, CaO and La₂O₃, did not seem to affect the penetration results, however residual projectile mass was somewhat lower for the calcia containing materials. Since these tiles were lower density and, from earlier measured mechanical properties, a weaker material, this result was unexpected and can not be readily explained. From the mushroom shape for most of spent rods, shown in figure 33, the primary penetrator failure mechanism is by plastic flow. For 3 out of 4 targets tested with thinner

ceramic tiles, penetrator "debris clouds" formed which resulted in disproportionately large residual mass values. Even with this larger residual mass, the thinner ceramics still had higher relative mass efficiencies. This concept can be effectively utilized when developing optimized and economical armor systems.

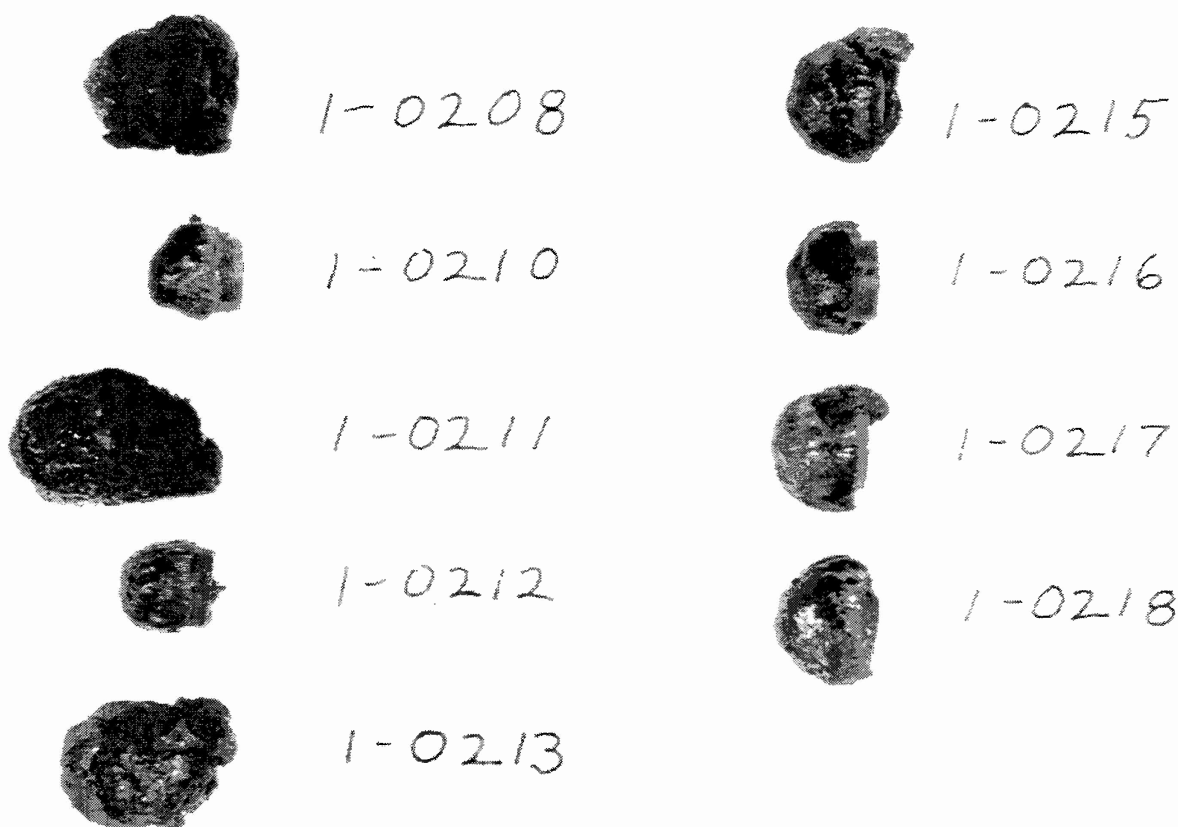


Fig. 33. Recovered penetrator masses for aluminum nitride targets.

When procedures were being established for evaluating the newly developed ceramic materials from current ARO/DARPA contracts, the question of a suitable screening method was discussed. Because per shot costs for LRP testing are high, the need for an alternative screening method is paramount.

Mechanical properties, for the most part, have been shown to be of little predictive value. Light caliber ballistic tests were informative, but still did not provide sufficient discriminating data to definitively guide the composition selection for the aluminum nitride LRP tests. A proposed alternative for screening AlN composites would be to use D.O.P. measurements with .50 caliber SLAP (Saboted Light Armor Penetrator) rounds. A schematic of the SLAP targets is shown in figure 34. The advantages this test offered were:

- 1) moderate cost (1/4 per shot cost compared to LRP);
- 2) round is tungsten alloy and similar to long rod penetrators of interest;
- 3) shot with .50 caliber barrel which is readily available;
- 4) ceramic is confined as in the LRP case;
- 5) limited number of ceramic targets required;
- 6) thickness of tiles needed was not a processing concern;
- 7) round is also extremely lethal, capable of penetrating 120 mm of Al;
- and 8) a limited ceramics database already existed with this method.

However, prior to testing AlN composites, there was an interest to first use to this ballistic test methodology to evaluate sintered AlN. Tiles, 12.7 cm dia. x 0.9 cm thick, were prepared from nine compositions including the three which were tested against the long rod penetrator. Preparation of these tiles was relatively straightforward and process yields were high. This was an obvious contrast to the difficulties encountered while producing the thicker sintered tiles. The only significant process modification which was incorporated during the manufacture of these tiles was during the sintering cycle. During this operation, the heating rate was reduced to 1°C/min between 1200°C and 1500°C and instead of flowing nitrogen, this interval took place under vacuum. This processing change was implemented to address the bloating problem observed with the latter batches. Because of the relatively small I/D ratio, density gradients, which likely was the major cause of cracking during binder removal and sintering of the thick AlN tiles, were not observed. The sintering temperatures were chosen to maximize density while approximating the microstructures which were previously evaluated. After sintering, the tiles were ground to yield a constant areal density of 3 g/cm².

.50 Caliber SLAP Targets

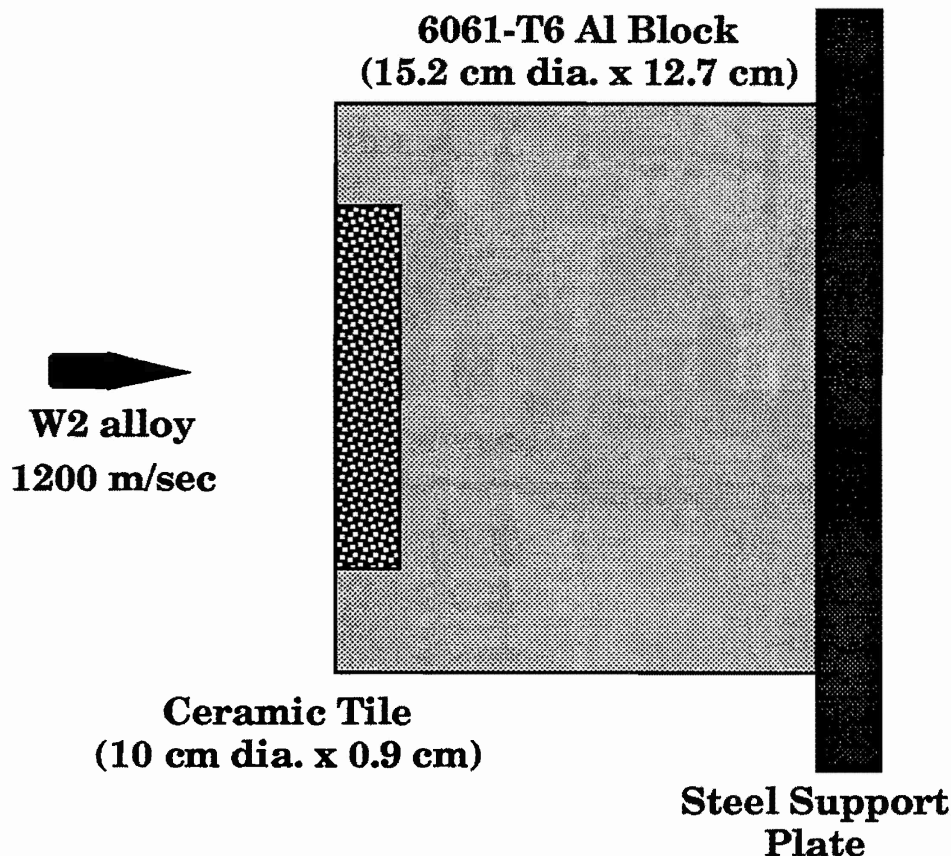


Fig. 34. Schematic of SLAP (Saboted Light Armor Penetrator) target assembly showing confined ceramic and semi-infinite aluminum backing plate.

The penetration results for these sintered aluminum nitride formulations are plotted in figure 35. The effectiveness of sintered AlN was initially overestimated and penetration approached the back surface of the 10.3 cm aluminum blocks which were used initially. The free surface created a change in stress state which caused the round to take a non-linear J-type path. The thickness of the aluminum backing was increased to 12.7 cm and better approximated a semi-infinite block. The penetration paths into these targets were relatively straight. Except for composition 34, the shot to shot variability was large and because of this scatter, differences in penetration resistance could not be established with any degree of confidence. While batch 29, which was equivalent to batch 11, the highest performing material during the earlier light caliber studies, had the lowest penetration values in this series as well, overall, these results did little to resolve composition/performance questions

for sintered aluminum nitride. The utility of this testing methodology as a suitable screening tool was seriously questioned. However, since the scatter was substantially reduced when the thicker aluminum blocks were used as the backing material, it was decided to proceed and use this method as the primary ballistic evaluator for the subsequent AlN composite work.

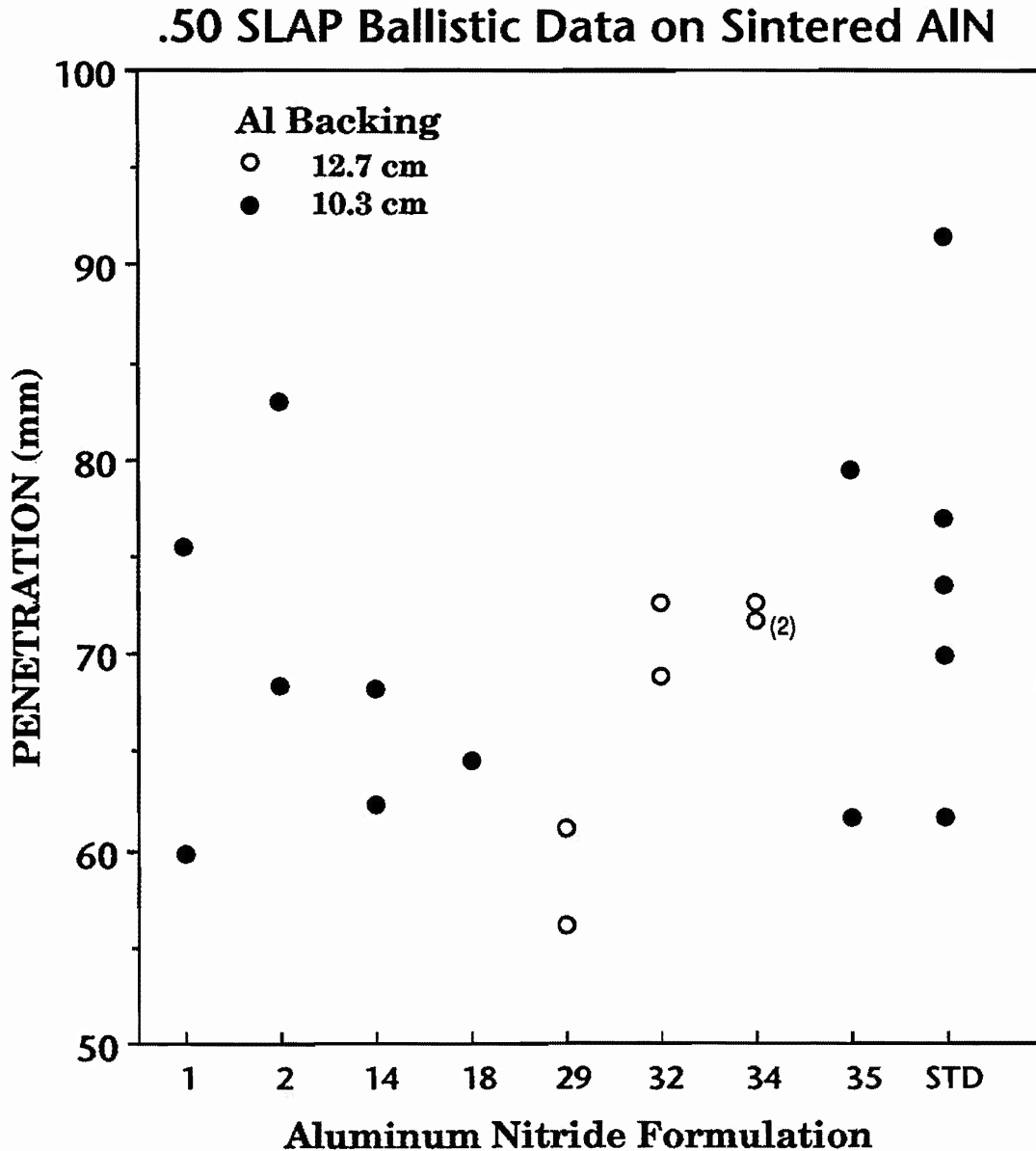


Fig. 35. Penetration values for .50 caliber SLAP rounds against sintered aluminum nitride targets. Initial targets had a aluminum block thickness of 10.3 cm. When penetration approached the back of these blocks, a thicker backing of 12.7 cm was used.

2.2.6 DISCUSSION

The development of cost-effective, high performance aluminum nitride was the ultimate objective of this contract. Through a series of statistically designed experiments, processing technology for fabricating large aluminum nitride bodies was established. Fabrication steps included spray drying formulated aluminum nitride powders, dry pressing, binder removal and pressureless sintering. This series of operations were selected based on their potential to economically produce large volumes of ceramics which would allow aluminum nitride containing systems to be competitive with alternative armor solutions. At large volumes, raw material costs, primarily aluminum nitride powder and the sintering aids, have the greatest influence on the price of fabricated tiles. Therefore, much effort was spent on examining different types of aluminum nitride powders and sintering aids to develop optimized (based on price and performance) products for armor applications. It was determined that the achievement of large high density tiles required the use of active, high surface area powders. The purity of these powders, over the range examined, did not seem to critically impact processability or ballistic performance. The most common sintering additive for aluminum nitride has been three weight percent of yttrium oxide. Because of the high price of this chemical, the reduction and ultimate elimination of that material represents a considerable opportunity for cost savings. Lower priced alternatives were successfully identified for sintering large aluminum nitride parts. CaCO_3 , CeO_2 and La_2O_3 , were found to be suitable substitutes for yttria from a processing standpoint. Ballistically, these sintering aids were also found to be as good as and in some cases better than the standard formulation.

During LRP penetration experiments, these sintered materials duplicated the performance of hot-pressed aluminum nitride and relative to steel, had mass efficiencies of 2.5. With the limited number of LRP shots, it was not possible to make a definite recommendation with regard to the best formulation for this application. The SLAP data contributed little to this end as well. However, it did reveal that options were available and composition selection could be based primarily on cost and ease of fabrication. From the light caliber results, it was concluded that large grained materials should be avoided and the amount of sintering aid should be minimized for enhanced ballistic protection.

To further explore the effect grain size and sintering aid had on penetration resistance, TEM (transmission electron microscopy) examination of four ballistic samples was undertaken. Samples 1,2 and 17,18 (see Tables XIV, XIX, and XX for description and properties) were fine and coarse grained paired sets which contained 5.0 and 0.5 v/o CeO_2 , respectively. Two types of specimens were prepared from the ballistically tested tiles. The powdered rubble was dispersed onto a TEM grid for one specimen and a thin section was prepared from a large fragment. It was assumed for each case that the powdered rubble originated near the impact zone while the fragment was from the outer portions of the tile.

As seen in figure 35, representative rubble particles for the four compositions are heavily deformed, characteristic of aluminum nitride ceramics. While there may be some concerns related to representative sampling, at least for the particles analyzed there appears to be little difference between these materials. In the fragment analysis, there were noticeable distinctions, beyond the obvious grain size and chemistry differences, among the four ceria doped compositions. For the 0.5% ceria samples, the fine grained material (batch 17) had a uniform microstructure with small pockets of the cerium aluminate. A minor presence of dislocations indicated some plastic deformation had occurred. For the same composition processed at the higher temperature (batch 18), there was also evidence of plastic deformation and more significantly, extensive microcracking. This comparison can be seen in figure 36. The fracture characteristics of batches 1 and 2, which contained 5.0 percent ceria were similar in nature, as reflected by the photomicrographs shown in figure 37. The frequency of microcracks was less in the batch 1 tile and the crack path was more tortuous due to the finer grain size. In both cases, the intergranular microcracking was the result of increased levels of ceria which concentrated at the grain boundaries as cerium aluminate. Based on these observations, ballistic performance for AlN compositions appears to be enhanced by delaying the onset of microcracking.

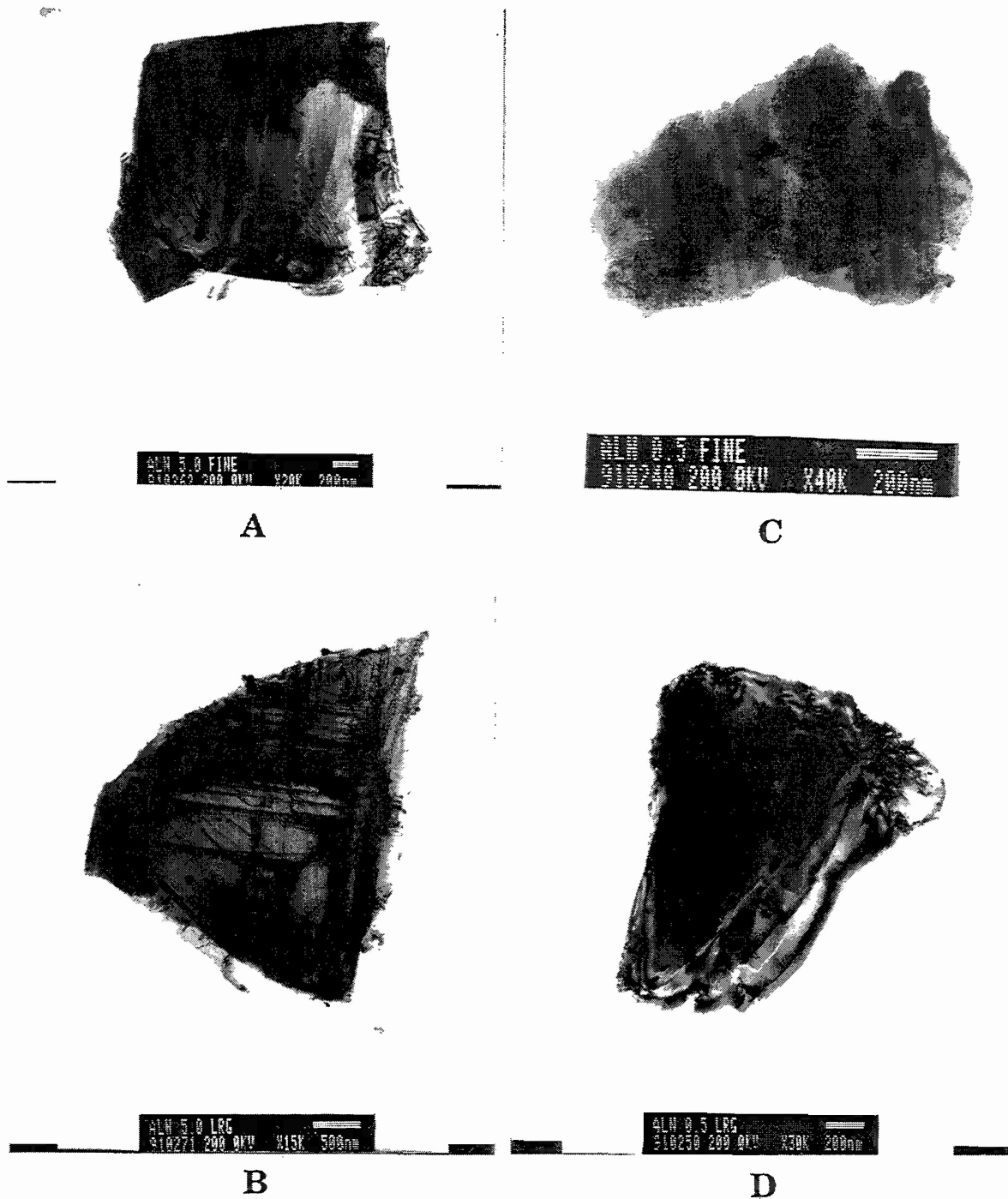


Fig. 36. TEM photomicrographs of fine rubble particles for four ceria doped aluminum nitride samples after .30 caliber AP ballistic testing: A) Batch 1, 5.0% ceria with fine grained microstructure; B) Batch 2, 5.0% ceria with coarse microstructure; C) Batch 17, 0.5% ceria with fine microstructure; and D) Batch 18, 0.5% ceria with coarse microstructure.

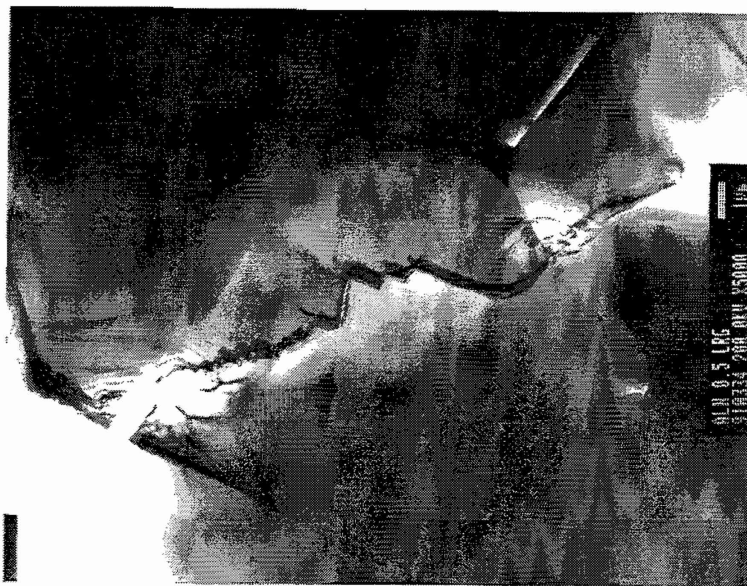


Fig. 37 TEM photomicrographs of thin sections taken from larger (>3 mm) ballistic fragments for two sintered AlN samples containing 0.5% cerium oxide. Batch 17 has a fine uniform microstructure (top), while batch 18 (bottom) has a substantially larger average grain size and clear evidence of microcracking.



Fig. 38. TEM photomicrographs of thin sections taken from larger (>3 mm) ballistic fragments for two sintered AlN samples containing 5.0% cerium oxide. The increased sintering aid level has led to grain boundary microcracking for both the fine (top) and coarse (bottom) grained materials. The average grain size difference appears less than reported due to a 2X magnification difference.

Another issue which was addressed during this study of aluminum nitride ceramics was whether any easily measured parameter could help guide materials development. Ceramic properties which have long been considered important for good ballistic performance include hardness, fracture toughness and compressive strength. Since the fracture toughness for sintered aluminum nitride compositions has not been shown to be sensitive to minor compositional or microstructural changes, it was not measured for these materials. During previous studies of aluminum nitride ceramics, scatter plots were generated for essentially every parameter which was correlated with ballistic performance. Considering the complex nature of the ballistic event and the influence of several independent parameters, such as the target configuration, and projectile shape and composition, the lack of a strong correlation between ballistic performance and these other measured values was not unexpected. However, since the breadth of this study was expanded considerably both from a compositional standpoint and from the type of measurements which were available, the current data was analyzed for correlations using a PC based statistics program. Correlation coefficients were easily generated for all of the parameters and were not limited to the two ballistic tests. The results of this analysis is given in Table XXV. In addition to the correlation coefficients, outliers were identified and scatter plots showing 95% confidence limits were also generated (figure 39).

TABLE XXV
Correlation Coefficients for all Parameters considered in this Study of AlN

	Flexure		Static		BR	Grain Size		% T.D.	Modulus		
	Hardness		Dynamic			DOP	Density		Speed		
Flex	1.000	0.562	0.628	0.730	0.379	-0.474	-0.630	0.193	0.429	0.417	0.534
Hard	0.562	1.000	0.697	0.841	0.217	-0.390	-0.260	-0.078	0.324	0.706	0.825
Static	0.628	0.697	1.000	0.859	0.424	-0.383	-0.502	0.210	0.560	0.565	0.705
Dynamic	0.730	0.841	0.859	1.000	0.395	-0.448	-0.548	0.020	0.473	0.701	0.841
BR(ϵ_r)	0.379	0.216	0.424	0.395	1.000	-0.821	-0.524	0.079	0.231	0.091	0.091
DOP	-0.474	-0.390	-0.383	-0.448	-0.821	1.000	0.610	0.268	-0.123	-0.332	-0.181
Grain Size	-0.630	-0.260	-0.502	-0.548	-0.524	0.610	-1.000	0.006	-0.191	-0.060	-0.172
Density	0.193	-0.078	0.210	0.020	0.079	0.268	0.006	1.000	0.604	-0.380	0.099
% T.D.	0.429	0.324	0.560	0.473	0.231	-0.123	-0.191	0.604	1.000	0.332	0.522
Speed	0.417	0.706	0.565	0.701	0.091	-0.332	-0.060	-0.380	0.332	1.000	0.741
Modulus	0.534	0.825	0.705	0.841	0.091	-0.181	-0.172	0.099	0.522	0.741	1.000

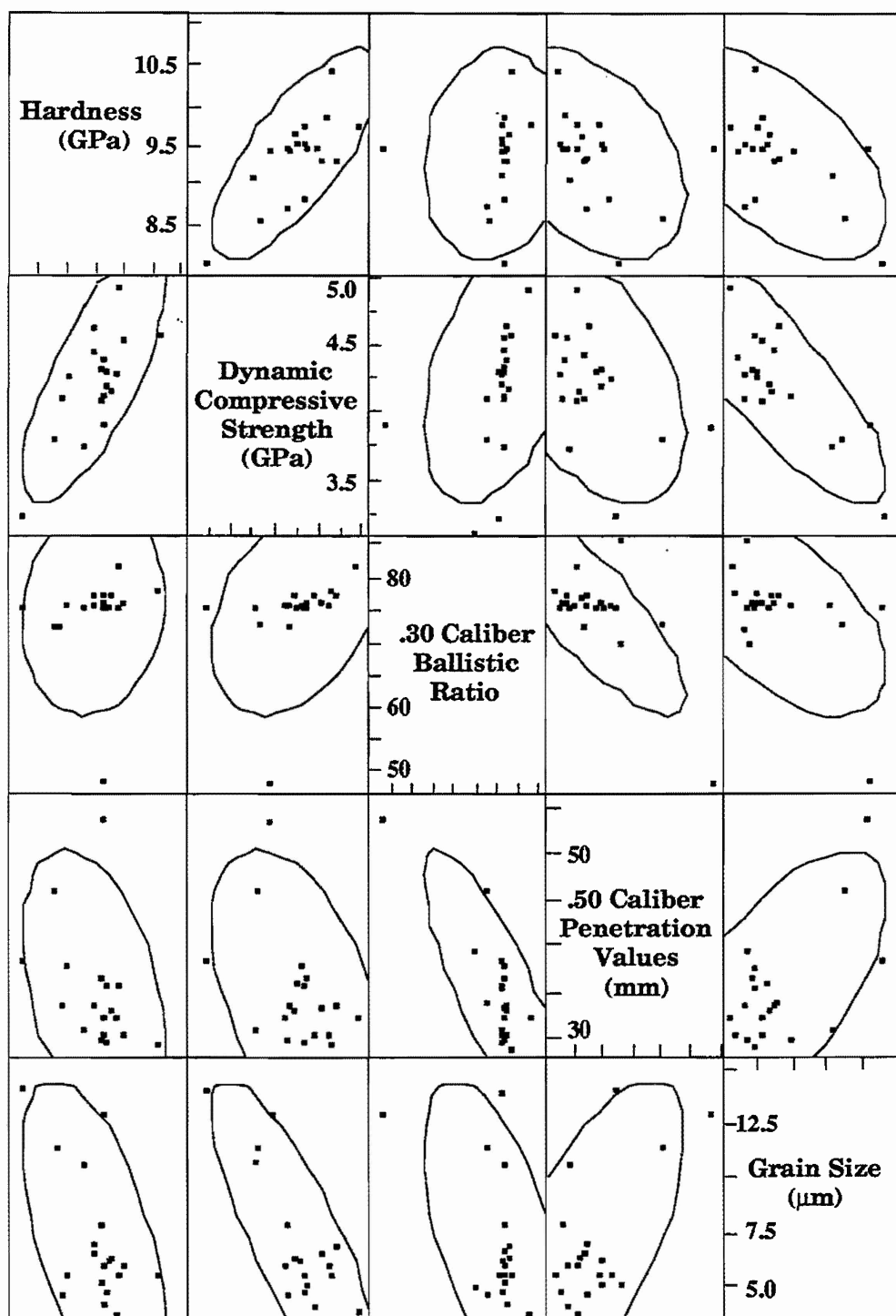


Fig. 39. Scatter plots for key mechanical properties, grain size and the two ballistic experiments, .50 caliber D.O.P. tests and the .30 caliber efficiency ratios. The elliptical figures represent the 95% confidence limits for each correlation. Thinner figures reflect a higher degree of correlation.

In general, none of the measured parameters were found to be strongly correlated with either of the ballistic tests. Grain size, consistent with the general observations which were discussed earlier, does appear to play a dominate role in not only ballistic performance but with the other mechanical properties as well. This conclusion is further reinforced when outlier data containing yttrium fluoride is extracted and not included in the analysis. Interestingly, density, absolute and percent of theoretical, sound speed and modulus did not have any influence on ballistic performance. Since a criteria used in the selection of these compositions was its ability to achieve high density, this observation was not totally unexpected. However, it might suggest for light caliber applications that the current density specification for armor ceramics of >98% T.D. could be relaxed. This data also indicates that there is a strong relationship between D.O.P. values and ballistic limit results and therefore strongly implies that measuring projectile penetration into semi-infinite backing is an appropriate ballistic materials screening tool.

Mechanical properties which appear to mimic ballistic performance the best are dynamic compressive strength and hardness. Dynamic compressive strength also appears to be a universal predictor of mechanical performance. It has the largest correlation coefficient with each of the other five mechanics parameters.

The ballistic event is a complex function of many factors, including several independent parameters such as the target configuration, and projectile shape and composition. In addition, the uncertainty in the individual data points was large due to experimental scatter and a limited data set. Therefore, the fact that there was no direct correlation between ballistic performance and other measured properties observed was not unexpected. However, it was still important to establish trends which could be reliably used to guide materials development. This then would suggest that a nonparametric statistical approach may be more appropriate for analyzing D.O.P. and ballistic limit tests. Therefore, instead of examining correlations between ballistic results and a given parameter, the relative rankings for each property were used. The rankings for hardness, flexure strength, compressive strength (static and dynamic) data, .30 caliber ballistic limit and .50 caliber penetration into an aluminum block were tabulated and compared using the Spearman rank

correlation coefficient.³⁰ The hypothesis which was tested for each combination of the six variables was whether the values were mutual independent or that there was a tendency for the larger values of one set to be paired with the larger values of another set. In the case of ties, the average value of that subgroup was used. The relative rankings for each of these six measured parameters are given in Table XXVI.

Table XXVI
Relative Rankings of Sintered Aluminum Nitride Compositions

Batch #	Flexure Strength	Hardness	Compressive Strength		.50 Caliber	.30 Caliber
			Dynamic	Static		
1	5	8	7	7	15	8.5
2	19	18	17	15	19	17.5
3	8	3	9	10	13	14
5	16	19	19	19	17	14
6	9	16	10	13	16	8.5
7	10	6	11	3	14	14
8	14	13	2	1	11.5	4
9	15	5	12	11	9	4
10	13	9	13	13	3	8.5
11	4	4	1	2	7.5	1
12	1	2	4	17	4.5	8.5
13	20	15	18	18	6	14
14	7	1	3	4	1	2
15	12	7	8	9	2	14
16	6	17	14	8	11.5	17.5
17	2	10	6	6	4.5	4
18	17	11	16	16	20	20
19	3	14	5	5	10	8.5
20	18	20	20	20	18	19
22	11	12	15	14	7.5	8.5

The Spearman rank correlation coefficients and the corresponding confidence level are shown in Table XXVII. Since the null hypothesis that the parameters were mutually independent was rejected at a confidence level of at least 99% for most of the interactions, improving the mechanical properties of aluminum nitride ceramics should lead to better ballistic materials. As expected from the earlier analyses of the actual data, dynamic compressive strength was the leading indicator of ballistic performance. While these trends may be valid for another family of ceramics, aluminum nitride has been the only ceramic to date which has undergone such extensive scrutiny and ballistic evaluation. Future work which focuses on improving the mechanical performance of aluminum nitride should lead to a better ballistic material as well. However, there is no basis to suggest that the ceramic material with the highest flexure strength, hardness or even dynamic compressive strength would be most efficient in defeating a given ballistic threat. More work is obviously needed before that easily measured property which can predict ballistic performance is identified or optimized ceramics can be microstructurally engineered for ballistic applications

TABLE XXVII
Rank Correlation Coefficients for Key Measured Parameters

	Flexure	Hardness	Static	Dynamic	DOP	BR(ϵ_r)
Flexure	• 0.504 0.985	0.504 0.985	0.608 0.997	0.750 0.999	0.401 0.960	0.530 0.991
Hardness	0.504 0.985	• 0.504 0.985	0.450 0.976	0.660 0.999	0.565 0.995	0.540 0.992
Static	0.608 0.997	0.450 0.976	• 0.450 0.976	0.783 0.999	0.303 0.905	0.593 0.997
Dynamic	0.750 0.999	0.660 0.999	0.783 0.999	• 0.750 0.999	0.497 0.984	0.765 0.999
DOP	0.401 0.960	0.565 0.995	0.303 0.905	0.497 0.984	• 0.401 0.960	0.602 0.997
BR(ϵ_r)	0.530 0.991	0.540 0.992	0.593 0.997	0.765 0.999	0.602 0.997	• 0.530 0.991

2.3 Hot-Pressed AlN/SiC Composites

Sintered aluminum nitride was shown to have significantly better long rod penetration resistance than the alumina ceramic standard. While performance was equivalent to hot-pressed AlN, substantial opportunity for enhancement exists. In addition, the potential for developing a material based on aluminum nitride with a broad threat window is also great. In developing these improved materials, maintaining attractive economics is essential. Particulate composites of aluminum nitride may meet both the performance and economic requirements. Of the high performance ceramics currently being considered for armor applications, SiC would be the preferred material to combine with aluminum nitride. SiC has extremely high HEL (Hugoneit Elastic Limit), which would complement the elastic-perfectly plastic characteristics of aluminum nitride. It is also a significant material of commerce which would not detract from the attractive economics which have been previously demonstrated for aluminum nitride. In addition, from a scientific standpoint, AlN/SiC composites are also interesting since materials with equivalent compositions can be prepared either as two-phased materials or homogeneous solid solutions. This unique feature will allow the effect of microstructural characteristics on ballistic performance to be studied without being encumbered by contributions caused by differences in chemistry.

Since the aluminum nitride/silicon carbide system has been thoroughly characterized,³¹⁻³⁷ this final phase of the contract primarily examined the ballistic characteristics of these composites. Several compositions in this system were examined and for each composition, two types of microstructures were prepared. Samples were all prepared by hot-pressing. .50 caliber SLAP penetration measurements were obtained for fourteen AlN/SiC composite materials. From these results, two of the compositions were chosen for evaluation against the L/D =10 LRP. Significant improvements in ballistic efficiencies were observed compared to the aluminum nitride baseline. In addition, some preliminary sintering experiments were also undertaken during this contract extension.

2.3.1 HOT-PRESSED OPTIMIZATION

Due to the previously reported influence of grain size on ballistic performance, to obtain a reliable comparison between the two-phased composites and solid solution materials it was essential that any grain size differences be minimized. It was also important to achieve high theoretical densities, >98%, for these samples as well. In order to achieve these program objectives, aluminum nitride composites with three SiC powders were evaluated. These included two β -SiC powders, Mitsui Toatsu BSC21[#] and Superior Graphite HSC 077[£] and one α -SiC powder, Starck A1[¢]. The powder characteristics for the four powders utilized during this task are described in Table XXVIII.

Table XXVIII
Powders Used During Tasks Associated with AlN/SiC Composites

POWDER Manufacturer	Mitsui Toatsu	Superior Graphite	Starck	DOW
GRADE	BSC21	HSC 077	A1	ARMOR
LOT #	ARP 5881	BH-19	165190	42021
TYPE	β -SiC	β -SiC	α -SiC	AlN
SIZE (μm)	0.9	3.2	1.3	1.9
SEM values				
High (μm)	0.7	6	3	1
Low (μm)	0.1	0.4	0.4	0.2
Mean (μm)	0.2	3	2	0.6
BET (m^2/g)	16.0	2.0	3.1	2.3
O (wt. %)	1.04	2.80	0.55	1.07
C (wt. %)	29.95	29.54	30.13	0.06
Fe (ppm)	190	667	310	26
Al (ppm)	75	692	100	60 (Si)
Ca (ppm)	<20	364	40	94

Metallic Impurities measured by X-ray Fluorescence (XRF).

[#] BSC21 SiC manufactured by Mitsui Toatsu, Japan and distributed by Performance Ceramics, Peninsula, OH.

[£] Superior Graphite Co., Chicago, IL

[¢] Hermann C. Starck, Inc., New York, NY

Scanning electron photomicrographs of the three SiC powders are shown in figure 39. The uniform, submicron BSC21 powder appears ideally suited for solid solution formation with aluminum nitride, while the angular, broadly distributed HSC 077 and A1 powders were evaluated for use in the two-phased composites. It was desirable that the A1 and HSC 077 SiC powders be in the 1 to 5 μm size range, since it was observed that the average grain size for AlN hot-pressed at 1900 to 2000°C was $\sim 3 \mu\text{m}$ and that the solid solution composites were expected to be similar. In order to achieve the desired characteristics for the hot-pressed ballistic samples, a detailed study of densification behavior and microstructural evolution for compositions ranging from 100 to 5 percent aluminum nitride was undertaken as a function of hot-pressing temperature with each of the three SiC powders.

Powder preparation for hot-pressing these composites consisted of attrition milling with 5 mm SiC media for one hour in ethanol. Batch sizes were 400 grams and the formulations were calculated on a volume basis. Since the theoretical density of SiC (3.217 g/cm³) is so similar to AlN (3.26 g/cm³), compositions based on weight rather than volume would be very similar. A dispersant which was found to be effective for both AlN and SiC was utilized. 0.4% of this butylated polyvinyl pyrrolidone polymer[¶] was mixed with ~ 350 ml of absolute ethanol. The powders, minor constituent first, were added and milled for one hour. The slurries were dried in a two step process. A standard rotary evaporator was used first to remove the majority of the ethanol. The final residual solvent was removed by drying overnight in a 100°C vacuum oven. The dried powders were then ground to -45 mesh. Five AlN/SiC formulations ranging from 90 to 5 volume percent aluminum nitride were initially prepared from each of the three SiC powders. Since it was not certain that the 5/95 AlN/SiC compositions could be densified without any sintering aids to >98% T.D., three additional mixes were prepared of this composition with 0.5% boron carbide.[§]

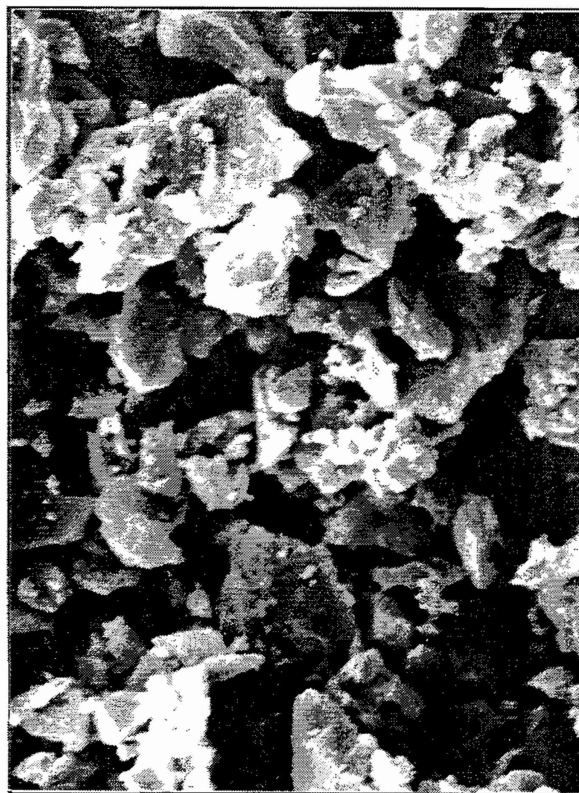
100g, 7.5 cm diameter AlN/SiC samples were hot-pressed in stacks of three using a graphite die arrangement similar to that described earlier for AlN. Each composite mix with the same AlN/SiC composition was hot-pressed

[¶] GANEX P-904, International Specialty Products, Wayne, NJ

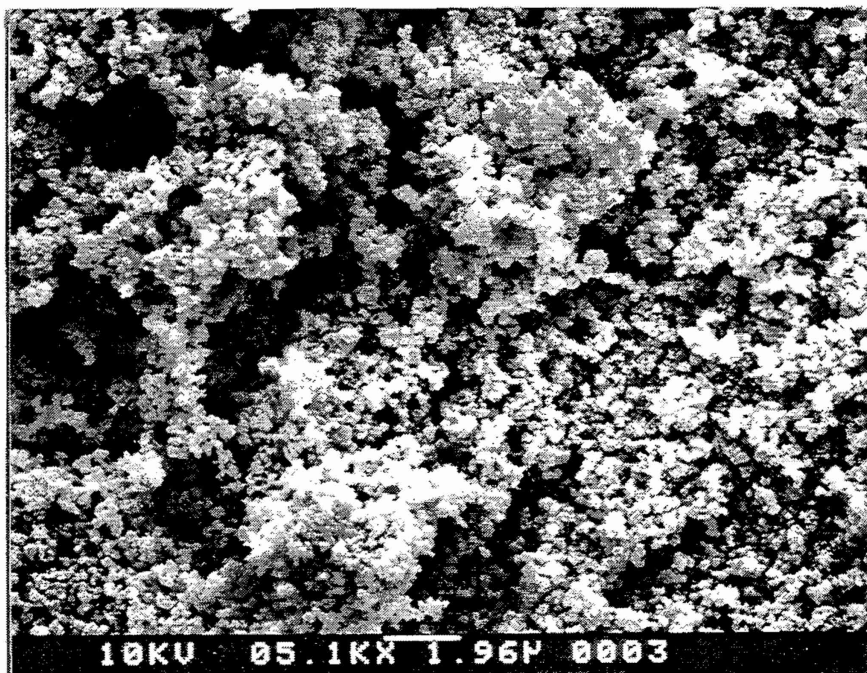
[§] ESK 1500, ESK Engineered Ceramics, New Canaan, CT



Starck A1 (5000x)



Superior Graphite HSC 077 (5000x)



Mitsui Toatsu (5000x)
(Ferro BSC21)

Fig. 39. SEM photomicrographs of the silicon carbide powders used for this study of AlN/SiC composites.

together in a single die assembly at three different temperatures and 34.5 MPa. One cm graphite spacers were used to separate the three mixes during powder loading and while pressing. The hot-pressing temperatures and resulting densities are given in Table XXIX. The highest composite densities at the intermediate temperatures were achieved using the relatively coarse Superior Graphite HSC 077 powder. While this powder did have the highest impurity levels which could have influenced the densification, this result was still unexpected particularly when the large surface area difference between BSC21 and HSC 077 is considered. The dominant factor may have been the position of the parts in the die during hot-pressing. For each run, the BSC21 powder was on the bottom, the Al containing mixes were in the middle and the HSC 077 materials were on top. Since the hot-press unit used had a single acting hydraulic system, which was applied from the top, a pressure gradient due to die wall friction was likely. During an initial AlN run with three stacked samples, the density after hot-pressing at 1700°C was almost 2% lower for the bottom disk relative to the top one. This effect, consistent with these results, would be expected to have the greatest impact at the intermediate temperatures, when the pressure component dominates the diffusion process. At low temperatures, there is not a sufficient driving force to allow densification to proceed. While at high temperatures, diffusion rates are relatively fast such that only modest pressure levels are needed to complete densification which would make the process relatively pressure insensitive.

Although standard x-ray diffraction methods are not sufficient to establish whether a complete solid solution has been achieved³³, the dynamics of SiC mobility and dissolution into the 2H AlN structure can clearly be monitored by this technique. Formation of AlN/SiC solid solutions can be established from shifts in the diffraction peak, but the absence of any SiC reflections was needed before this transformation was considered complete. While the driving force sufficient to achieve a single phase homogeneous composition at 2100°C, which is above the miscibility temperature for all compositions³⁶, is high, the higher SiC compositions required increasingly greater hot-pressing temperatures to achieve this state. Consistent with observations reported in the literature³⁸, solid solution formation occurred more readily when β -SiC was used. These X-ray diffraction analyses have been qualitatively summarized in Table XXIX.

Table XXIX
Density and Phase Analysis for AlN/SiC at Different HP Temperatures

AlN/SiC	Temperature 1 °C			Temperature 2 °C			Temperature 3 °C		
	Density (g/cm ³) Solid Solution			Density (g/cm ³) Solid Solution			Density (g/cm ³) Solid Solution		
Silicon Carbide	BSC	A1	HSC	BSC	A1	HSC	BSC	A1	HSC
100/0		1700 3.248 YES			1825 3.254 YES			1950 3.236 YES	
90/10	3.243 NO	1750 3.240	3.221 NO	3.231 close	1875 3.235 NO	3.235 NO	3.232 YES	2050 3.231 YES	3.232 YES
75/25	3.134 NO	1800 3.22 NO	3.161 NO	3.222 NO	1925 3.212	3.224	3.229 YES	2100 3.246 close	3.216 close
50/50	2.854	1825 2.983	2.899	3.047 NO	2000 3.210 NO	3.181	3.227 YES	2200 3.216 close	3.217 close
25/75	2.749	1900 2.704	2.744	3.029 NO	2100 2.974	3.231 NO	3.206 YES	2300 3.210 NO	3.223 YES
5/95	2.992 NO	2100 2.992 NO	3.228	3.201 NO	2300 3.213 NO	3.226			
5/95/0.5 B ₄ C	3.166 NO	2100 3.215	3.200	3.186 NO	2300 3.219 NO	3.200			

BSC, Mitsui Toatsu β -SiC; A1, Starck α -SiC; and HSC, Superior Graphite, β -SiC.
No, SiC peaks still strong; Close, a significant reduction in SiC phase; Yes, no SiC reflections.

The samples containing the BSC SiC powder tended to form a homogeneous material more readily than the coarser HSC powder, but the effect was not as large as anticipated from the factor of eight difference in surface area. Figures 40 and 41 show the microstructural evolution as a function of temperature and SiC powder for two AlN/SiC compositions. Hot pressing conditions and SiC powder which will be used for preparing the ballistic targets were determined from these results.

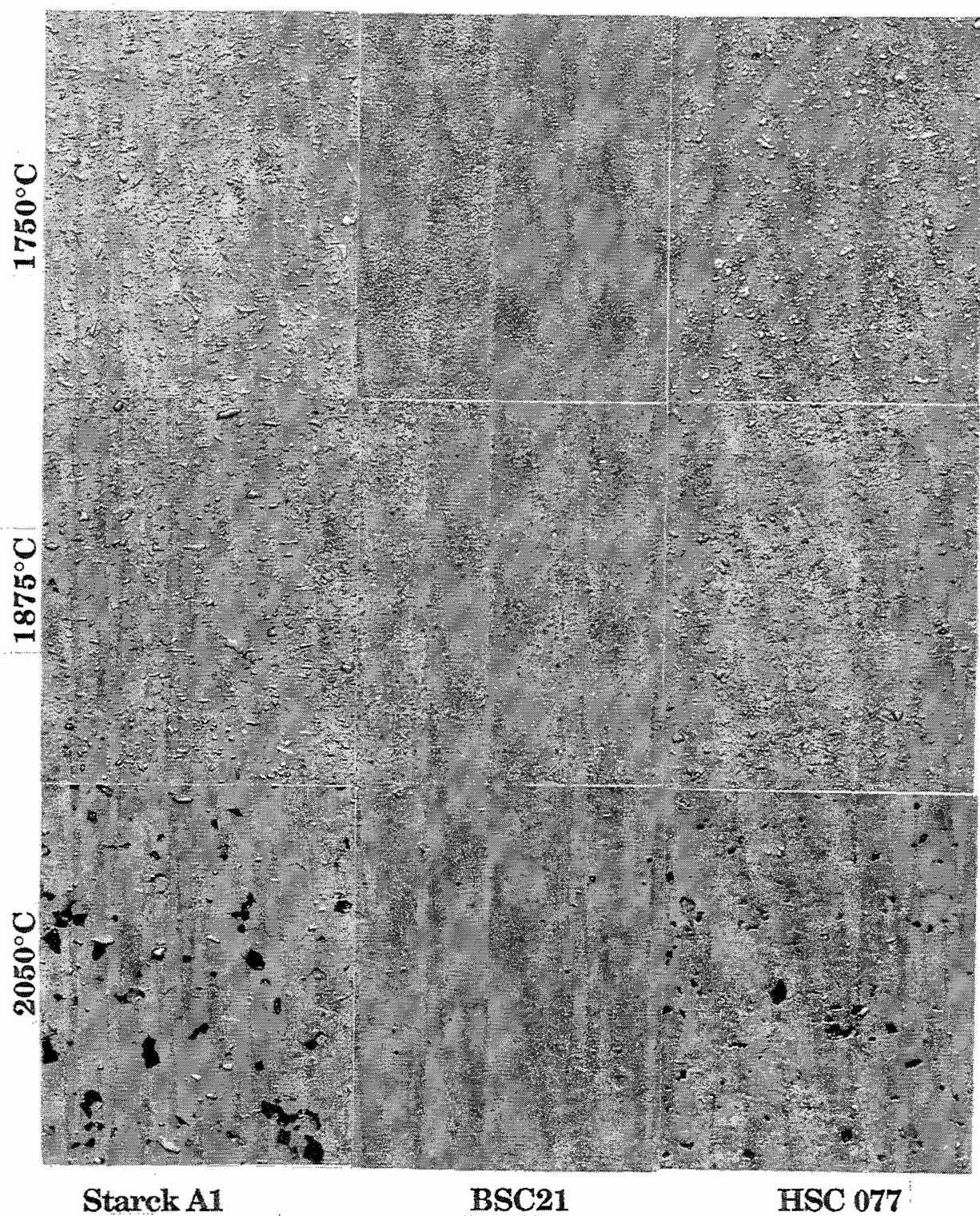


Fig. 40 Optical photomicrographs (500x magnification) of polished 90/10, AlN/SiC samples, using three SiC powders and hot-pressed at three temperatures.

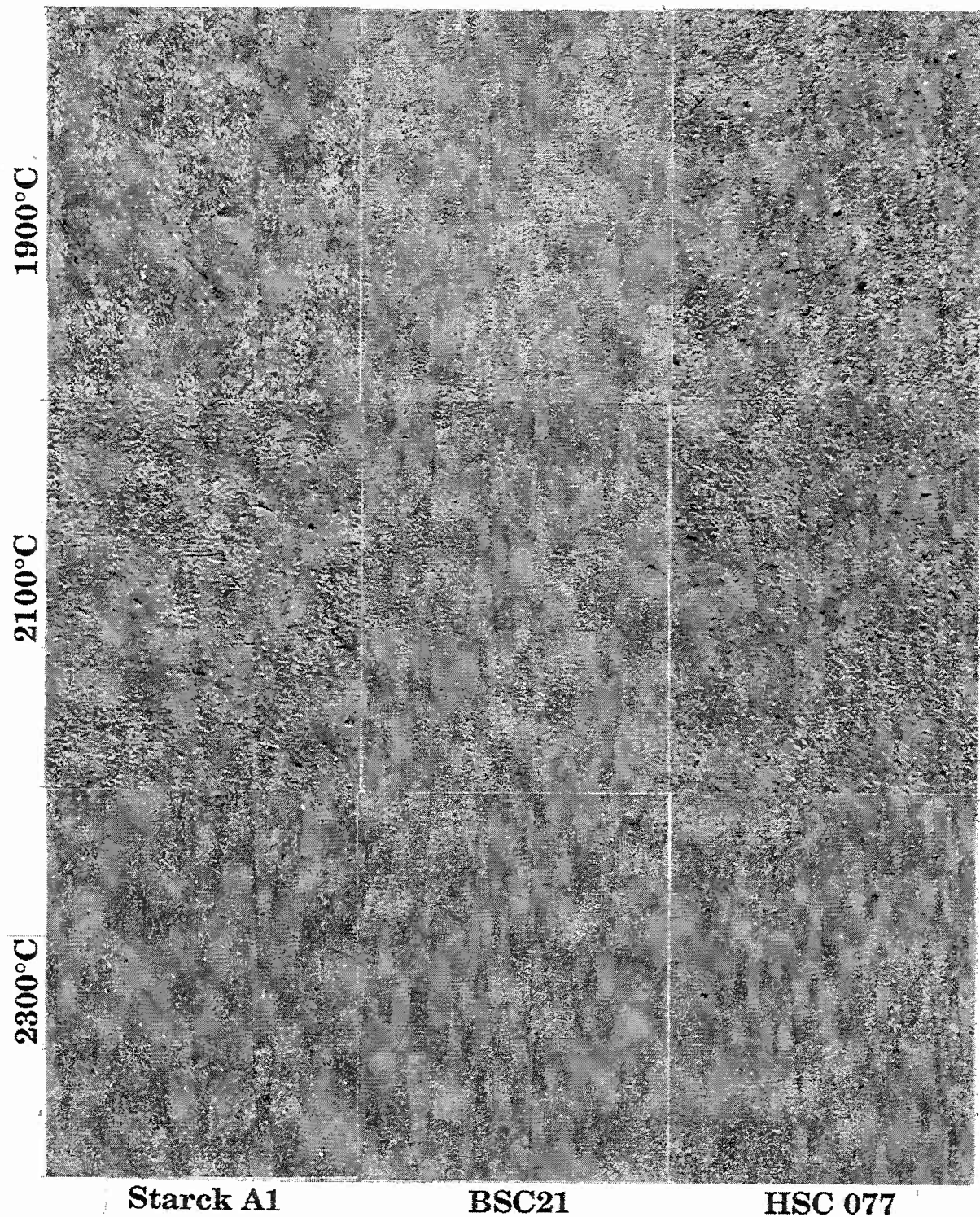


Fig. 41 Optical photomicrographs (500x magnification) of polished 25/75, AlN/SiC samples, using three SiC powders and hot-pressed at three temperatures.

2.3.2 COMPOSITE TILE PREPARATION

Fourteen formulations were prepared using mixing procedures outlined earlier. 625 gram batches provided enough powder to prepare the required two 10 cm diameter tiles for .50 caliber SLAP penetration tests. Based on the earlier hot-pressing results, it was determined that the BSC21 β -SiC offered the greatest opportunity for achieving homogeneous, solid solution composites. For the two phased materials, all three SiC powders could have been utilized. However, in order to minimize any potential grain size effects, the coarse HSC 077 powder was chosen. Its average particle size closely matched that of the aluminum nitride powder used and it was expected to result in a composite with an average grain size similar to the solid solution materials.

After drying and grinding to -45 mesh, 270 grams of formulated powder were loaded into a fiber reinforced graphite die. A graphite spacer was added and then another 270 grams of powder were poured into the die. This arrangement allowed both parts to be hot-pressed at the same time and substantially reduced the number of runs needed to fabricate all of the samples. The position in the die was recorded for each tile and identified throughout the tests as either T (top) or B (bottom). Hot-pressing conditions used during the fabrication of the fourteen composites are listed in Table XXX. The times and temperatures were adjusted from the earlier experiments to enhance the uniformity of the samples. For the composites containing BSC21, where a complete solid solution was desired higher temperatures and longer times were often used. For the other set of composites, where a two-phased microstructure was desired, the minimum conditions which would achieve high density and avoid co-diffusion of aluminum nitride and silicon carbide were employed. After densification, the tiles were machined to an areal density of 3 g/cm².

Density measurements for this series of tiles are shown in figure 42. While the goal of achieving at least 98% of theoretical density was met for most samples, the tiles located in the bottom position of the hot-press die did tend to have a lower density. The only sample set which did not meet this density criteria was the 5/95 AlN/SiC composite prepared with the BSC21 silicon carbide powder. This result is somewhat of an anomaly since it used the higher surface area SiC powder compared to HSC 077 plus a higher processing

Table XXX
Hot-Pressing Conditions for AlN/SiC Ballistic Samples

AlN/SiC	Solid Solution	Two-Phased Composites
Silicon Carbide	BSC21	HSC 077
100/0	1900°C, 30 min	-
90/10	2050°C, 30 min	1850°C, 60 min
75/25	2200°C, 120 min	1950°C, 60 min
60/40	*1950°C, 60 min	2000°C, 60 min
50/50	2300°C, 30 min	2050°C, 60 min
40/60	-	2100°C, 60 min
25/75	2300°C, 60 min	2150°C, 60 min
5/95	2300°C, 60 min	2200°C, 30 min

*Two-phased material. All samples were pressed at ~33 MPa.

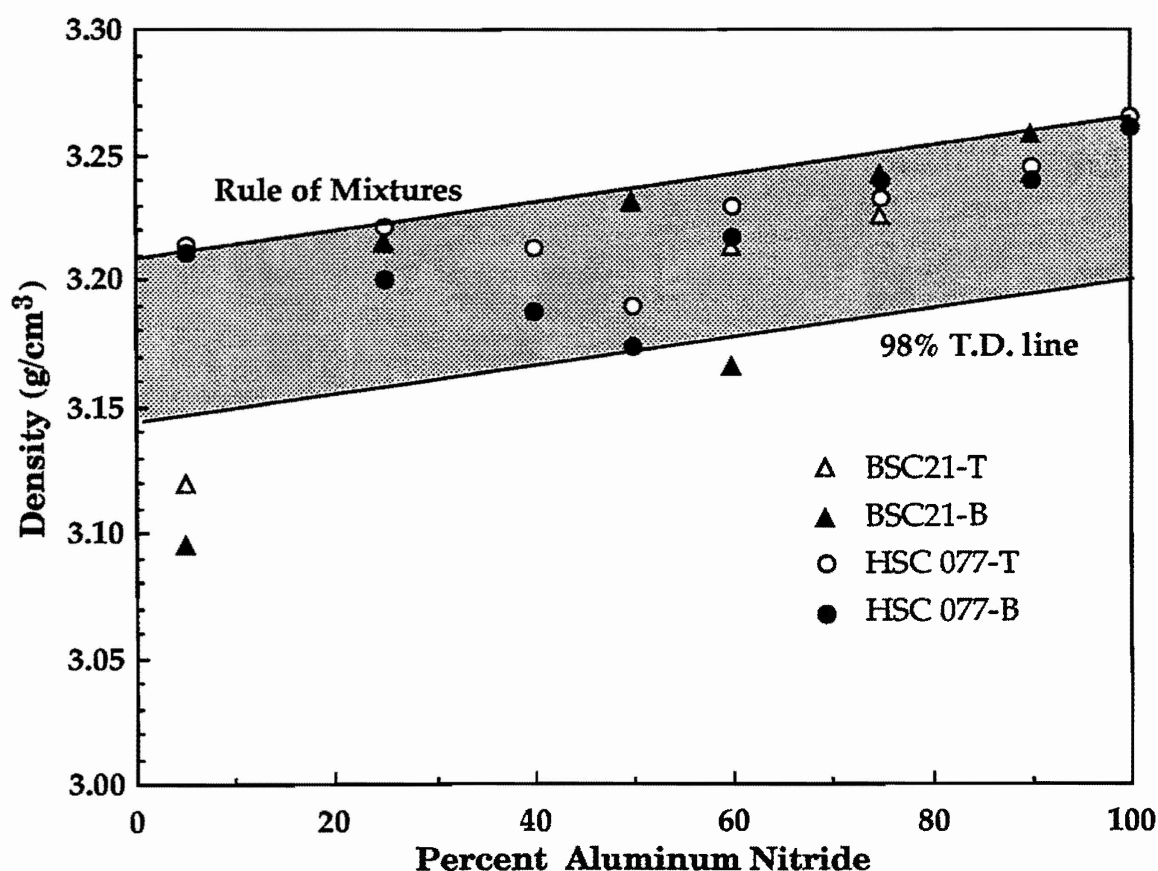


Fig. 42 Density of AlN/SiC tiles showing effect of position, Top (T) and Bottom (B), in die during hot-pressing. Density goal reflected by shaded area.

temperature. The 60/40 compositions, which were prepared to study second phase particle size effects, also reflected the enhanced sinterability of the HSC 077 containing composites. These results suggest that the higher impurity levels of the HSC 077 silicon carbide powder had a substantial impact on the densification of these AlN/SiC composites, since hot-press die position, which was alluded to earlier as affecting density results, was equivalent for both sets of composites.

Two AlN/SiC compositions were selected for further evaluation. One composite was a 50/50 solid solution material which was hot-pressed at high temperatures (2300°C) using the BSC21 silicon carbide powder. The other composite was a 75/25 two-phased AlN/SiC material which was hot-pressed at moderate temperatures (2000°C) and used HSC 077 silicon carbide powder. For these materials, ~5000 grams of formulated powder were needed to meet the program objectives. However, due to capacity limitations of the laboratory attritor mill, instead of one large batch, ten batches, 625 grams each, had to be mixed. During the drying step, these batches were dried two at a time in the rotary evaporator. All of the dried formulated product was then homogenized by first rolling in a large plastic jar, followed by grinding to -45 mesh. Several tiles with thicknesses ranging from 1.2 to 4.7 cm (areal densities of 4 to 15 g/cm²) were hot-pressed individually from both mixes, using conditions similar to those which were established earlier for these two compositions. Probable pressure gradients which existed during the pressing of these thick tiles did not significantly impede densification, since most densities exceeded 99% T.D. for these thicker tiles.

2.3.3 BALLISTIC RESULTS

For screening the ballistic characteristics of the initial fourteen AlN/SiC formulations, penetration experiments into a semi-infinite aluminum block with the .50 caliber SLAP round were performed. The target configuration for these ballistic tests was described previously in figure 34. The thickness of the aluminum backing was 12.3 cm for all of the AlN/SiC tests. The results of these ballistic experiments are detailed in figure 43. The average velocity was 1220 m/sec and the standard deviation for these 28 shots was less than 1%.

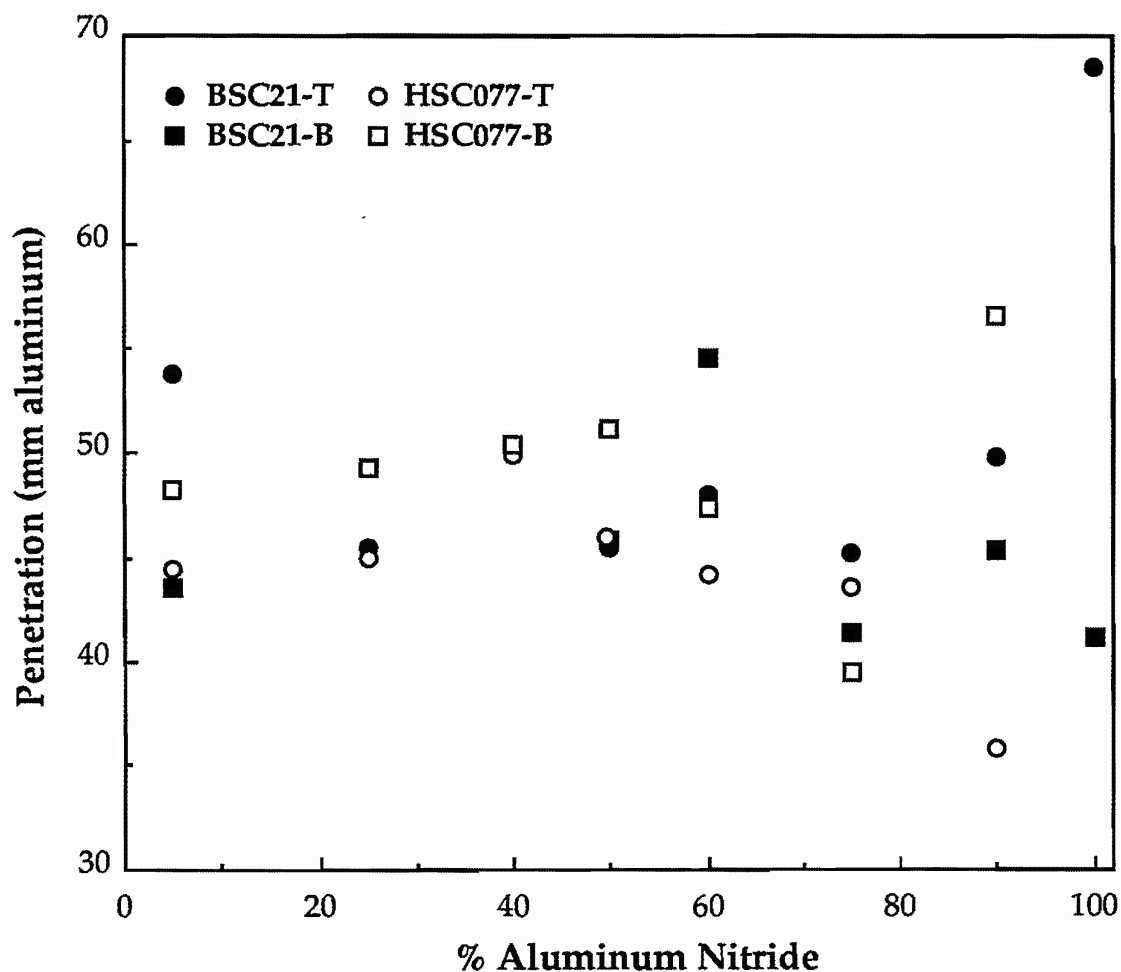


Fig. 43 Residual penetration of .50 caliber SLAP rounds in AlN/SiC composite targets. Tiles from the bottom of the two tile hot-press stack tended to have a lower penetration resistance than the top tile.

When analyzing this series of ballistic results, it was apparent that this limited number of tests did not adequately differentiate these compositions and microstructures. There appeared to be no consistent compositional or microstructural effects which could be established. Although the highest penetration resistance was usually obtained with a two phased composite, statistically these microstructural data sets would be indistinguishable. There appeared to be a performance disadvantage for only those samples for which the bottom die position had a significant impact on the hot-pressed density. In the experiments where the size of the second phase was evaluated, the microstructure with the larger SiC particulates had lower penetration values. The range in penetration values (35 to 55 mm) more closely approximated

measured values for SiC (30 to 45 mm) than sintered aluminum nitride (55 to 90 mm). In fact, it appeared that even minor additions of SiC (10%) had a positive impact on improving penetration resistance. While these trends were promising, wide scatter in the aluminum nitride baseline experiments have clearly decreased confidence levels in these rationalized conclusions.

After the screening experiments, the work statement called for two compositions to be scaled up and further evaluated against the long rod penetrator. However, based on the existing data, it was not obvious which compositions and microstructures should be selected. Since the objective of this phase of the program was to develop materials with enhanced ballistic protection without sacrificing the cost advantages of aluminum nitride, it was important to choose compositions which could realistically be expected to be pressureless sintered. It was expected that compositions with SiC contents greater than 50% would not practically meet these program objectives. While the 90/10 compositions should be easily sintered, inconsistent performance made these materials less attractive. The two-phased 75/25 AlN/SiC composition was chosen since it had the lowest average penetration value and was considered to be a formulation which could be pressureless sintered. The second formulation chosen was the consistent 50/50 solid solution material. It was obvious from the above SLAP penetration results that establishing a preferred microstructure and composite chemistry would require additional ballistic experiments. It was hoped that by changing both parameters some differentiation could be established for these two AlN/SiC composites which would ultimately improve our understanding of how ceramic materials fail under ballistic conditions.

During the lower caliber screening tests, ballistic performance was evaluated at a constant areal density of 3 g/cm². Since the ceramic targets were largely overmatched by the .50 caliber SLAP round, there was excessive scatter which made material comparisons extremely difficult. An alternative depth of penetration type of ballistic test would be to increase the areal density of the ceramic targets until the point of zero penetration is reached. This method has been successfully utilized to compare ceramics³⁹ and also allows the determination of an effective strength parameter.²⁸ Tiles with areal densities of 4.5 g/cm² were prepared from AlN and the two selected AlN/SiC composites.

Because of the large scatter at 3 g/cm² for AlN, this thickness was also retested. During testing with the .50 caliber SLAP round, performance improvement over AlN was clearly demonstrated under these test conditions by both composites. Additional tiles were hot-pressed and ballistically evaluated to establish the point of zero penetration and further confirm the performance advantage of the AlN/SiC composites. Because of time constraints, these later tiles were tested as pressed. The results of this series of ballistic experiments are summarized in figure 44.

Over the areal density range tested, aluminum nitride penetration resistance was relatively constant. Except for two obviously different data points at 4.5 and 5.3 g/cm², penetration into the aluminum backing decreased linearly with increases in areal density. The correlation coefficient for this linear fit was 0.9 for the selective data set. Examination of the targets for the two low penetration values revealed that the projectile in both cases had rotated such that it was traveling sideways into the aluminum. While the cause of the rotation is unclear and may be related to the characteristics of the ceramic target, these observations provided ample justification for excluding these two data points from the analysis.

At 4.5 g/cm², penetration into both composites was less than 1 cm and was rapidly approaching the zero penetration value. Targets with 5.3 g/cm² of ceramic had effectively no penetration into the aluminum. The measured depths for these composite targets were determined with a profilometer since the deformation into the aluminum was more crater like rather than a deep narrow cavity like was shown earlier (figure 30). The performance of the two AlN/SiC materials was essentially indistinguishable and was at least equivalent to sintered SiC (high density product made at Dow) and significantly better than the aluminum nitride standard. Hot-pressed AlN, at an equivalent areal density, had penetration depths of almost 50 mm. While this comparison is illustrative, it does not establish the weight savings or relative efficiency of these composites. The preferred value to quantify the improvement advantage offered by the AlN/SiC composites would be a comparison of the zero penetration values or the respective areal densities at any other given penetration depth. However for determining this parameter some estimation, either extrapolating to some penetration depth for AlN or

interpolating a value for the composites, is also required. Since the areal density of AlN needed to yield a depth of 5 mm would be 9.6 g/cm², the relative efficiency of the AlN/SiC composites is more than twice that of AlN for this threat and target configuration. This improvement is both substantial and potentially very significant.

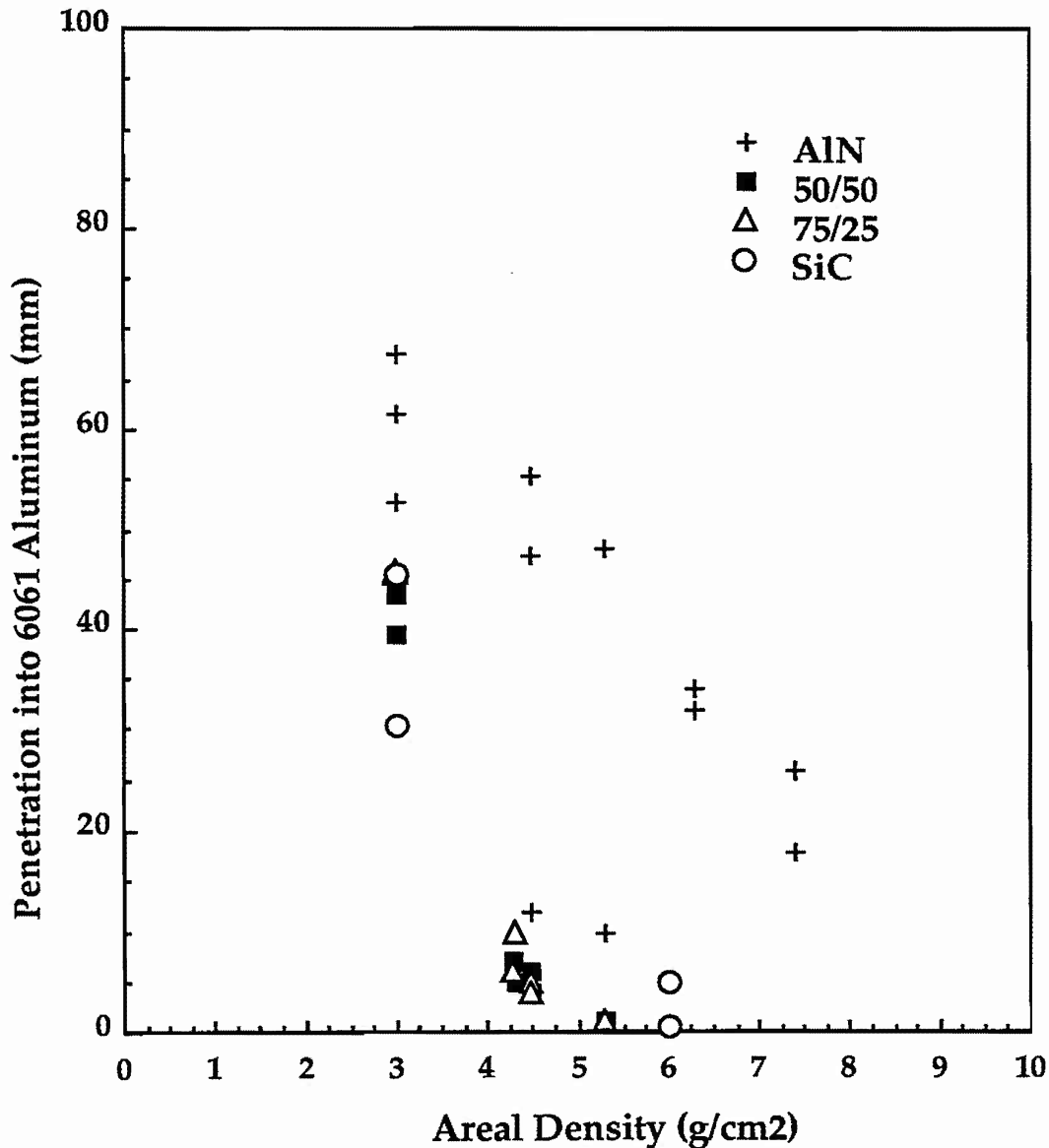


Fig. 44 Residual penetration of .50 caliber SLAP rounds in hot-pressed AlN/SiC composite targets as a function of areal density. Silicon carbide samples were pressureless sintered using a proprietary process.

Test parameters and results for the L/D 10 long rod penetrator experiments are summarized in Table XXXI. The test configuration was described earlier in section 2.2.5.2 and was similar to the target set-up shown in figure 8. As seen in figure 45, the performance of the AlN/SiC composites was equally impressive against this tungsten penetrator compared to AlN and the alumina baseline. However, unlike the .50 caliber SLAP experiments, some differentiation between the two AlN/SiC composite compositions was evident. The 75/25, two-phased AlN/SiC composite was clearly superior to the 50/50 solid solution material. In three out of the four shots, the mass efficiency, e_m , for this ceramic compared to the steel backing material exceeded 4. These results represent a significant advancement in ballistic protection and clearly exceeded the performance objectives of this program.

Table XXXI
L/D = 10 LRP Penetration Results into Al Backed AlN/SiC Composites

Tile ID	Density (g/cm³)	A.D. (g/cm²)	SHOT #	Velocity (m/sec)	Total Yaw	D.O.P. (mm)	e_m	Residual Mass (g)
50F818	3.21(99.2)	9.97	1-263	1542	2.0	42.8	2.75	11.3
50F801	3.21(99.2)	9.97	1-269	1546	1.8	36.2	3.29	9.1
75S802	3.22(99.2)	9.96	1-265	1546	0.5	15.4	4.92	5.2
75SG85	3.23(99.5)	9.97	1-266	1558	0.9	17.1	4.89	5.1
50F30	3.22(99.6)	14.99	1-264	1551	1.2	26.7	2.72	5.9
50F31	3.23(99.8)	15.00	1-267	1552		32.0	2.80	8.7
75S801	3.23(99.5)	15.02	1-270	1533	0.2	0.1	4.02	4.6
75SG31	3.23(99.5)	15.01	1-268	1571	1.0	22.4	3.04	6.8

$$e_m = (p_{ref} - p_c) \rho_{ref} / AD_c$$

Typical of most ceramic materials, the mass efficiency was lower for the targets with the thicker ceramic tiles. Although the shot to shot reproducibility was in general excellent, shot 1-268 resulted in a 30% lower performance rating for the 75/25 composition compared to its matching target (1-270). The velocity was ~2% higher for that test, but it is unlikely that this difference could completely account for the observed increase in penetration. There were also no obvious ceramic issues which may have contributed to this result. The consistent performance of this composition for the targets with a

result. The consistent performance of this composition for the targets with a ceramic areal density of 10 g/cm², strongly suggests that this lower result is the anomaly. Even as such, this "low" value is still better than any of the other compositions tested against this threat.

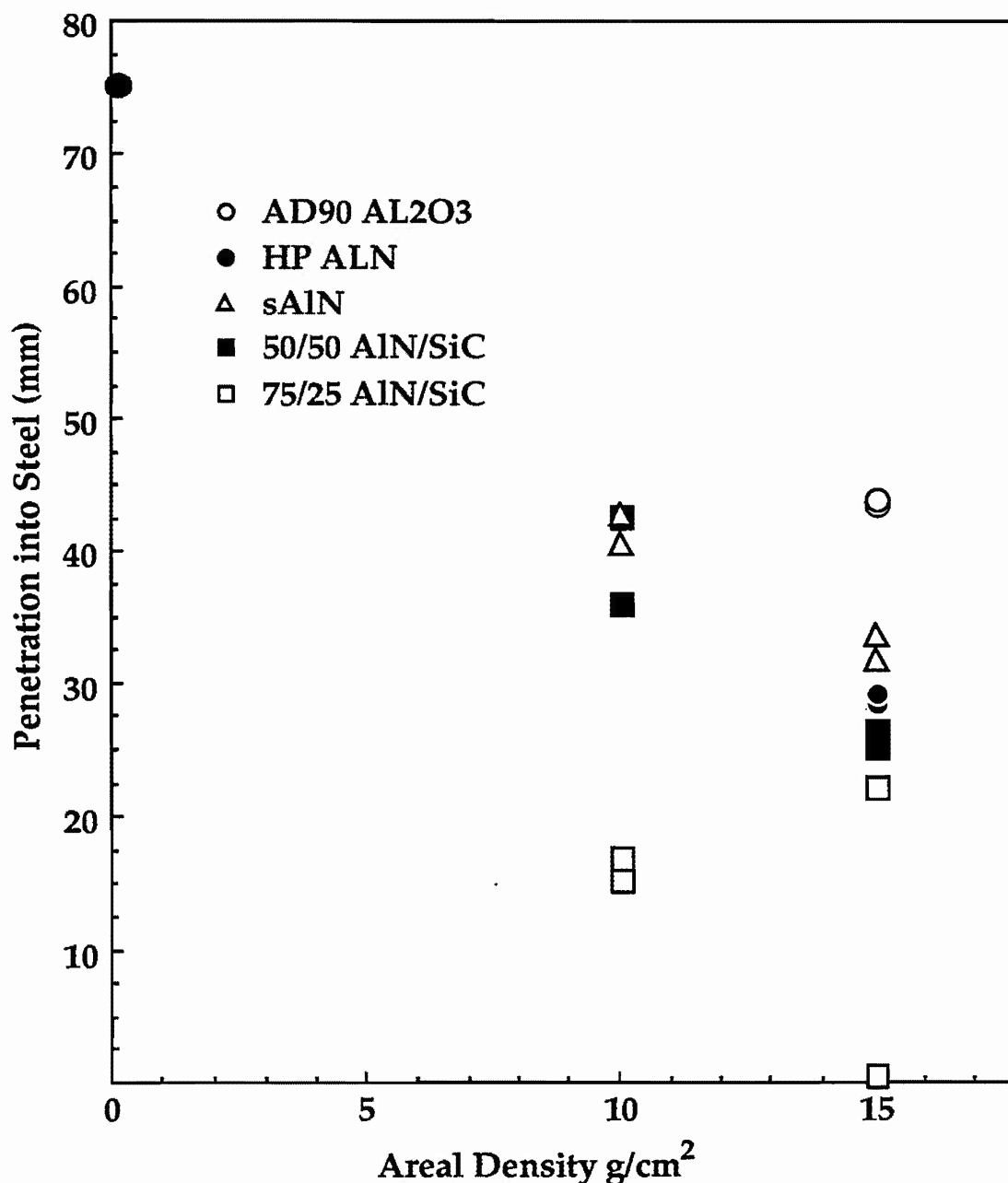


Fig. 45 Comparison of residual penetration of tungsten long rod penetrators in hot-pressed AlN/SiC composite targets at two areal densities with aluminum nitride ceramics and the program baseline material, AD90 alumina. The 65 gram LRP had a L/D ratio of 10 and was fired at ~1540 m/s.

2.3.4 DISCUSSION

This effort has established that silicon carbide additions to aluminum nitride based ceramics can substantially reduce the effectiveness of tungsten penetrators. During this ballistic study, three issues developed which warrant explanation and discussion. Substantial improvements in penetration resistance were demonstrated with as little as 10% silicon carbide. Against the .50 caliber SLAP round, no optimum composition or preferred microstructure could be identified in the initial screening study or during the more extensive evaluation which focused on two AlN/SiC compositions. Ultimately, some differentiation did occur when the heavier LRP threat was employed. The 75/25 two-phased formulation was found to be significantly better than the 50/50 solid solution material during the LRP tests.

Since mechanical characterization of these composites was not a substantial part of this program, an attempt will be made to rationalize why the two-phased 75/25 composition out-performed the 50/50 solid solution material by considering previous studies of the properties of AlN/SiC composites. Several properties are obviously affected by additions of SiC into aluminum nitride. Hardness and elastic modulus effectively follow the rule of mixtures in this compositional range and increase with higher SiC levels.³¹ Mechanical properties in this system improved primarily above 30% SiC.³⁷ The dramatic increase occurred above 60% silicon carbide, where there was a two-fold improvement in the average flexure strength to 800 MPa. The microstructures of these high strength materials were primarily single phase or mixtures of solid solution compositions. From the assumptions that flexure strength accurately reflects a material's inherent strength and that stronger materials have better ballistic characteristics as was the case for aluminum nitride, these literature values would imply that penetration resistance would be highest for silicon carbide rich, solid solution composites. However, when comparing a 75/25 AlN/SiC two-phased composite with the 50/50 solid solution, the experimental observations did not support this premise.

Since it is well recognized that ballistic penetration is a complex process involving many defeat mechanisms, there have been several attempts to simplify this event. Tate developed a model which described the penetration of

a projectile into a metal and recently this same methodology was shown to be applicable to ceramic targets as well.²⁸ Tate's theory predicts that there is a critical velocity (V_c) below which the projectile will not penetrate the target. This velocity (equation 1) is dependent upon the difference between the effective strength of the target (R_t) and then yield strength of the penetrator (Y_p). ρ_p is the density of the penetrator.

$$V_c = (2(R_t - Y_p)/\rho_p)^{1/2} \quad (1)$$

During the SLAP ballistic experiments, the AlN/SiC composites had similar penetration values and were all substantially better than aluminum nitride. Based on the earlier discussion of this system's mechanical properties, a continuous relationship between SiC content and ballistic performance may have been expected. However, the penetration results were instead more similar to a step function. By analogy with Tate's theory, if SiC additions to aluminum nitride targets increase the effective target strength, then the critical velocity for penetration would also increase. While penetration had occurred in all aluminum nitride and AlN/SiC composite targets with 3 g/cm² of ceramic, the penetration characteristics had changed from one smooth, regular cavity typical of rigid rod penetration to an irregular shaped cavity created by a heavily fragmented threat. This change in the mode of penetration could also have a critical velocity similar to but higher than V_c . Since these experiments were done at constant velocity, it is conceivable that the enhanced strength of the AlN/SiC composites resulted in this new critical velocity which was greater than the test velocity. If that was the case, then a step-like relationship between penetration and composition would be expected.

It was mentioned earlier that a ballistic event is a complex process which is dependent on many variables including the target configuration, and penetrator composition, geometry and velocity. For ceramic containing targets, the composition of the ceramic, the size of the tile and the level of confinement are particularly critical. In addition to these parameters, there is the potential for numerous energy absorbing mechanisms which can be evoked while defeating the projectile. Many of these effects are also time dependent with early time events being significantly different than late time ones. Since the LRP and SLAP round were both made of a tungsten alloy and

were fired at similar velocities, it is likely that elements of the response by the ceramics would be equivalent in both cases. The primary difference between these two threats and target configurations is the duration of the high pressure wave created by the length of the LRP. While the early time component and magnitude of the impact pulse should be very similar for these two threats, which could account for the improvement compared to AlN in both tests, it is the next level of response which may be controlling performance in the LRP case and allowing the 75/25 composite to be differentiated. Since it is assumed that the strength of both of these ceramics was sufficient to begin the break up of the penetrators, some other characteristic of these materials must be responsible for the 75/25 composite outperforming the 50/50 solid solution material. Additional experiments were needed to explore this issue further. However, only a transmission electron microscopy study was within the scope of this effort. Clearly, measuring the dynamic compressive strength of these specific composites would also have been highly desirable in order to confirm whether proposed suppositions with regard to the strength of these composites were valid.

When starting this program, it was hoped that additions of silicon carbide would increase the strength of aluminum nitride without sacrificing its ductility. Based on the ballistic performance, it is clear that the strength has been enhanced. By examining both rubble particles and ballistic fragments with a TEM, the effect on plasticity was explored. In figure 46, representative rubble particles from the two AlN/SiC composites are compared with hot-pressed AlN. While dislocations were present in both composites, the defect concentration was in general less than the aluminum nitride baseline material. The shape of the particles were also different. AlN particles tend to be irregularly shaped with few sharp edges. The 50/50 AlN/SiC particles examined had many angular edges which was indicative of intergranular fracture. The shape of the 75/25 composite particles consisted of both types of structures. As expected, isolated SiC particles were also found in this composite. The SiC particles were smaller than the typical grain size and fracture surfaces were very sharp and reflective of brittle failure.

While long range plasticity was not observed in any of the composites examined, the 75/25 composite which had the excellent ballistic performance

had extensive microcracking, as seen in figure 47. The microcracking was primarily along grain boundaries and the path was clearly affected by the presence of the added SiC particles and the elongated SIALON grains which formed during processing. The tortuous path of the microcracks would also suggest that this composition would have a higher fracture toughness which would provide some added benefit. It was noted earlier that microcracking was also observed in some of the aluminum nitride materials (figures 37 and 38). However, unlike this situation, ballistic performance was actually lower for the microcracked AlN samples. While the cause of this microcracking was clearly different in the AlN cases, these results indicate that ballistic performance can not be enhanced strictly by controlling this microstructural feature. More knowledge is obviously needed about the role microcracking away from the impact zone plays on penetration and ceramic performance. For instance a primary issue which needs to be considered is whether this microcracking is an early or late time event and whether it is representative of the fracture behavior of the material under the eroding penetrator.

Despite being hot-pressed at substantially higher temperatures, the average grain size for the 50/50 solid solution material was 2 to 5 times smaller than the 75/25 composite. If only the silicon carbide source was considered then this size difference would be consistent. However, the aluminum nitride powder which was used during the preparation of these composites was identical for both cases. The fine submicron silicon carbide powder then not only enhanced the formation of the AlN/SiC solid solution but it also substantially reduced grain growth. This property may be very beneficial when the pressureless sintering of these composites are investigated.

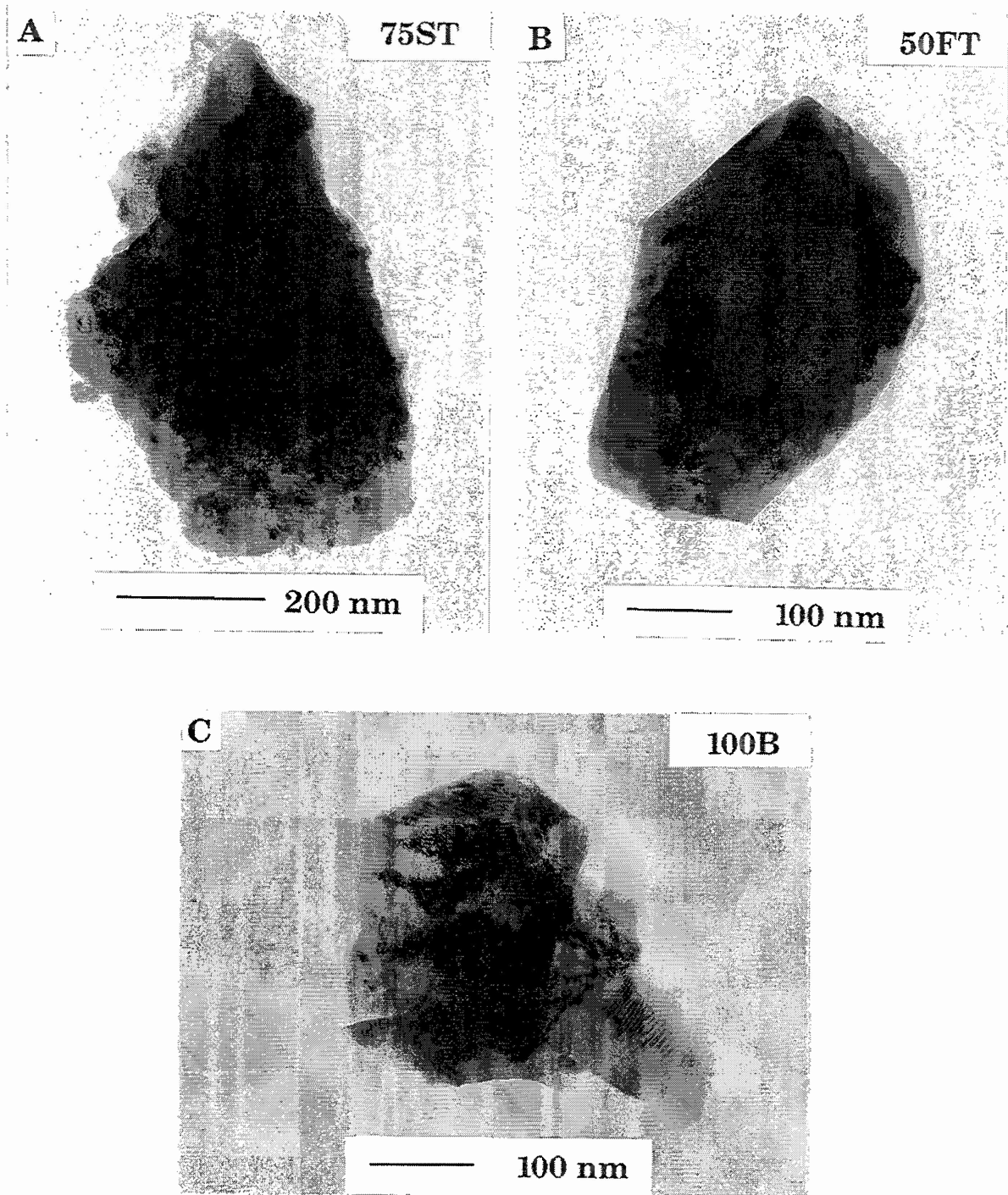


Fig. 46. TEM photomicrographs of typical fine rubble particles for hot-pressed AlN and two AlN/SiC composites after .50 caliber SLAP ballistic testing: A) aluminum nitride particle from 75/25 AlN/SiC two-phased composite; B) solid solution particle from 50/50 AlN/SiC composite; and C) heavily deformed microstructure typical of hot-pressed AlN materials.

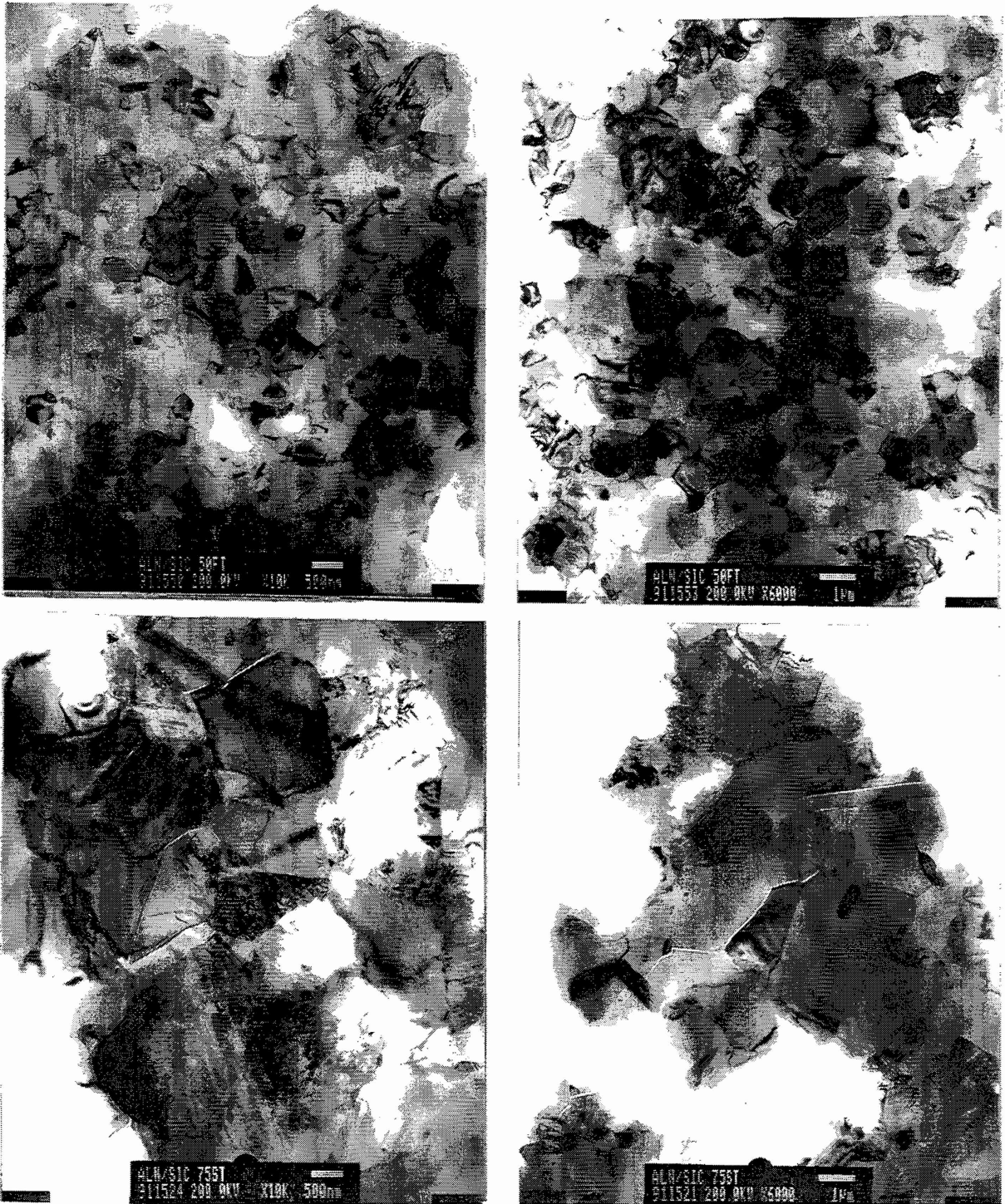


Fig. 47 TEM photomicrographs of thin sections taken from larger (>3 mm) ballistic fragments for two sintered AlN/SiC composite samples. Top photos show representative, uniform equiaxed microstructure of 50/50 AlN/SiC solid solution material. In addition to AlN (large light grains) and SiC (darker striated grains) grains, a platelike SIALON phase was also observed in the 75/25 AlN/SiC composite (bottom photos).

2.4 Sintering of AlN-SiC Composites

AlN/SiC composites have been shown to offer significant promise as ballistic materials. However, the practical development of AlN/SiC ceramic armor requires that these materials be prepared using low cost fabrication methods. This cost requirement precludes the use of hot-pressing and necessitates the development of a suitable pressureless sintering method. Building on the earlier aluminum nitride work and previous AlN/SiC studies⁸, the sintering characteristics of AlN/SiC composites were studied. The goal of this task was to establish formulations which would allow the achievement of high density parts using manufacturing technology based on pressureless sintering. Scale-up of these compositions and ultimate evaluation as ballistic materials would be an appropriate follow on program to this work.

2.4.1 PROCESS OPTIMIZATION

The intent of this current study was to establish the critical processing parameters for obtaining high density AlN/SiC compositions. A 70/30 AlN/SiC composition with 2 wt% Y_2O_3 which was shown to be sinterable to high densities by Lee and Wei⁸, was selected for this process optimization study. Processing variables examined in this study included, starting silicon carbide powder source (the characteristics of the three SiC powders which were evaluated here were described earlier in Table XXVIII), the burnout environment used (nitrogen or nitrogen/air), sintering environment (the use of a AlN/SiC powder bed), and the type of crucible (graphite or boron nitride) used during sintering. To determine the main effects and possible interactions between various processing variables a full factorial screening design was created.

Three batches, each using a different silicon carbide powder, were prepared with 2 weight percent yttria using the standard dry-press formulation and mixing procedures used throughout this contract. The dispersant (Ganex P-904) was first mixed with ethanol (absolute) to form a solution for dispersing the ceramic components. The slurry, including the ceramic components, were then milled for 2 hours. The premixed binder solution, consisting of 2:1 PEG/ECB ratio in ethanol, was then added to the slurry. Mixing was

continued by ball milling for 4 additional hours to obtain a homogeneous mixture. The solvent was then removed from the slurry using a rotary evaporator. The resulting powder was then crushed and sieved through a 45 mesh screen. 5 cm diameter disks by 1 cm thick were pressed at 82 MPa.

The organics were then thermally extracted from the compacts using a 2°C/minute ramp to 600°C in nitrogen. Upon reaching 600°C, the nitrogen atmosphere was either maintained or the inlet gas was switched to air depending on the sample. All runs had a 1 hour dwell before being cooled at a rate of 2°C/minute. A constant flow rate of 6 liters/minute was used. Other constants in the study included a sintering heating rate of 10°C/minute and a sintering temperature of 2075°C with a 1 hour dwell. Green densities were measured geometrically and were found to be somewhat dependent on the source of SiC powder. The high surface area BSC21 powder had the highest average green density (1.89 ± 0.01 g/cm³). Samples containing Starck A1 and Superior Graphite HSC 077 had similar green densities. Average values were 1.74 ± 0.02 and 1.77 ± 0.07 g/cc, respectively. Sintered densities were measured by immersion in water. The relative extent of solid solution formation and grain boundary phases present were determined by x-ray diffraction using CuK α radiation at a scan rate of 2°/minute from 20° to 80° two-theta. The process parameters and sintering results of these 25 experiments are summarized in Table XXXII.

The measured density values, grouped by silicon carbide powder, are shown graphically in figure 48. Sinterability of this AlN/SiC composition was primarily determined by the choice of SiC selected. From the main effects plot, figure 49, burnout atmosphere was the only other processing variable in this study which played a significant role. The type of crucible and the use of a powder bed were parameters which did not substantially influence the densification of this AlN/SiC composition. Since a full factorial design was utilized during this study, the interaction terms could also be evaluated. From Table XXXIII, the interaction between the burnout condition and Starck A1 powder was the only term which was found to be statistically significant. This SiC powder had an oxygen level which was 2 to 4 times lower than that of the other two powders. Since the presence of sufficient levels of oxide is required for sintering AlN based materials and the burnout environment strongly

Table XXXII
Process Optimization Study for Sintered AlN/SiC

RUN	BURNOUT	POWDER	CRUCIBLE	POWDER BED.	DENSITY (%TD*)	<110> Peak **
1	N ₂	Starck A1	Graphite	None	71.13	67
2	N ₂ /air	BSC21	Graphite	AlN/SiC	97.45	22
3	N ₂ /air	BSC21	BN	None	98.03	0
4	N ₂ /air	Starck A1	Graphite	None	88.66	NA
5	N ₂	BSC21	BN	None	96.86	22
6	N ₂	Starck A1	BN	None	65.73	NA
7	N ₂	BSC21	BN	AlN/SiC	94.93	NA
8	N ₂ /air	BSC21	Graphite	None	97.86	16
9	N ₂	HSC 077	BN	AlN/SiC	88.75	44
10	N ₂ /air	Starck A1	BN	None	90.05	17
11	N ₂	BSC21	Graphite	None	92.03	NA
12	N ₂	HSC 077	BN	None	86.82	28
13	N ₂	Starck A1	BN	AlN/SiC	83.11	67
14	N ₂ /air	HSC 077	BN	None	87.00	NA
15	N ₂ /air	Starck A1	BN	AlN/SiC	73.71	NA
16	N ₂	BSC21	Graphite	AlN/SiC	97.80	80
17	N ₂	HSC 077	Graphite	AlN/SiC	85.75	11
18	N ₂	Starck A1	Graphite	AlN/SiC	78.60	56
19	N ₂ /air	HSC 077	BN	AlN/SiC	93.20	78
20	N ₂ /air	BSC21	BN	AlN/SiC	97.02	7
21	N ₂	HSC 077	Graphite	None	82.90	11
22	N ₂ /air	HSC 077	Graphite	AlN/SiC	91.37	NA
23	N ₂ /air	HSC 077	Graphite	None	91.11	11
24	N ₂ /air	Starck A1	Graphite	AlN/SiC	90.07	100
25	N ₂ /air	BSC21	BN	None	97.85	NA

NOTE: Run 25 is a duplicate of run 3. NA indicates sample was not analyzed

* Theoretical density was assumed to be 3.267 g/cc for 70/30/2 AlN/SiC/Y₂O₃ composition.

** Peak width is relative value at a 25% relative intensity level.

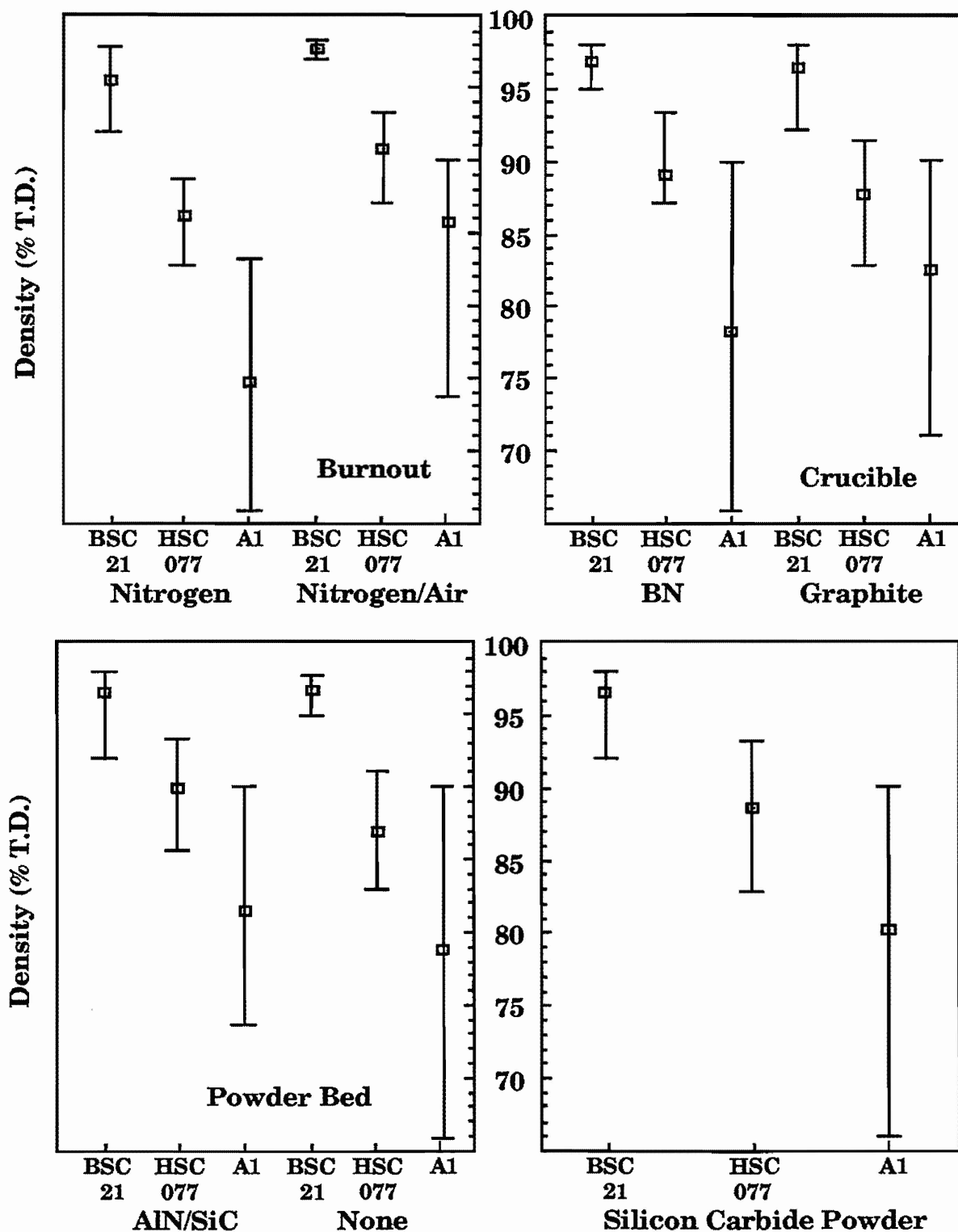


Fig. 48 Graphical representation of AlN/SiC results. The percent theoretical density are shown as a function of silicon carbide powder for the main design parameters. Average values are shown for each data subset. High and low values are indicated by the error bars.

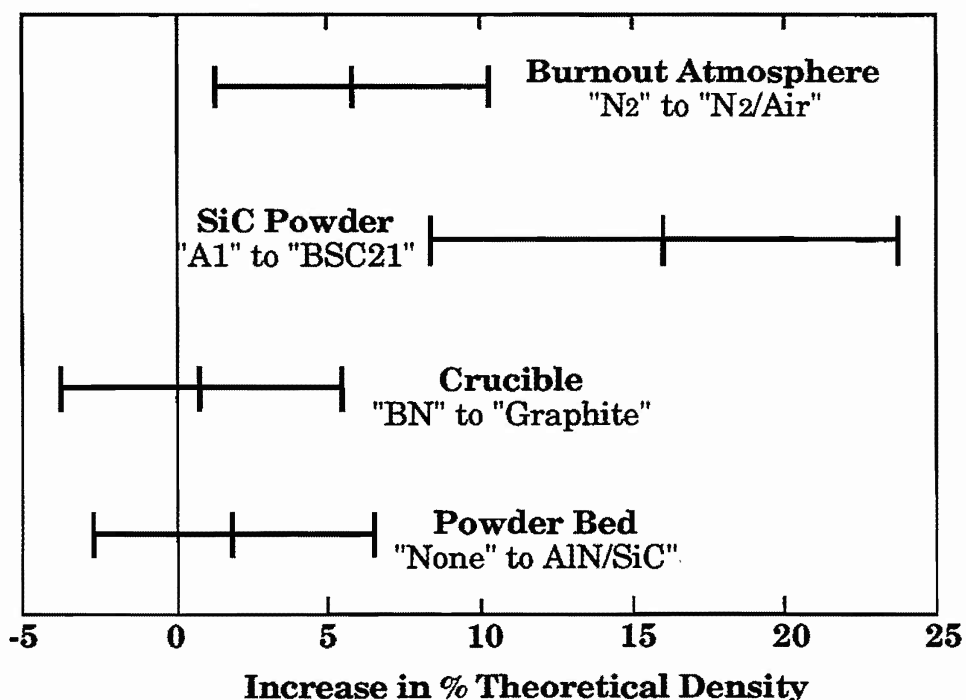


Fig. 49 Main effects plot showing the influence on percent theoretical density. 95% confidence intervals are also shown.

influences this level, this interaction could have been anticipated, particularly when a similar result was observed during the earlier AlN powder study.

Based on the X-ray diffraction data, it was also found that samples containing BSC21 SiC had a greater tendency to form the AlN/SiC solid solution than samples containing Starck A1 SiC. This observation is consistent with the earlier hot-press results and verified that finer β -SiC powders are easily dissolved within the aluminum nitride grains. The amount and composition of the grain boundary phases were found to vary depending on the processing conditions. Compositions richer in oxygen showed the typical secondary phases seen in sintered AlN - Y_2O_3 compositions including $Al_5Y_3O_{12}$, $AlYO_3$, $Al_2Y_4O_9$, and Y_2O_3 . Since there was no indication of silica based materials, it was likely that modest levels were incorporated either into the yttrium aluminate grain boundary phase or the solid solution matrix. Al_2OC , having the wurtzite structure, is isomorphic and has extensive mutual solubility with AlN and SiC. This would imply that this crystal structure can accommodate substantial amounts of oxygen contaminants and could account for the lack of x-ray diffraction peaks from silica containing species.

Table XXXIII
Least Square Coefficients for AlN/SiC Process Optimization Study

Term	Coefficient	Std. Error	T-value	Significance
Constant	88.634060	1.101931	80.44	0.0001
BO<1df>				0.0142
nitrogen	-3.266560	1.101931	-2.96	0.0142
nitrogen/air	3.266560	1.101931	2.96	0.0142
P<2df>				0.0007
Ferro	7.821870	1.537724	5.09	0.0005
Starck	-7.550310	1.568584	-4.81	0.0007
Superior	-0.271560	1.568584	-0.17	0.8660
C<1df>				0.5240
BN	-0.727607	1.101931	-0.66	0.5240
Graphite	0.727607	1.101931	0.66	0.5240
E<1df>				0.2608
None	-1.313440	1.101931	-1.19	0.2608
AlN/SiC	1.313440	1.101931	1.19	0.2608
BO*P<2df>				0.1637
nitrogen*BSC21	2.215630	1.537724	1.44	0.1802
nitrogen*A1	-3.174690	1.568584	-2.02	0.0705
nitrogen*HSC 077	0.959060	1.568584	0.61	0.5546
nitrogen/air*BSC21	-2.215630	1.537724	-1.44	0.1802
nitrogen/air*A1	3.174690	1.568584	2.02	0.0705
nitrogen/air*HSC 077	-0.959060	1.568584	-0.61	0.5546
BO*C<1df>				0.2347
nitrogen*BN	1.393440	1.101931	1.26	0.2347
nitrogen*Graphite	-1.393440	1.101931	-1.26	0.2347
nitrogen/air*BN	-1.393440	1.101931	-1.26	0.2347
nitrogen/air*Graphite	1.393440	1.101931	1.26	0.2347
BO*E<1df>				0.2101
nitrogen*None	-1.475726	1.101931	-1.34	0.2101
nitrogen*AlN/SiC	1.475726	1.101931	1.34	0.2101
nitrogen/air*None	1.475726	1.101931	1.34	0.2101
nitrogen/air*AlN/SiC	-1.475726	1.101931	-1.34	0.2101
P*C<2df>				0.4031
BSC21*BN	0.898536	1.537724	0.58	0.5719
BSC21*Graphite	-0.898536	1.537724	-0.58	0.5719
A1*BN	-2.206143	1.568584	-1.41	0.1899
A1*Graphite	2.206143	1.568584	1.41	0.1899
HSC 077*BN	1.307607	1.568584	0.83	0.4240
HSC 077*Graphite	-1.307607	1.568584	-0.83	0.4240
P*E<2df>				0.7910
BSC21*None	0.969370	1.537724	0.63	0.5426
BSC21*AlN/SiC	-0.969370	1.537724	-0.63	0.5426
A1*None	-0.877810	1.568584	-0.56	0.5881
A1*AlN/SiC	0.877810	1.568584	0.56	0.5881
HSC 077*None	-0.091560	1.568584	-0.06	0.9546
HSC 077*AlN/SiC	0.091560	1.568584	0.06	0.9546
C*E<1df>				0.5025
BN*None	0.766560	1.101931	0.70	0.5025
BN*AlN/SiC	-0.766560	1.101931	-0.70	0.5025
Graphite*None	-0.766560	1.101931	-0.70	0.5025
Graphite*AlN/SiC	0.766560	1.101931	0.70	0.5025

2.4.2 SCREENING STUDY

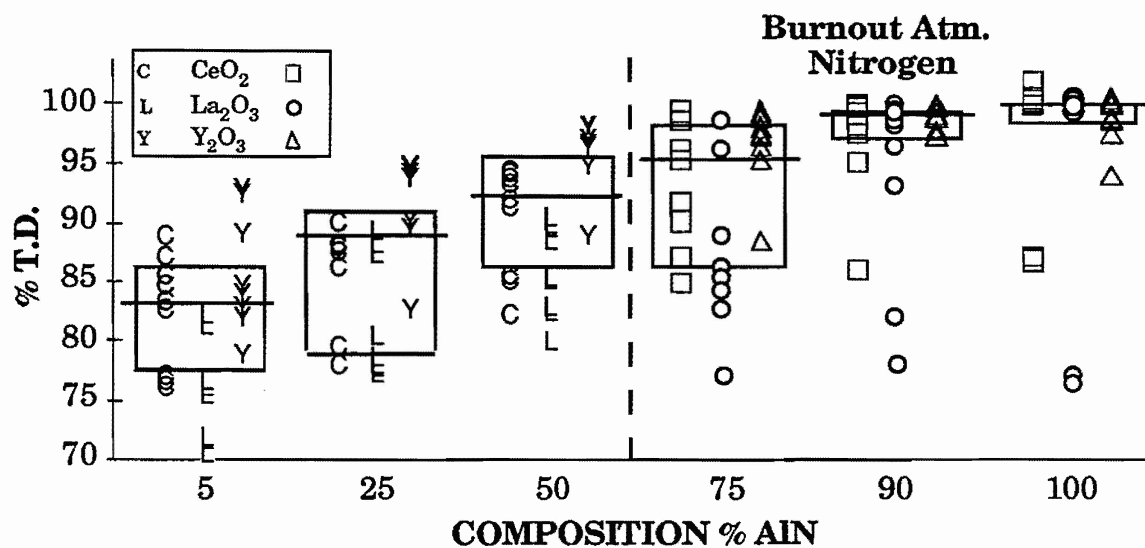
During this study of the sintering characteristics of AlN/SiC composites, five processing parameters were examined. The entire compositional range from 100 to 5% AlN was evaluated. Using our earlier AlN work as a guide, yttria, ceria and lanthana at three levels, 0.5, 1.75 and 3.0 v/o were selected as the sintering aids. While the sintering temperatures studied ranged from 1800 to 2200°C, due to the anticipated differences in sinterability in the AlN/SiC phase system, for any given composition only three temperatures were used. The three compositions rich in aluminum nitride were sintered at 1800, 1900 and 2000°C. The samples which had SiC as the major phase were sintered at 2000, 2100 and 2200°C. This difference in temperature range for the two sets of compositions created some difficulties in generating an efficient, balanced experimental design. To avoid this problem, three independent full factorial designs were generated. The first design, consisting of 54 runs, examined the six AlN/SiC compositions with three levels of the three sintering aids at a constant temperature of 2000°C. The other designs had temperature as a variable, but only looked at the three compositions in that temperature range with the nine sintering aid and level combinations. In addition, the burnout environment, which has a critical role in determining the oxide level available during the sintering process, was another variable which was considered in this study. The burnout process was treated as a constant, which in essence doubled the total number of experimental models which were generated to six.

The preparation of these samples was similar to previous studies except there were no binders used. Because of the previous density results, the source of silicon carbide powder for all of these batches was the BSC21. The dispersant, ISP Ganex P-904, was first added to ethanol then the raw materials were added in order from the minor to the major constituents. The samples were dried in a rotary evaporator, crushed to -100 mesh, then dry-pressed at 34.5 MPa in a 2.2 cm die. Since there were no binders used the green densities after dry-pressing were not adequate, so disks were also isopressed at 207 MPa. Initially, the intent was to sinter the disks as-pressed without incorporating a burnout step. However, 0.8% of this dispersant was more than adequate to generate enough free carbon to impact the chemistry, appearance and sinterability of the sintered parts. It was at this point that the decision was

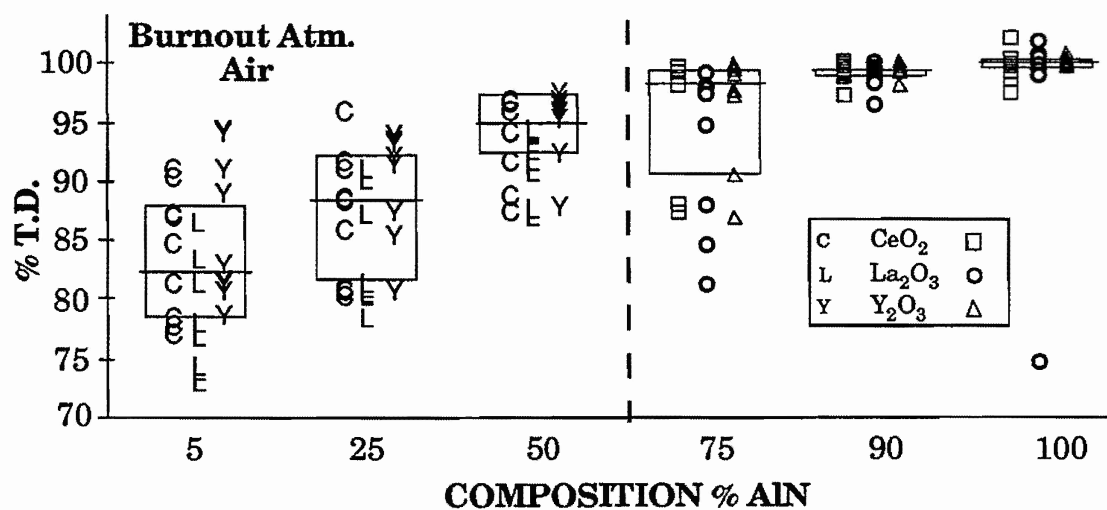
made to add the burnout step as a process variable. For some of the compositions, hydrate and/or carbonate species were generated when the samples were burned out in an open air muffle furnace. After this observation, all of the specimens were burned out under controlled conditions using either dry nitrogen or air. Based on the previous process optimization study, the sintered pellets were placed in BN crucibles without an embedding powder.

The results of this statistically designed experimental study are described in a series of box plots shown in figure 50. The values listed below each plot represent the mean percent theoretical density for all samples with that specific AlN/SiC composition. IQR equals the difference of the means for the first and third quartiles for each data set. Overall, percent theoretical density decreased with increases in SiC content above 10%. Yttrium oxide was the most effective sintering aid and it offered the most options relative to achieving high density parts. The number of samples which had densities >98% T.D., based on the initial starting materials decreased dramatically below 75% SiC. The air burned-out samples tended to achieve higher fired densities at a given sintering condition than their nitrogen equivalents. The importance of the liquid phase volume and composition to the densification process is clearly reflected by these results. For the 25/75 and 5/95 AlN/SiC composites only a few, primarily yttria doped, samples achieved densities near 95% of theoretical. While the attainment of high density materials was limited to AlN based compositions, these results were encouraging since this was the compositional regime which was the primary focus of this effort.

Some of the samples achieved densities which calculated to be greater than the theoretical density for the planned composition. Since this is an outcome which is not possible to achieve, there must have been either an error in calculating the theoretical density or that the composition had changed from the initial mixture of raw materials. An examination of the greenware chemistry prior to sintering revealed substantial oxygen pick-up in the air burned-out samples containing cerium and lanthanum oxide. These results could have significantly impacted the density observations described above, and also suggests a catalytic effect on AlN oxidation by these sintering aids.



# Pts	27	27	27	27	27	27
Mean	82.7	87.0	91.6	91.7	96.5	96.9
IQR	8.97	11.56	9.47	12.31	2.38	1.58



# Pts	27	27	27	27	27	27
Mean	83.7	88.4	94.5	95.5	99.2	99.1
IQR	9.55	10.79	4.87	8.99	0.76	0.82

Fig. 50 Box plot showing the influence of sintering aid, composition, and burnout atmosphere on percent theoretical density for AlN/SiC composites. 95% confidence intervals and average values for each composition group are also shown. The three compositions rich in AlN were sintered at 1800, 1900 and 2000°C, while the other SiC rich materials were sintered at 2000, 2100 and 2200°C.

Since a full factorial design was used for this series of sintering experiments, contour plots could be generated which would enable the selection of conditions needed to achieve high density parts for any given AlN/SiC composition. Contour plots for 100, 90 and 75% AlN using yttrium oxide as the sintering aid are shown in figure 51. Similar plots were generated for the other sintering aids.

By combining these results with the ballistic data for hot-pressed AlN/SiC composites, formulations could be chosen for preparing large sintered AlN/SiC tiles with enhanced ballistic protection. Using the ballistic experiments as the guide, the 75/25 AlN/SiC composition would be the primary choice for any future development activities. Fortunately for this composition, it would be possible to select appropriate sintering aid levels and firing temperatures for each of the three oxide additives studied during this task. However, it must be recognized that the 75/25 AlN/SiC composition which was found to have excellent ballistic characteristics utilized the micron sized Superior Graphite HSC 077 SiC powder, and not the finer BSC21 required for achieving high densities. While there has been no indication which would suggest that the size of the SiC particles affects the materials performance, this issue would have to be addressed and resolved before committing to a sintered AlN/SiC armor product.

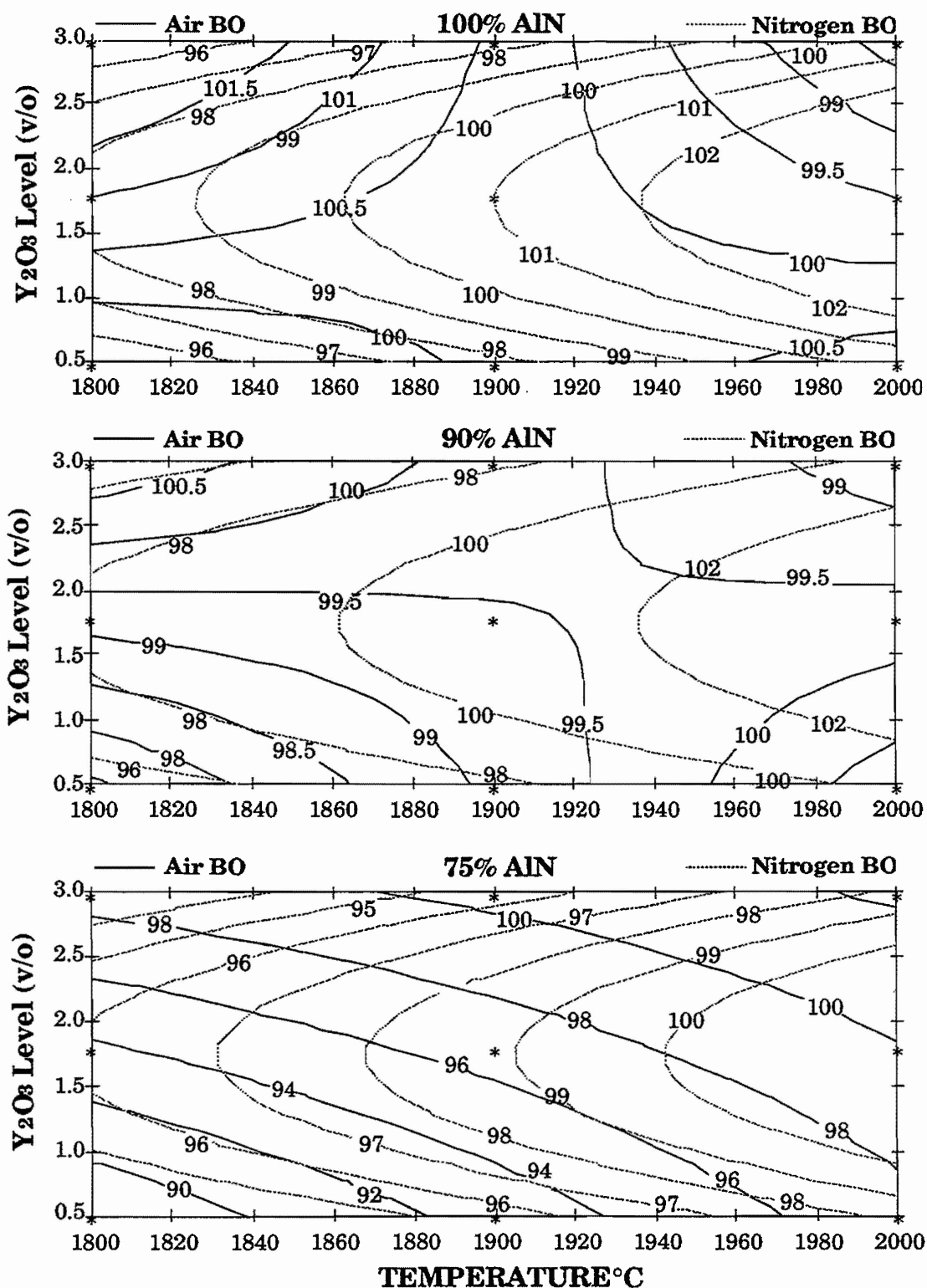


Fig. 51 Contour plots showing the influence of sintering aid (Y_2O_3), composition (100, 90 and 75% AlN), and burnout atmosphere (air or nitrogen) on % T. D. for AlN/SiC composites.

3.0 SUMMARY

When this contract started in 1988, aluminum nitride was receiving serious consideration as an electronic material, but was strictly a curiosity as a ceramic armor material. Cost was and continues to be the major impediment to the use of ceramic based armor. The objective then of this contract was to establish aluminum nitride, because of its potential as a dual use material, as a viable cost-effective high performance armor material. Two major goals had to be achieved in order to meet this objective. Processing technology suitable for large scale manufacturing had to be developed for producing AlN armor tiles and then it had to be demonstrated that the manufactured product offered superior ballistic protection compared to standard ceramic materials.

Through the extensive use of statistically designed experimentation, the capability to produce large aluminum nitride bodies using low cost manufacturing methods was achieved. During the development of this fabrication process, sinterability, without the use of external pressure, had to be established for each aluminum nitride powder examined. Surface area and powder size distribution was found to be the critical powder characteristics which controlled densification. While the powder preparation method was not found to have an inherent influence on its sinterability, powders produced by the carbothermal nitridation process because of their more narrow particle distribution had better sintering characteristics than nitrided powders with an equivalent surface area. Several cheaper sintering aid alternatives were identified, although none offered the same flexibility as yttrium oxide, the industry standard. Greenware were prepared by uniaxially pressing formulated spray-dried powders. Appropriate binder removal and sintering schedules were determined for producing tiles as large as 5 cm. This developed technology package was successfully transferred to Dow's Market Development Plant for ceramic parts in Traverse City, MI. Aluminum nitride tiles 15 cm x 15 cm x 3 cm are now routinely manufactured at this site.

Hot-pressed aluminum nitride was shown to offer a 40% improvement in ballistic protection compared to the alumina standard. While this was encouraging, it was the sintered product which needed to achieve this level of performance if this program was to be considered successful. Based on

previous studies of ceramic materials for armor application, where ballistic protection had fallen off considerably when sintered materials were compared to hot-pressed products, it was expected that the performance of sintered AlN would be less than the hot-pressed product. The fact that during some earlier light caliber tests, sintered AlN actually exceeded the performance of hot-pressed AlN, created some optimism that the performance would be comparable in these experiments as well. Because of the many combinations of powders, formulations and processing conditions which were evaluated, there was significant variation in the ballistic performance of the sintered aluminum nitride materials. However, as in previous studies, the performance of the better sintered products met or exceeded the ballistic protection of the hot-pressed ceramics for each of the threats tested. Therefore, the primary objective of this contract to develop an economical high performance ceramic material for use in armor applications for achieved. Since these materials were also thoroughly characterized both before and after ballistic testing, it was hoped that some fundamental insights into the performance of aluminum nitride and ceramics in general could also be achieved which would enhance our understanding of this complex event. While there was some progress towards this scientific goal, the identification of the most critical parameters which control performance was not achieved.

It has been well documented that non-oxide ceramics, as a class of materials offer superior ballistic protection against most penetrators. However, the relative ranking of these non-oxide ceramics is specific to the threat and target geometry of the test. It was hoped then that by forming composites of these materials, a ceramic with a broad performance window could be developed. AlN and SiC were chosen to be studied because of their ballistic characteristics and attractive economics. By measuring the ballistic properties of hot-pressed AlN/SiC composites, the effect of composition and microstructure was studied. With only modest additions of silicon carbide to aluminum nitride, ballistic performance increased dramatically against the SLAP and LRP tungsten rounds. Relative mass efficiencies compared to steel exceeded 4 for the 75/25 AlN/SiC composite. Several sinterable formulations were also identified for this AlN/SiC composition. The combination of these two discoveries could significantly enhance the utilization of ceramic based armor due to the increase in protection level and the broadening of the application window.

4.0 PUBLICATIONS AND TECHNICAL REPORTS

The following presentations and publications have been supported wholly or in part by this contract:

"Aluminum Nitride and AlN Composite Ceramic Armor, W. Rafaniello, presented at the 2nd Annual Combat Vehicle Survivability Symposium, April, 1991, Gaithersburg, MD.

"Processing of Aluminum Nitride Ceramics", F. Skeelee and W. Rafaniello, Proceedings of the 37th Sagamore Army Materials Research Conference, Plymouth, MA, Oct., 1990.

"Development of Low Cost Ceramic Armor Based on Aluminum Nitride," W. Rafaniello, F. Skeelee and I. Khoury, presented at the 92nd Annual Meeting of the American Ceramic Society, April, 1990, Dallas, TX.

"Effect of High Impact Loading on the Microstructure of AlN and other Ceramic Materials," D. Susnitzky and W. Rafaniello, presented at the 92nd Annual Meeting of the American Ceramic Society, April, 1990, Dallas, TX.

"Examination of Commercial AlN Powders", W. Rafaniello, M. Paquette and T. Rey, Proceedings of the Third International Conference on Ceramic Powder Processing Science, Feb. 4-7, 1990, San Diego, CA. Ceramic Powder Science III, *Ceramic Transactions*, Vol. 12, 865-874 (1990).

"Evaluation of Low-Cost Aluminum Nitride Armor Tiles", W. Rafaniello, B. Brubaker and R. Hoffman, The Dow Chemical Company, Proceedings of the Fifth TACOM Armor Coordinating Conference, 7-9 March 1989, Monterey, CA

5.0 REFERENCES

1. J. M. Weatherall, "Advanced Armor Materials," Kline & Co., Fairfield, NJ, in *American Ceramic Society Bulletin*, **69** [3] 294 (1990).
2. D. Viechnicki, W. Blumenthal, M. Slavin, C. Tracy, and H. Skeelee "Armor Ceramics -- 1987," presented at the Third TACOM Armor Coordinating Conference, Feb. 1987, Monterey, CA.
3. R. G. Young, K. A. Epstein and R. J. Hoffman, "The Cost Effectiveness of Ceramic Armor," Proceedings Fourth TACOM Armor Coordination Conference for Combat Vehicles, March, 1988, Monterey, CA., Battelle Columbus Division, Columbus, OH
4. H. C. Heard and C. F. Cline, "Mechanical behavior of polycrystalline BeO, Al₂O₃ and AlN at high pressure," *J. Mat. Sci.*, **15** 1889-1897 (1980).
5. P. T. B. Shaffer, J. R. Schorr and R. L. Hexemer, Jr., "Green Light to Aluminum Nitride," *Ceramic Industry*, **132** [5] 25-27 (1989).
6. R. A. DiChiara and I. A. Khoury, "Ceramic Greenware Formulation for Dry-Pressed Greenware," Dow Chemical Internal Report.
7. P. Woolsey, D. Kokidko and S. A. Mariano, "Progress Report on Ballistic Test Methodology For Armor Ceramics," Proceedings of the TACOM Combat Vehicle Survivability Symposium, March, 1990, Gaithersburg, MD.
8. W-C. J. Wei and R-R. Lee, "Pressureless Sintering of AlN-SiC Composites," *J. Mater. Sci.*, **26** [4] 2930-36 (1991).
9. A.J. Kamp, M.S. Paquette, A.K. Knudsen, I.A. Khoury, and K.L. Scanlon, "High Thermal Conductivity Aluminum Nitride in Advanced Packaging Applications," NEPCON West - Proceedings (1988).
10. W. Rafaniello, M. S. Paquette, and T. D. Rey, "Examination of Commercial AlN Powders," Ceramic Powder Science III, *Ceramic Transactions*, Vol. 12, 865-874 (1990).
11. W. Rafaniello, F. Skeelee and I. Khoury, "Development of Low Cost Ceramic Armor Based on Aluminum Nitride," Presented at the 92nd Annual Meeting of the American Ceramic Society, April, 1990, Dallas, TX.
12. E. P. Papadakis, "Absolute Accuracy of the Pulse-Echo Overlap Method and the Pulse-Superposition Method for Ultrasonic Velocity, *J. Acoust. Soc. Am.*, **52** [3] 843-46 (1972).
13. C. A. Tracy, "A Compression Test for High Strength Ceramics," *J. of Testing and Evaluation*, **15** [1] 14-19 (1987).

14. J. Lankford, "Compressive Strength and Microplasticity in Polycrystalline Alumina," *J. Mater. Sci.*, **12** [4] 791-96 (1977).
15. P. Woolsey, D. Kokidko and S. A. Mariano, "Alternative Test Methodolgy For Ballistic Performance Ranking of Armor Ceramics," U. S. Army Materials Technology Laboratory, MTL TR 89-43 (1989).
16. J. Lankford, "Mechanisms Responsible for Strain-Rate Dependent Compressive Strength in Ceramic Materials," *J. Am. Cer. Soc.*, **64** [2] C-33 - C-34 (1981).
17. M. Adams and G. Sines, "A Statistical, Micromechanical Theory of the Compressive Strength of Brittle Materials," *J. Am. Cer. Soc.*, **61** [3-4] 126-131 (1978).
18. W. Rafaniello, B. Brubaker and R. Hoffman, "Evaluation of Low-Cost Aluminum Nitride Armor Tiles," Proceedings Fifth TACOM Armor Coordination Conference for Combat Vehicles, March, 1989, Monterey, CA., Battelle Columbus Division, Columbus, OH.
19. K. Komeya, "Development of Aluminum Nitride Ceramics", *Seramikkusu*, **20**(6), 505-12, (1985).
20. R. D. Cook and C. J. Nachtsheim, "A Comparison of Algorithms for Constructing Exact D-Optimal Designs," *Technometrics*, **22**(3), 315-322 (1980).
21. T. J. Mitchell, "An Algorithm for the Construction of D-Optimal Experimental Designs," *Technometrics*, **16**(2), 203-210 (1974).
22. H. P. Wynn., "The Sequential Generation of D-Optimum Experimental Designs," *The Annals of Mathematical Statistics*, **41**(5), 1655-1644 (1970).
23. W. O. Cochran and G. M. Cox, Experimental Designs, John Wiley & Sons, Inc., (1957).
24. J. A. Cornell, Experiments with Mixtures: Designs, Models and the Analysis of Mixture Data, John Wiley & Sons, Inc., (1981).
25. D. K. Shetty, A. R. Rosenfield, P. McGuire, G. K. Basal, and W. H. Duckworth, "Biaxial Flexure Tests for Ceramics," *Am. Ceram. Soc. Bull.*, **59**(12), 1193-1197 (1980).
26. R. A. Thompson, "Mechanics of Powder Pressing: I, Model for Powder Densification," *Am. Ceram. Soc. Bull.*, **60**(2), 237-243 (1981).
27. Z. Rosenberg, S. J. Bless, Y. Yeshurun and K. Okajima, "A New Definition of Ballistic Efficiency Based on the Use of Thick Backing Plates," Presented at the Impact 87 Conference, Bremen, Germany, (1987).

28. Z. Rosenberg and Y. Tsaliah, "Applying Tate's Model for the Interaction of Long Rod Projectiles with Ceramic Targets," *Int. J. Impact Eng.*, **9**, 247-51 (1990).
29. M. L. Wilkins, C. F. Cline and C. A. Honodel, "Fourth Progress Report of Light Armor Program," **UCRL-50694**, (1969).
30. W. J. Conover, Practical NONPARAMETRIC Statistics, John Wiley & Sons, Inc., (1971).
31. W. Rafaniello, K. Cho and A. V. Virkar, "Fabrication and Characterization of SiC-AlN Alloys," *J. Materials Science*, **16**(12), 3479-88 (1981).
32. R. Ruh and A. Zangvil, "Composition and Properties of Hot-Pressed SiC-AlN Solid Solutions," *J. Am. Ceramic Soc.*, **65**(5) 260-5 (1982).
33. W. Rafaniello, M. R. Plitcha and A. V. Virkar, "Investigation of Phase Stability in the System SiC-AlN," *J. Am. Ceramic Soc.*, **66**(4) 272-6 (1983).
34. R. Ruh, A. Zangvil and J. Barlowe, "Elastic Properties of SiC, AlN and Their Solid Solutions and Particulate Composites," *Am. Ceram. Soc. Bull.*, **65**(10), 1368-74 (1985).
35. A. Zangvil and R. Ruh, "Solid Solutions and Composites in the SiC-AlN and SiC-BN Systems," *Materials Science and Engineering*, **71** 159-64 (1985).
36. A. Zangvil and R. Ruh, "Phase Relationships in the Silicon Carbide - Aluminum Nitride System," *J. Am. Ceramic Soc.*, **71**(10) 884-90 (1988).
37. M. Landon and F. Thevenot, "The SiC-AlN System: Influence of Elaboration Routes on the Solid Solution Formation and its Mechanical Properties," *Ceramics International*, **17**(1), 97-110 (1991).
38. S. Y. Kuo, Z. C. Jou, A. V. Virkar and W. Rafaniello, "Fabrication, thermal treatment and microstructure development in SiC-AlN-Al₂O₃ ceramics," *J. Materials Science*, **21**(12), 3019-24 (1986).
39. J. Reaugh, A. Holt, B. Cunningham and M. Wilkins, "Ballistic Evaluation of Five Ceramics and Pyrex as a Function of Velocity and Thickness," Classified Proceedings of 1989 Hypervelocity Impact Symposium, San Antonio, TX, (1990).

